Masters Theses   Graduate School

12-2000

Investigating the feasibility of monitoring dynamic behavior of a fluidized bed using a piezoelectric accelerometer

Tiang-Yong Teh

Follow this and additional works at: https://trace.tennessee.edu/utk_gradthes

To the Graduate Council:

I am submitting herewith a thesis written by Tiang-Yong Teh entitled "Investigating the feasibility of monitoring dynamic behavior of a fluidized bed using a piezoelectric accelerometer." I have examined the final electronic copy of this thesis for form and content and recommend that it be accepted in partial fulfillment of the requirements for the degree of Master of Science, with a major in Metallurgical Engineering.

George Pharr, Major Professor

We have read this thesis and recommend its acceptance:

R. A. Buchanan, R. S. Benson
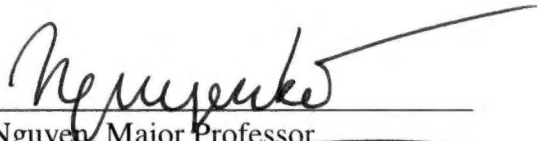
Accepted for the Council:
Carolyn R. Hodges

Vice Provost and Dean of the Graduate School

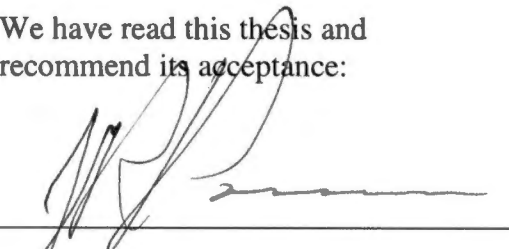(Original signatures are on file with official student records.)

To the Graduate Council:

I am submitting herewith a thesis written by Tiang-Yong Teh entitled "Investigating the Feasibility of Monitoring Dynamic Behavior of a Fluidized Bed Using a Piezoelectric Accelerometer." I have examined the final copy of this thesis for form and content and recommend that it be accepted in partial fulfillment of the requirement for the degree of Master of Science, with a major in Mechanical Engineering.
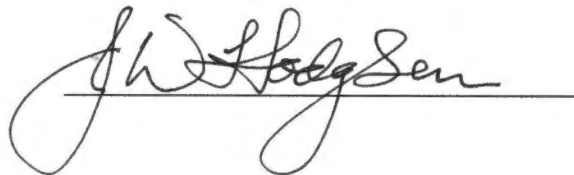
Ke Nguyen, Major Professor

We have read this thesis and
recommend its acceptance:

Accepted for the Council:

Associate Vice Chancellor and
Dean of The Graduate School

INVESTIGATING THE FEASIBILITY OF MONITORING DYNAMIC BEHAVIOR OF A FLUIDIZED BED USING A PIEZOELECTRIC ACCELEROMETER

A Thesis

Presented for the

Master of Science

Degree

The University of Tennessee, Knoxville

Tiang-Yong Teh

August 2000

ACKNOWLEDGEMENTS

ABSTRACT

Results obtained from the Geldart's group B and D solids in a laboratory-scale fluidized bed indicate that significant information about the bed dynamics can be obtained from acoustic sensors With simple pre-processing of acoustic signals with RMS filtering, the bed dynamics can be monitored by extracting the low-frequency acoustic-intensity modulation Both linear and nonlinear analysis techniques show that pressure and acoustic signals share significant amount of information by characterizing various fluidization regimes associated with near minimum fluidization, developing slugs, slugging, and breaking slugs.

Results demonstrate that piezoelectric accelerometer can be a useful tool for monitoring the dynamic behavior of fluidized bed, especially in hazardous systems where limited direct contact with the process is an advantage Such monitoring capability shows great promise of becoming a valuable supplemental diagnostic tool for detecting anomalous or undesirable behavior such as defluidization and solid agglomeration in commercial fluidized bed reactors and combustors

TABLE OF CONTENTS

LIST OF TABLES

LIST OF FIGURES

ix

CHAPTER 1

INTRODUCTION

Fluidization is a process in which a mass of fine solids is transformed into a fluid-like state by the upward flow of a gas or liquid. A fluidized bed is formed by passing an upward flow of a gas or liquid through a bed of particles contained within a reactor vessel. The bed of particles behaves like a liquid when the fluid flow exceeds the minimum fluidization velocity, at which the drag between the solids and fluid counterbalances the gravitational force of the solid particles. Thus, denser particles will sink to the bottom of the bed and lighter particles will tend to float, creating a bed of wave motion particles. This phenomenon creates many processing advantages where solids can be removed and added to the bed continuously. Increasing the flow velocity above the minimum value enhances the degree of mixing between the solids and fluid. Therefore, the mixing of the gas and solids results in highly efficient rates of mass and heat transfer.

There are attractive advantages of using fluidized bed as a chemical or physical-processing tool due to its ease of large-scale operation, continuous processing, rapid mixing of solids leading to nearly isothermal conditions throughout the reactor and impressive heat and mass transfer between gas and particles [Kunii, D., and Levenspiel, O., 1969]. Nevertheless, fluidized beds are not without its numerous design and operating deficiencies. These include significant erosion/corrosion of the bed walls and heat transfer surfaces, elutriation of solids in the gas flow, and agglomeration of particles at certain operation conditions. Despite the above problems, the overwhelming

1

advantages of fluidized beds have been widespread in industrial operation such as chemical reactors, dryers and combustors.

However, understanding the dynamic behavior of the fluidized bed is the key to the successful operation of many operating commercial fluidized beds Dynamic pressure measurements are commonly used to characterize the quality and regime of fluidization The fluidization states of the bed mainly depend on the properties of the solids and operating conditions The properties of the solids are largely dependent on a combination of mean particle size and density, whereas the operating conditions are fluid velocity, pressure, and temperature. A fluidization diagram was created by D Geldart to classify the variation of fluidization behaviors for different solid sizes Several common classifications of fluidization is shown in Figure 1 based on gas-solid contacting [Kunii D, and Levenspiel, O., 1969]. When the flow rate is below the minimum fluidization velocity, fluid passes through the void spaces between the stationary solids, a state referred to as a fixed bed As the flow rate increases to a point when the drag forces between the fluid and particles are sufficient enough to overcome the gravitational force, the solids will be lifted upward, allowing the bed to expand A bed is said to be incipiently fluidized when the drag is just sufficient to balance the weight of the particles As the flow rate increases above the minimum fluidization velocity, a smooth expansion of the bed without any large scale of bubbling is classified as a particulately fluidized bed or a smooth fluidization. At higher gas flow rates, more violent and movement of solids such as bubbles can be observed in the bed. This state is referred to as an aggregative fluidized bed or bubbling fluidization With further increase in flow rate, bubbles coalesce and grow as they rise in the bed. Depending on vessel geometry, particle

2
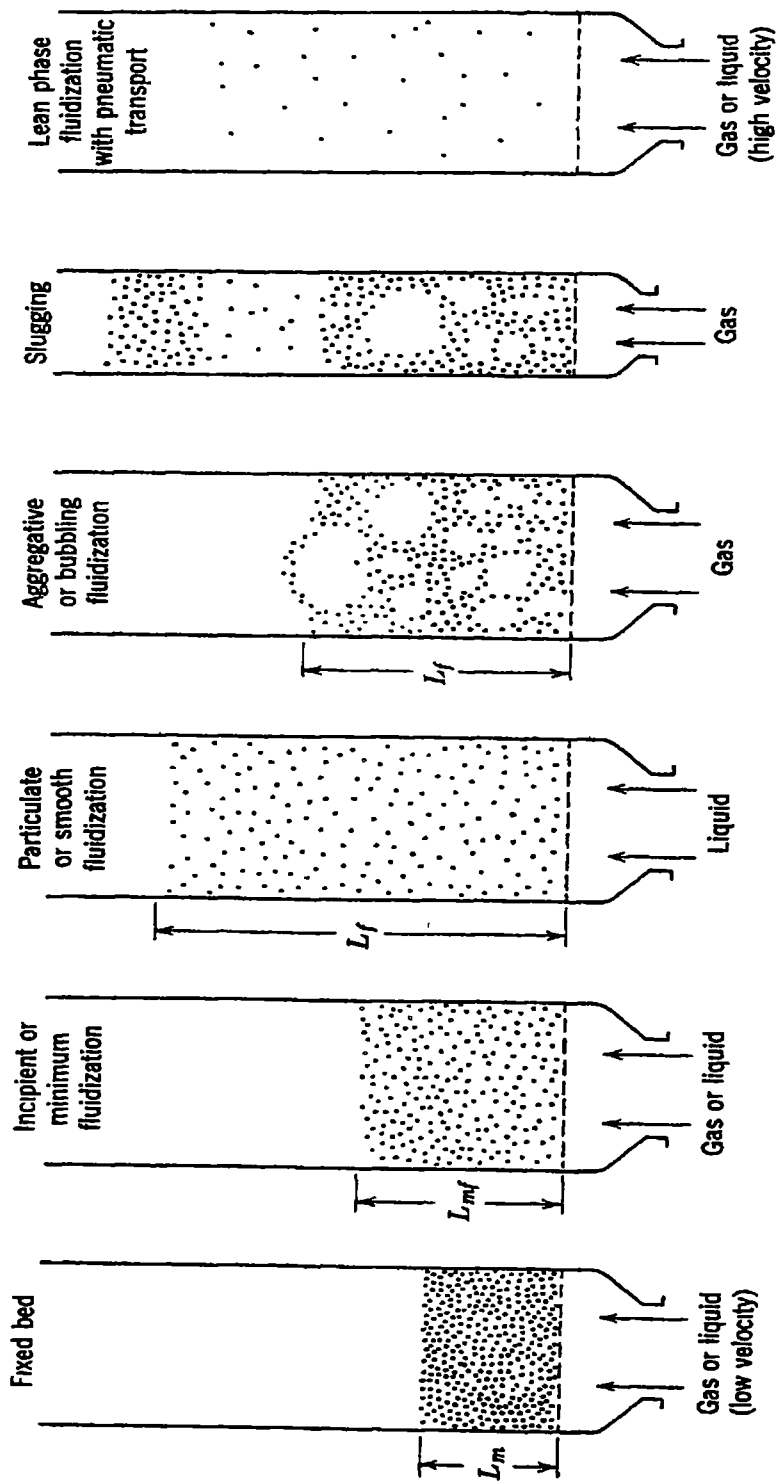
Figure 1. Classification of fluidization behaviors based on various kinds of contacting of a batch of solids by fluid

Source "Fluidization Engineering", 1969, edited by Kunii, D , Levenspiels, O , Robert E Krieger Publication Company, Inc

3

size and density, large bubbles can spread across the entire cross section of the bed creating a piston-like situation where a portion of the bed above the bubble is pushed upward, a phenomenon known as slugging Further increase in gas velocity results in particles being carried along with the flow stream resulting in a lean-phase fluidized bed with pneumatic transport of solids. Figure 2 illustrates four different regimes of group A, B, C, and D to characterize the particles according to their fluidization behavior in the air at ambient conditions. Numerous studies have been conducted showing that pressure measurements are extremely useful in monitoring the dynamic behaviors of fluidized beds, but they often introduce some engineering difficulties The most common problems involved fluidized bed are tap penetration of the vessel wall, plugging of the taps by particles, and modulation of the dynamic signal by lines connecting the taps and pressure sensors. Moreover, installation and maintenance of pressure taps due to the long-term wear of process operations introduces another financial burden All these difficulties provide the need to introduce an alternative measurement to replace conventional pressure measurements Acoustic measurements promise to be a powerful, nonintrusive technique for extracting process information, because they are not subjected to erosion, corrosion or even plugging in adverse operating conditions such as high temperature, erosive or chemically reactive materials

Since industrial processes are always accompanied by energy outputs (i e , heat, sound, vibration, etc), emission of audible noise can be used to characterize many production, manufacturing, transportation and propulsion processes Some of this noise is produced in the form of vibrational energy, which can be measured and analyzed For instance, a new concept using acoustic sensors for characterizing the flow of particulate

4
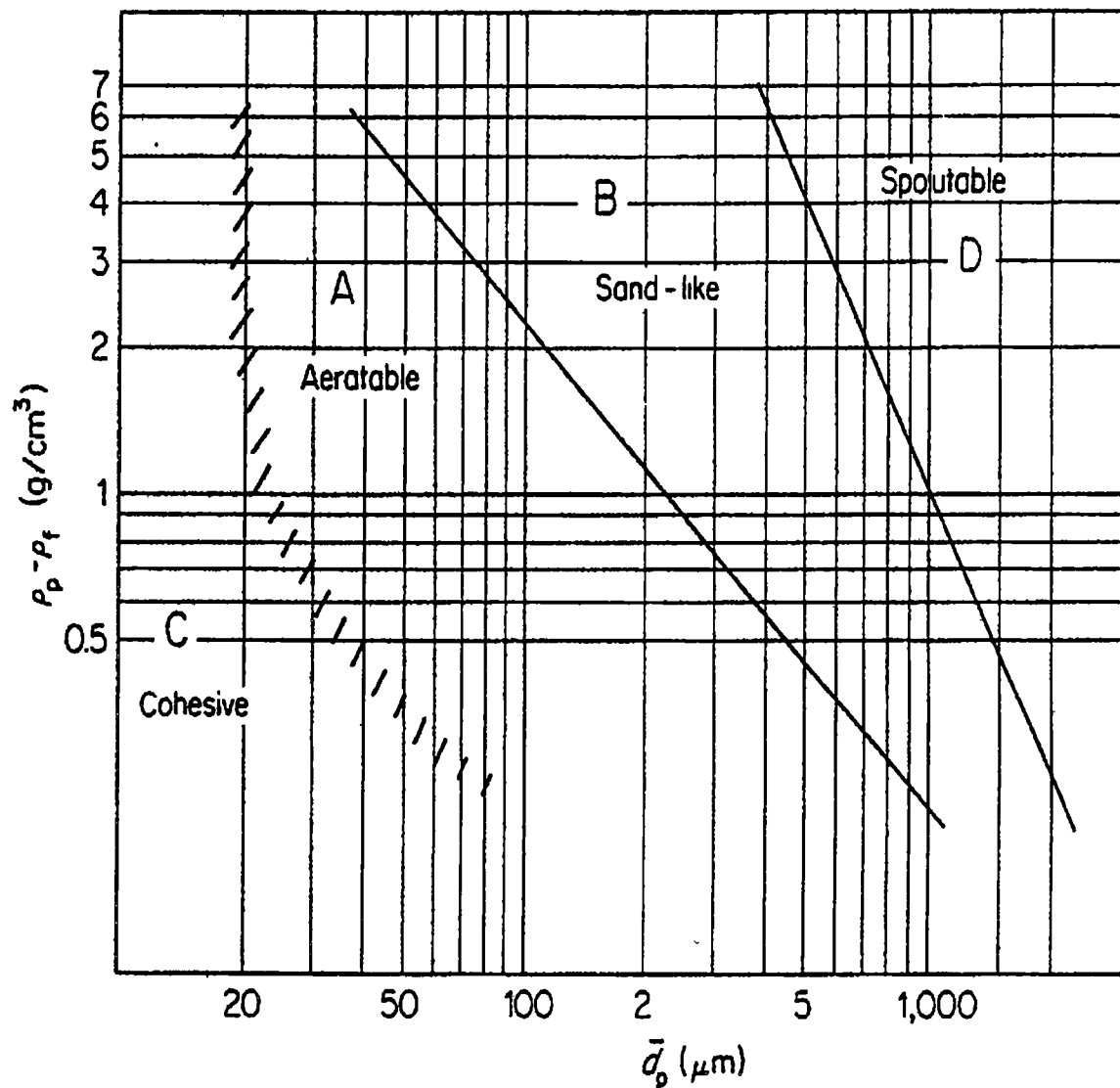
Figure 2. Classification of solids based on their fluidization behavior in air at ambient conditions, where $(\rho_p - \rho_f)$ is the density difference between the solids and fluidization air and $\bar{d}_p$ is the mean diameter of the solids.

materials in pneumatic-conveying pipelines has been developed by the Applied Chemometrics Research Group at the Power Science and Technology Group, Tel-Tek within the last few years [Halstensen, M., Silva, S., Esbensen, K., 1998] This group has established empirical correlations describing the connection between the flow behavior of representative types of materials and nonmvasive acoustic measurements of pipeline surface A similar application of nonintrusive passive acoustic sensors has been used for online monitoring of pipeline flows [Hou, R, Hunt, A, Williams, R A, 1999] The general approach has been to use statistical and spectral characteristics of the collected acoustic signal to build quantitative models to infer related process parameters such as solid concentration, volumetric flow rate and mass flow rate of the dense slurries of fine silica particles. The results indicate that passive acoustic signals can be a viable tool for on-line monitoring of slurry flows.

Acoustic sensor, including generic accelerometers, portable recorders or desktop microphones, are all practical approaches for recording useful sound signals from the operating system. In the operation of fluidized beds, fluidization states can be distinguished by human ears For instance, the whooshing sounds can be observed with the rising bubbles in the bed and thumping of particles can be correlated with rising bubbles and the slugging in the bed, respectively. This occurrence seems to be a characteristic behavior of relatively low flow velocity in the fluidized bed

Recently, studies have shown that acoustic sensors can be used to measure slugging bed dynamics [Finney, C.E.A, Daw, C S, Halow, J S., 1997] These studies demonstrate that significant information about dynamic behaviors of fluidized beds can be extracted using simple acoustic signal recording and processing Pre-processing of

acoustic signals with analog and digital filters is a key step in separating information about micro-scale and macro-scale processes. Both linear and nonlinear analyses are used for analyzing acoustic measurements. Nonlinear time-series analyses such as Kolmogorov entropy and correlation dimension appear to be especially useful for practical diagnostics. Results indicate that acoustic signals from slugging bed dynamics contain both similar and complementary information relative to dynamics pressure signals [Finney, C.E.A., Daw, C.S., Halow, J.S., 1997]. Therefore, this technique could be prove useful for monitoring fluidized bed systems, especially in hazardous systems where minimal or no direct contact with the process is an advantage These developments have motivated the present study.

The objective of this study is to investigate the feasibility of using wall-mounted accelerometer to monitor the dynamics behavior of in a laboratory-scale fluidized bed to characterize Geldart's group B and D particles Both pre-filtering of the acoustic signals and subsequent linear and nonlinear characterization are used to developed practical diagnostics. A laboratory-scale fluidized bed operated at various flow conditions using Geldart's group B and D particles is used to generate the acoustic data evaluated in this study The data generated include signals from a piezoelectric accelerometer and differential-pressure measurements The latter are already known to correlate well with the dynamic behaviors of fluidized beds.

This thesis is organized as follows Chapter 2 describes the experimental apparatus and procedures used in this study. Chapter 3 presents a brief review of theoretical background of data-analysis techniques and the calculation procedures used in this study. Chapter 4 discusses the results obtained from this study, and Chapter 5

7

presents the conclusions drawn from this study and recommendations for further research

work.

CHAPTER 2

EXPERIMENTAL APPARATUS AND PROCEDURES

The experimental apparatus and procedures used in this study are discussed in this chapter Sections 2.1 and 2.2 describe the experimental apparatus and the test conditions, respectively. An overview of the experimental procedures is presented in Section 2.3

2.1   DESCRIPTION OF THE EXPERIMENTAL APPARATUS

This section describes the experiment apparatus used in this study Section 2 1 1 describes the laboratory-scale fluidized bed. A description of the air distributor plate design is given in Section 2.1.2. Data acquisition is described in Section 2 1 3   Section 2.1.4 presents the dual analog filters used in this study. Section 2.1.5 reviews the differential-pressure transducers. The piezoelectric accelerometer used in this study is described in Section 2.1 6. The physical properties of the solid particles are given in Section 2 1.7.

2.1.1   LABORATORY-SCALE FLUIDIZED BED

A schematic of the experimental apparatus is shown in Figure 3   The fluidized bed used in this study is fabricated from a plexiglass cylindrical tube with 10 2 cm (4 inch) inner diameter and 252 cm (99.2 inch) height The plexiglass tube is fabricated in two sections of 82 cm (bottom section) and 107 cm (top section) long connected

9
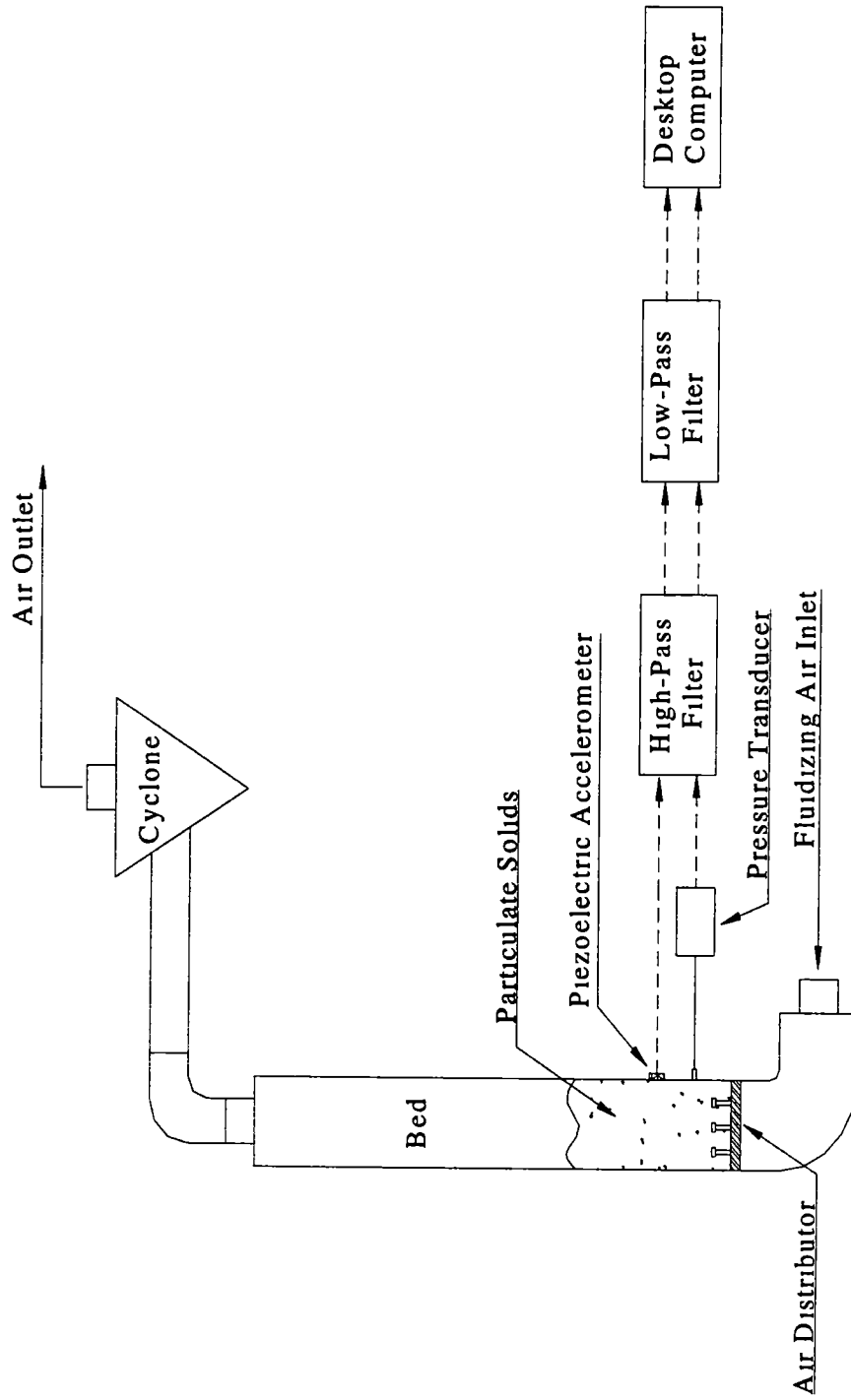
Figure 3. Schematic of the experimental apparatus

with flanges. Rubber gaskets are used to seal the flanges from leaking A tuyere-nozzle type air distributor mounted at the bottom of the fluidized bed is used to distribute fluidizing air uniformly across the bed cross section. Building air is introduced into the plenum chamber via the cut off valve, pressure regulator, flow meter (rotameter), and throttle valve. The plenum chamber is constructed of a 90° PVC elbow (10 2 cm inner diameter) is located at the bottom of the fluidized bed. The fluidized bed exit is connected to a cyclone dust collector via a flow reducer and flexible rubber hose The whole fluidized bed assembly is supported on a steel stand For rigidity the bed is attached to the wall by an aluminum bracket located at the exit section of the fluidized bed (top flange).

Four equally-spaced pressure taps located on the bed circumference at an elevation of 10.16 cm (4 inch) above the air distributor to measure the pressure drop across the bed. The pressure taps are fitted on the bed circumference by the 0 3175 cm (0 125 inch) pipe fittings and wire meshes are glued on the tap openings to prevent plugging of pressure tabs by solid particles. The pressure taps are connected using the 0.3175 cm (0.125 inch) diameter vinyl tubing The pressure taps are horizontally interconnected such that the average pressure drop over the bed cross section is obtained In this study, the average pressure drop from the taps to atmosphere is referred to as the global pressure drop. The arrangement and the location of the pressure taps are shown in Figures 4

In order to correlate the acoustic measurement with the measurement obtained from the pressure transducer, a piezoelectric accelerometer is used to capture the acoustic signal generated by the fluidized bed at various flow conditions The

11
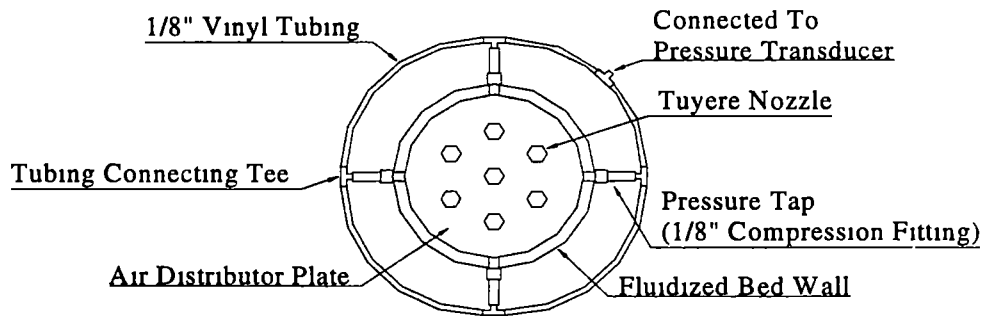
a. Cross sectional view of the lower portion of the bed showing pressure tap arrangement and interconnections.
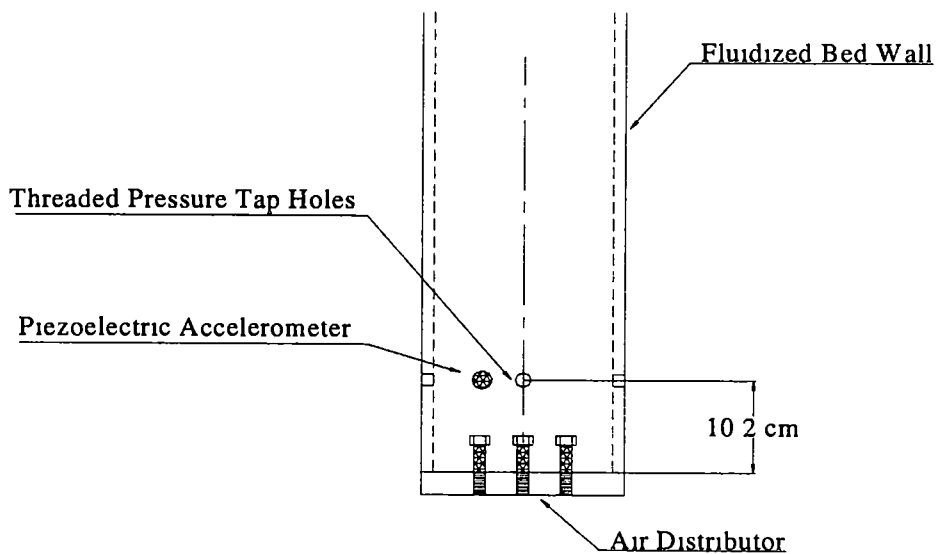
b. Front view of the lower portion of the bed showing pressure tap locations, piezoelectric accelerometer and air distributor.

Figure 4. Arrangement and location of pressure tabs and piezoelectric accelerometer.

piezoelectric accelerometer is mounted externally on the wall of the fluidized bed at the same elevation as the pressure taps. In this study, a piezoelectric accelerometer is used to monitor the dynamical behaviors of the bed for four different solid particles at different flow conditions.

In order to avoid static charge built-up in the fluidized bed, two equally-spaced 1 27 cm (0.5") wide copper strips are glued on the inside wall of the lower plexiglass section of the fluidized bed The copper strips and the air distributor are grounded to prevent the build-up of static charge

2.1.2   AIR DISTRIBUTOR PLATE

A tuyere-nozzle type air distributor is used to distribute fluidizing air uniformly across the cross section of the fluidized bed. A schematic of the air distributor plate is shown in Figure 4b The air distributor plate is constructed of an aluminum disk 15 9 cm in diameter and 1 27 cm in thickness. Six equally-spaced 0 95 cm diameter holes are drilled on the circumference of a 3.5 cm radius circle centered on the distributor plate, and one hole is drilled at the center of the air distributor plate. All the holes are then threaded to accommodate the tuyeres The tuyeres are fabricated from 3 81 cm long and 1 27 cm diameter brass tubes with threaded ends. Eight 6.3 mm diameter holes located at two different elevations are drilled 90° apart along the length of the center nozzle, whereas six 6.3 mm diameter holes located at two different elevations are drilled 90° apart for the other nozzles. The tops of the nozzles are capped in order to prevent solid particles from entering the plenum chamber Fine mesh screens are wrapped and wired

around the tube circumference to avoid solids from entering the air supply through the tubes. The tuyeres are then screwed into the threaded holes in the aluminum disk to serve as nozzles The six outer nozzles are screwed into the aluminum disk with the holes of nozzles facing away from the wall to prevent erosion on the fluidized bed wall

2.1.3 DATA ACQUISITION

A National Instrument Data Acquisition Board (DAQ) installed in a Pentium II desktop computer is used to record signals from the fluidized bed National Instrument LabVIEW™ 5.0 software is used in conjunction with the board to acquire the signals obtained from piezoelectric accelerometer and the rapid response differential-pressure transducer. The software interface is configured as shown in Figure 5 In this study a maximum sampling rate of 10,000 Hz is used for a duration of 60 seconds for each run A total of 600,000 data points are simultaneously recorded to two different channels at each operating condition. All data points from these two channels are then saved in ASCII format under specific filename into the hard disk of the PC for later analyses

2.1.4 DUAL ANALOG FILTERS

Two Wavetek Model 452 Dual analog filters are used to remove low and high-frequency artifacts from the sensor signals. The signal from the pressure transducer is band-pass filtered between 0 1 Hz and 50 Hz to remove unwanted D.C bias thereby increasing resolution of the dynamic signals and to reduce 60 Hz contamination from
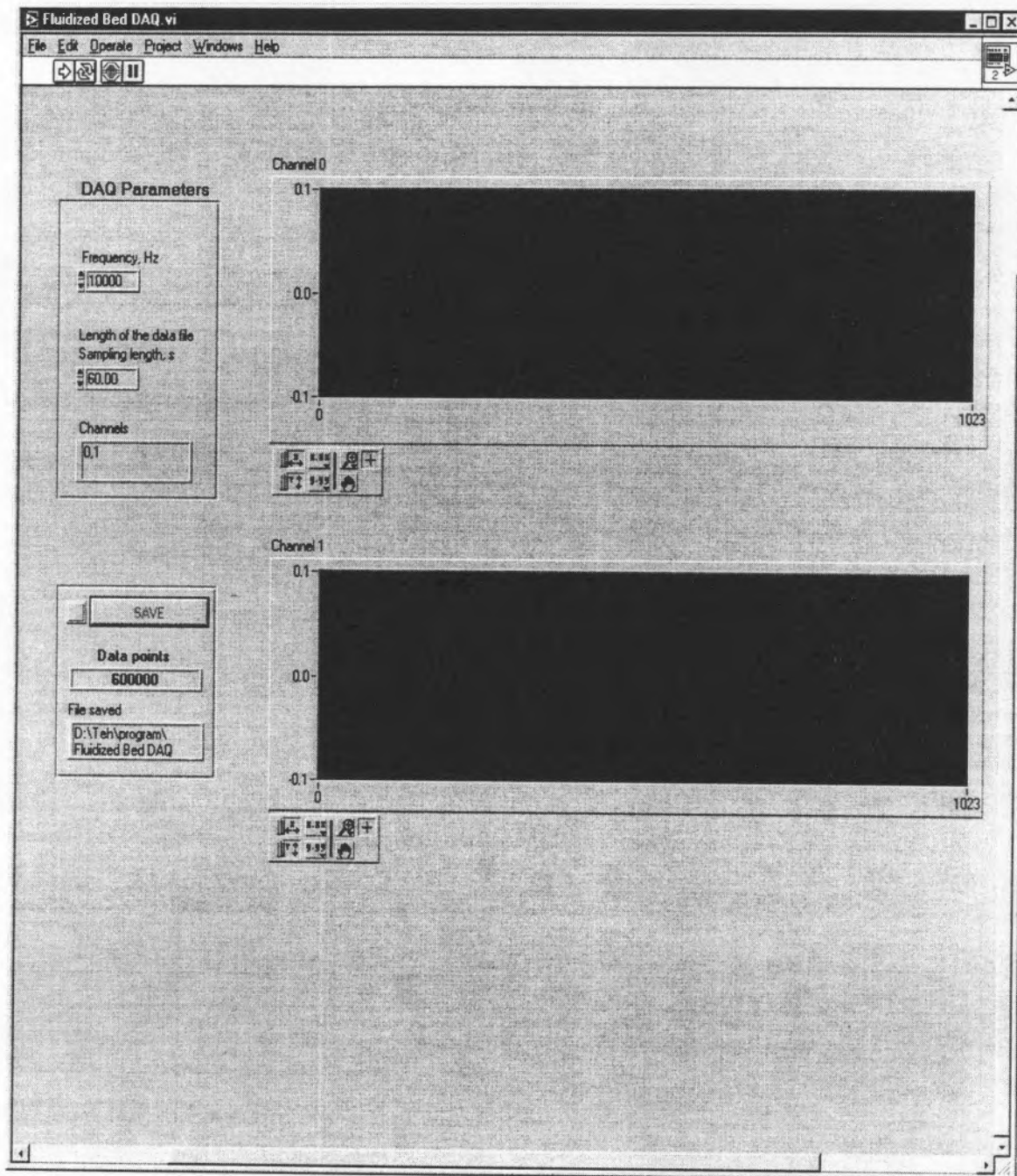
Figure 5. Configuration of dual channels virtual instrument acquisition window.

nearby the AC power system   The signal from the piezoelectric accelerometer is band-pass filtered between 500 Hz and 5000 Hz   Experience has shown that most extraneous room sounds and vibrations fall below 500 Hz   Likewise, extraneous noises such as the sound of airflow in the supply line and distributor nozzles are typically above 5 kHz   The accelerometer signal between these limits appears to correlate with the solids motion in the bed.

Each Wavetek Model 452 Dual analog filter consists of two identical channels in a common cabinet. Each channel has a separate input/output terminal which offers high and low pass filter functions.

2.1.5   DIFFERENTIAL-PRESSURE TRANSDUCERS

A Baratron Model 223 BD rapid response differential pressure transducer is used to measure the global pressure drop in the fluidized bed. The pressure transducer has a nominal input range of 50 inches of water column (12.5 kPa) and an output of between 0 to 5 VDC

The two major components of the Baratron transducer are the sensor and the signal conditioner   The sensor contains a tensioned metal diaphragm, one side of which is exposed to the gas whose pressure is to be measured   The other (reference) side is adjacent to an electrode assembly that is terminated in another like port. The diaphragm deflects with varying differential pressures, causing a capacitance change between the diaphragm and the adjacent electrode assembly   The signal conditioner consists of a fixed frequency oscillator, amplifier, demodulator, and calibration circuitry   The

capacitance change with pressure generates an AC voltage which is amplified, demodulated, and then converted into a DC output voltage linear with pressure

2.1.6 PIEZOELECTRIC ACCELEROMETER

A PCB Piezotronics, Integrated-Circuit-Piezoelectric (ICP) Accelerometer, Model 303A is used as the piezoelectric accelerometer for capturing the sound signals generated from the fluidized bed. The frequency response ranges from 10 Hz to 10,000 Hz with the amplitude deviation of –2.3 % to 5.0 %. With such a frequency response range the accelerometer is capable of capturing almost all the acoustic energy generated by the particles inside the bed. The accelerometer has a voltage sensitivity of 9.88 mV/g and a resonant frequency of 86.5 kHz. The calibration data and key specifications of the piezoelectric accelerometer are shown in Table 1 and Table 2, respectively

Table 1. Calibration data of the accelerometer

Voltage Sensitivity	9 88 mV/g
Transverse Sensitivity	2 2 %
Resonant Frequency	86 5 kHz
Discharge Time Constant	0 5 s
Output Bias Level	10 2 V

Table 2. Key specifications of the accelerometer.

Range	± 500 g
Resolution	0 01 g
Temperature Range	-100/+250 °F

$$g = 9\ 8\text{ms}^{-2}$$

2.1.7 PHYSICAL PROPERTIES OF THE FLUIDIZING BED PARTICLES

Four different particulate solids of Geldart's group B and D are selected for this study These solids are 35×100 mesh 316 stainless steel particles (35x100 SS), 4.5 mm spherical steel ball bearings (BB), 2.9 mm glass bead (Glass) and 18×50 mesh 316 stainless steel (18×50 SS). Of the four solid particles used in this study, only 35x100 mesh stainless steel is Geldart's group B and all other solid particles are Geldart's group D The steel BB's are uniform in size and shape, whereas the glass beads, 18×50 SS, and 35×100 SS are distributed between the upper and lower mesh sizes. The mean diameters of 18x50 SS and 35x100 SS are determined using weight fraction method [Kunni, D , Levenspiel, O., 1969].

The minimum fluidization velocity (U_{mf}) is found experimentally for each individual solid. The minimum fluidization velocity is defined as the minimum gas velocity at which the drag on an individual particle exceeds the force exerted by the gravity (Geldart, 1986) A wide range of fluidizing velocities is performed to determine the minimum fluidization velocities by using the time average pressure drop across the

10.2 cm (4 inch) fluidized bed with 23.5 cm static particle bed height Initially, the airflow is increased to turbulent fluidizing velocity such that the particles in the bed are observed to be well fluidized. Airflow is then reduced in small increments and the average pressure drop is recorded until the airflow is reduced to the point where no particle motions are observed in the bed. Minimum fluidization velocity is determined by plotting a semi-log of the time average pressure drop versus the gas velocity. For the relatively low flow rates, the pressure drop is approximately proportional to the gas velocity which is referred as fixed bed slope. With a further increase in flow rate, the particles in the bed tend to "unlock" themselves and a nearly constant (or slightly increasing) pressure drop is observed An intersection between extrapolations of these two distinctive regions is identified as the minimum fluidization velocity. Figure A 1, A 2, A.3 and A.4 in the appendix A illustrate the curves for determining minimum fluidization velocity for the four solids used in this study. All the physical properties and minimum fluidization are summarized in Table 3

Table 3. Physical properties of particles and minimum fluidization velocities

Description	35×100 316SS	18×50 316SS	Glass	Steel BB
Particle Density [gm/cc]	8 0	8 0	2 6	7 5
Mean Diameter [mm]	0 175	0 565	2 9	4 5
Geldart's Group	B	D	D	D
Minimum Fluidization Velocity [m/s]	0 10	0 67	1 47	3 60

2.2   TEST CONDITIONS

In the present study, all fluidized bed operation is carried out at room temperature and atmospheric pressure The fluidizing air is dried and compressed building air with a maximum air pressure of 100 psig The air pressure feeds to the bed distributor never exceeds 50 psig.

2.3   OVERVIEW OF EXPERIMENTAL PROCEDURES

In this study, the signals obtained from accelerometer and differential pressure measurements are used to characterize the dynamic behavior of a laboratory-scale fluidized bed.   Signals from the accelerometer and pressure sensors are acquired simultaneously so that their degree of correlation could be evaluated The initial static bed height is set at 23.5 cm above the distributor plate for all four solids

The pressure taps and accelerometer are located at the same elevation above the air distributor plate. The superficial airflow velocity (U) is obtained by dividing the volumetric flow rate from the rotameter corrected to standard temperature and pressure by the cross sectional area of the fluidized bed. The fluidizing gas velocity range (U/U_{mf}) is limited by the amount of particles entrained in the flow and carried out of the fluidized bed. Consequently, Geldart's group B particles (35x100 SS) has the largest fluidizing gas velocity range due to small bed expansion On the other hand, Geldart's group D solids such as 18x50 SS, glass, and steel BB have smaller fluidizing gas velocity ranges due to the large bed expansion which allows solid particles exiting from the fluidized bed at a

Table 4. Fluidizing gas velocity ranges for four solid particles.

Solid Particles	Fluidizing Gas Velocity Range [U/U$_{mf}$]
35x100 Mesh 316 SS	1 11 – 13 69
18x50 Mesh 316 SS	1 01 – 4 75
Glass	1 01 – 2 52
Steel BB	1 06 – 1 96

much lower flow rate. Pressure and sound signals are then generated for each material over a wide range of fluidizing gas velocity shown in Table 4

Initially, the airflow is increased to approximately minimum fluidization velocity such that small particle movements are visible in the bed. Airflow is increased to the point where the solid particles reach two-third of the bed height to prevent solid particles from exiting the fluidized bed. For each increment of airflow, the bed is allowed to run for approximately 2 minutes to reach steady state operating condition. Once the steady state is reached, filtered signals from the pressure transducer and accelerometer are recorded simultaneously by the National Instrument Data Acquisition Board (DAQ) and LabVIEW 5.0 at the sampling rate of 10,000 Hz for a period of 60 seconds Both signals are then stored in separate ASCII files The same procedures are repeated for each fluidizing solid over a wide range of fluidizing velocities.

CHAPTER 3

DATA-ANALYSIS TECHNIQUES

Both linear and nonlinear time-series analysis techniques are used to characterize the acoustic and pressure signals from the fluidized bed. Linear analysis methods include the Fourier power spectrum and cross-correlation function, whereas nonlinear time-series methods include correlation dimension and Kolmogorov entropy. This chapter reviews the theoretical background for the time-series analysis techniques and computational used in this study.

3.1   PRE-PROCESSING ACOUSTIC SIGNALS

A finite-length, moving-window, root-mean-square (RMS) filter is used to pre-process the raw acoustic time series. Acoustic signals contain two types of information from the fluidized bed. Particle-particle and particle-wall collisions produce audible vibrations in the kHz range. Dynamic fluidization phenomena such as bubbles and global solids circulation produce modulation of these audible sounds at frequencies typically below 20 Hz. A RMS filter is capable of recovering the low frequency modulation, which contains the information of interest. The moving-window size is selected by determining the size that produces the maximum cross-correlation between the filtered acoustic and the pressure signals.

The RMS of each record at temporal index i is calculated using a window of the previous records (p), the current record, and future records (a) and is expressed as

$$RMS(i) = \sqrt{\frac{\sum_{j=i-p}^{i+a} x_j^2}{p+a+1}}$$

where x is the acoustic time series. As a concrete numerical example, Table 5 shows an indexed series, its values and the RMS results for $p = a = 2$.

Table 5. Sample calculation for RMS of a given indexed series.

Index	1	2	3	4	5	6	7	8	9	10
Value	4	3	2	6	4	3	1	3	5	6
RMS			4 02	3 85	3 63	3 44	3 46	4 00		

For $i = 3$, the RMS is calculated according to

$$RMS(3) = \sqrt{\frac{(4 \cdot 4 + 3 \cdot 3 + 2 \cdot 2 + 6 \cdot 6 + 4 \cdot 4)}{2+2+1}} = 4\ 02$$

The computer routine is written such that RMS values are not calculated for the first p and last a records, and only the filtered time-series values are used for further analysis. The term "filtered time series" refers to the bandpass-filtered pressure signals and the RMS-filtered acoustic signals. For subsequent analysis, the filtered acoustic signals are down-sampled at 100 samples/s to match the pressure signals

3.2   FOURIER POWER SPECTRUM

A Fast Fourier Transform power spectral density (PSD) estimate is used to determine the frequency content of the filtered time series This is a common technique to characterize the time scales and their relative strength or power present in the signal The amplitude of each Fourier frequency is squared to determine the power Each data set is divided into an input block of 2^n records, where n is typically 10 to 12 Five consecutive, nonoverlapping blocks are averaged to generate the overall PSD composite These blocks are conditioned using a modified Hanning window function. Power spectra from acoustic and pressure signals can be compared, and they should exhibit similar dominant frequencies if the same phenomena are measured.

At minimum fluidization velocity, the movements of the particles are localized and highly complex producing a broad PSD for both the pressure and acoustic signals As the flow velocity increases to slugging conditions, a single dominant frequency can be easily revealed. With further increase in flow rate, wider power spectra are observed for both acoustic and pressure signals due to the violent mixing of particles in the bed

3.3   CROSS-CORRELATION FUNCTION

The cross-correlation function is used to evaluate correlation between two simultaneously measured time series.   Cross-correlation measures the amount of statistical covariance between the test signal (i.e. RMS filtered acoustic) and reference signal (i.e. pressure). This technique is used in this study to determine the degree of

correlation between the filtered acoustic and pressure signals Cross-correlation r_{xy} (τ) is defined by

$$r_{xy}(\tau) = \frac{\langle x(i)y(i+\tau) \rangle}{\sigma_x \sigma_y}$$

where τ is the lag time, σ is the correlation length and $<\cdot>$ is the expected value [Burgess, J.C., 1998; Pope, J., 1998].

When the fluidizing air velocity is below or close to the minimum fluidization velocity, both the acoustic and pressure signals are very complex due to the local movement of individual particles in the bed. Consequently, the correlation between the two signals is fairly low In slugging conditions, it is expected that the cross-correlation between the acoustic and pressure signals will be close to 1. For flows above slugging, cross-correlation drops again as the particle motion becomes more complicated

3.4   CORRELATION DIMENSION

Correlation dimension is an estimation of signal complexity. This technique is used to estimate the minimum dynamical degrees of freedom of a reconstructed attractor in phase space. An attractor can either be constructed directly from the dynamical variables or by using time-series embedding of a single variable [Packard, N H , Crutchfield, J.P , Farmer, J D., and Shaw, R.S., 1980, Takens, F., 1981] These attractors are categorized by a correlation exponent D that is defined on a basis of a time-series $\{X_i\}$ of N records and the correlation integral defined as

25

$$C_l = \frac{1}{N(N-1)} \sum_{i \neq j} H(l - \|X_i - X_j\|)$$

where H is the Heaviside function[1], X_i and X_j are the embedded vectors, $\|X_i - X_j\|$ is the Euclidean norm between embedded trajectory points i and j, l is a tolerance or cutoff length, and N is the number of trajectory points used to calculate C_l [Grassberger, P and Procaccia, I.., 1983a]. Generally speaking, the correlation integral is the probability of two points on the attractor within the region designated by the distance l. As $l \rightarrow 0$ and $N \rightarrow \infty$, the correlation integral C_l scales to a power law as

$$C_l = l^D$$

where l is a small distance and D is the correlation dimension defined as

$$D = \lim_{l \to 0} \frac{\ln[C_l]}{\ln[l]}$$

This technique is limited in analysis of experimental data, because the values of correlation integral will tend to be inaccurate at very small values of l due to the very few qualifying pairs and noise of the experimental systems.

The present studies use an estimation procedure based on a maximum-likelihood method [Schouten, J.C , Takens F. and Van den Bleek, C.M, 1994] In this method, the interpoint distances between the M randomly chosen pairs of embedded points $(X_i - X_j)$ are generated. In this case, the maximum norm is used for calculating interpoint distances Distances are normalized with respect to a chosen cutoff length, denoted l_o Therefore, a new set of distances r_i, where $0 \leq r_i \leq 1$ and the correlation integral $C(r)$

---

[1] The Heaviside Function is H(a) = 1 if a ≥ 0 and H(a) = 0 if a < 0

represents a normalized cumulative probability distribution

$$C(r) = r^D$$

According to Fisher's maximum-likelihood rule, the probability P_M for seeking a sampled

pairs in $\{(r_1, r_1+dr_1), (r_2, r_2+dr_2), (r_3+dr_3), \ldots, (r_M, r_M+dr_M)\}$ dependent on D is given by

$$P_M = \prod_{i=1}^{M} D \cdot r_i^{D-1} \ dr_i$$

When P_M is maximum, the value of D is defined as follows

$$D_{ML} = -[\ln(r_i)]^{-1}$$

Generally speaking, the value of the correlation dimension D_{ML} is equal to the inverse of

the average value of $[-\ln(r_i)]$, with a given sample $(r_1, r_2, \ldots, r_M)$ as $i = (1, 2, 3, \ldots, M)$

where M is the number of sampled pairs [Schouten, J C., Takens F and Van den Bleek,

C.M, 1994; Vasudesevan, M.,1995].

The Schouten et al. procedure recommends a particular embedding lag of a

sample time step and an embedding time window of an average cycle time about the

mean The average absolute deviation about the mean is used as the cut-off length A

standard 30 replicate random sampling is set to determine 30 estimates of the D_{ML}

Therefore, the final D_{ML} estimate is calculated by averaging 30 independent estimates and

the uncertainty is estimated as two times the standard deviation of the D_{ML} replicate

estimates

For this study, correlation dimension is determined at various flow velocities for

the pressure and filtered acoustic signals It is expected that the plots should exhibit the

same trend if both pressure and piezoelectric acoustic signals measure the same

phenomenon. When the bed is in steady slugging condition, the movement of the bed

becomes periodic, and the correlation number of the signal is very low as compared to when the bed is in a turbulent regime. Significant amount of information about transition in the fluidization regime can be observed from the trends over a wide range of fluidizing velocity.

3.5 KOLMOGOROV ENTROPY

Kolmogorov entropy measures the rate of information loss or a measure for the degree of predictability of points along the signal by giving an initial point A form of the maximum-likelihood estimator of Kolmogorov entropy (K_{ML}) is based on the calculation of the average time for initial trajectory segments to diverge beyond a specified tolerance [Schouten, J.C., Takens F., Van den Bleek, C M, 1994 and Grassberger, P. and Procaccia, I., 1983c]. K_{ML} has been to be a proven reliable standard measure of fluidized bed pressure signals [Schouten, J C., Stappen, M L.M vander, Van den Bleek, C.M., 1996; Stappen, M.L.M. vander, 1997].

Entropy values are calculated by tracking initially neighboring orbits of an attractor over a period of time. The rate of divergence of these orbits is expected to be exponential for nonlinear system. A pair of close orbits can be evaluated when the points on the orbits are within a set length of time (average cycle time) as well as within a maximum cut-off distance (average absolute deviation). A function of qualifying pairs of orbits $F(t)$ can be calculated by tracking the randomly selected orbits pairs that are not diverged exit the cut-off distance over a period of time. According to Schouten et al , the undiverged trajectory pairs from the initial sample population decays according to the

relation

$$F(t) = e^{-kt}$$

where k is decay constant and t is the time-step size. A maximum-likelihood estimate of Kolmogorov entropy is calculated by

$$K_{ML} = -\log_2 F(t)$$

where the unit of K_{ML} is in *bits*.

Thirty random sample replicates are typically used to calculate the average entropy value and its uncertainty. Kolmogorov entropy is zero when the signal is periodic or cyclic, whereas the infinite entropy indicates that the signal is random. A nonlinear system is considered to have finite entropy values.

The values of entropy are calculated and plotted at various flow velocities for the pressure transducer and piezoelectric accelerometer. The plots generated from the acoustic and pressure signals should exhibit the same trend for different solids at various flow velocities if they measure the same phenomena. At the minimum fluidization velocity, the entropy values for both piezoelectric accelerometer and pressure transducer are very large due to the local movement of particles that has a very low degree of predictability. When the bed is in steady slugging condition, the movement of the bed becomes periodic and the entropy of the signal is very low due to the very high degree of predictability for periodic condition. As the bed becomes turbulent at very high flow rate, the entropy number increases due to the random and complicated behaviors in the bed. The entropy curves obtained from the pressure and acoustic signals provide information about transition in fluidization regime. If the same amount of information is

obtained from the acoustic signal, it is expected that the acoustic signal will exhibit the

same (or similar) entropy curve to those obtained from pressure signal

CHAPTER 4

EXPERIMENTAL RESULTS AND DISCUSSIONS

This chapter discusses experimental results obtained for four different solids (35x100 mesh stainless steel, 18x50 mesh stainless steel, glass beads, and spherical steel ball bearings) over a range of fluidizing velocities. Selection of representative results of each solid are presented since it would not be practical to present the entire collection of data. Section 4 1 explains the preprocessing of acoustic signals with RMS filter Fourier power spectrum results are described in Section 4.2 Section 4.3 addresses the cross-correlation function between acoustic and pressure signals. Correlation dimension and Kolmogorov entropy are presented in Sections 4.4 and 4.5, respectively

Linear and nonlinear analysis results are used to compare signals from a piezoelectric accelerometer and a pressure transducer. Complete experimental results for all conditions investigated in the present study are presented in the Appendices

4.1 FILTERING ACOUSTIC SIGNAL WITH A MOVING-WINDOW RMS

A root-mean-square (RMS) filter is used to preprocess the acoustic signals obtained from the fluidized bed for each fluidizing solid over the range of flow velocities Acoustic signals obtained from the fluidized bed are originally sampled at a frequency of 10,000 samples per second for a duration of 60 seconds, giving a total of 600,000 data points per run. The low-frequency amplitude modulation of the acoustic signals are

observed to reflect the dynamic behaviors of the fluidized bed such as bubbling, slugging, breaking slugs, and near turbulent.

The RMS filter window size is determined such that the cross-correlation between the filtered acoustic and pressure signals is maximum over a range of fluidizing conditions. Note that the dominant frequencies for 35x100 mesh stainless steel, 18x50 mesh stainless steel, glass, and BB are between 0 and 6 Hz [Skrzycke, D.P., Nguyen, K., Daw, C.S., 1993; Vasudevan, M., 1995]. Typically, the results of this study indicate that a window size of 1250 points, corresponding to a low-pass cutoff of 8 Hz, gives the best correlation between the filtered acoustic and pressure signals.

Figure 6 shows the pressure and RMS filtering the raw acoustic signals for 18x50 mesh stainless steel at a slugging condition ($U/U_{mf} = 1.19$) All time series are scaled to standard units (zero mean and unit variance) for comparative purposes Figure 6a displays raw pressure and acoustic signals. From this figure, it is apparent that the raw acoustic signals are very complex and noisy looking However, there does appear to be some type of correspondence between the two time series. Figure 6b illustrates the process of RMS filtering using a window size of 1250 data points (RMS-1250) to extract useful information from raw acoustic signals. Note that the RMS-1250 acoustic signal is down-sampled to match the sampling rate of the pressure signal (100 samples/s) The low-frequency modulation of the raw acoustic signal is reflected in the peaks and troughs of the filtered signal Figure 6c shows the final time-series plot between pressure and RMS-1250 acoustic signals. It is apparent that there is a phase difference between these two measurements. The phase difference is a result of bubbles traversing pass the pressure taps and piezoelectric accelerometer. Negative pressure-drop deviations are

32
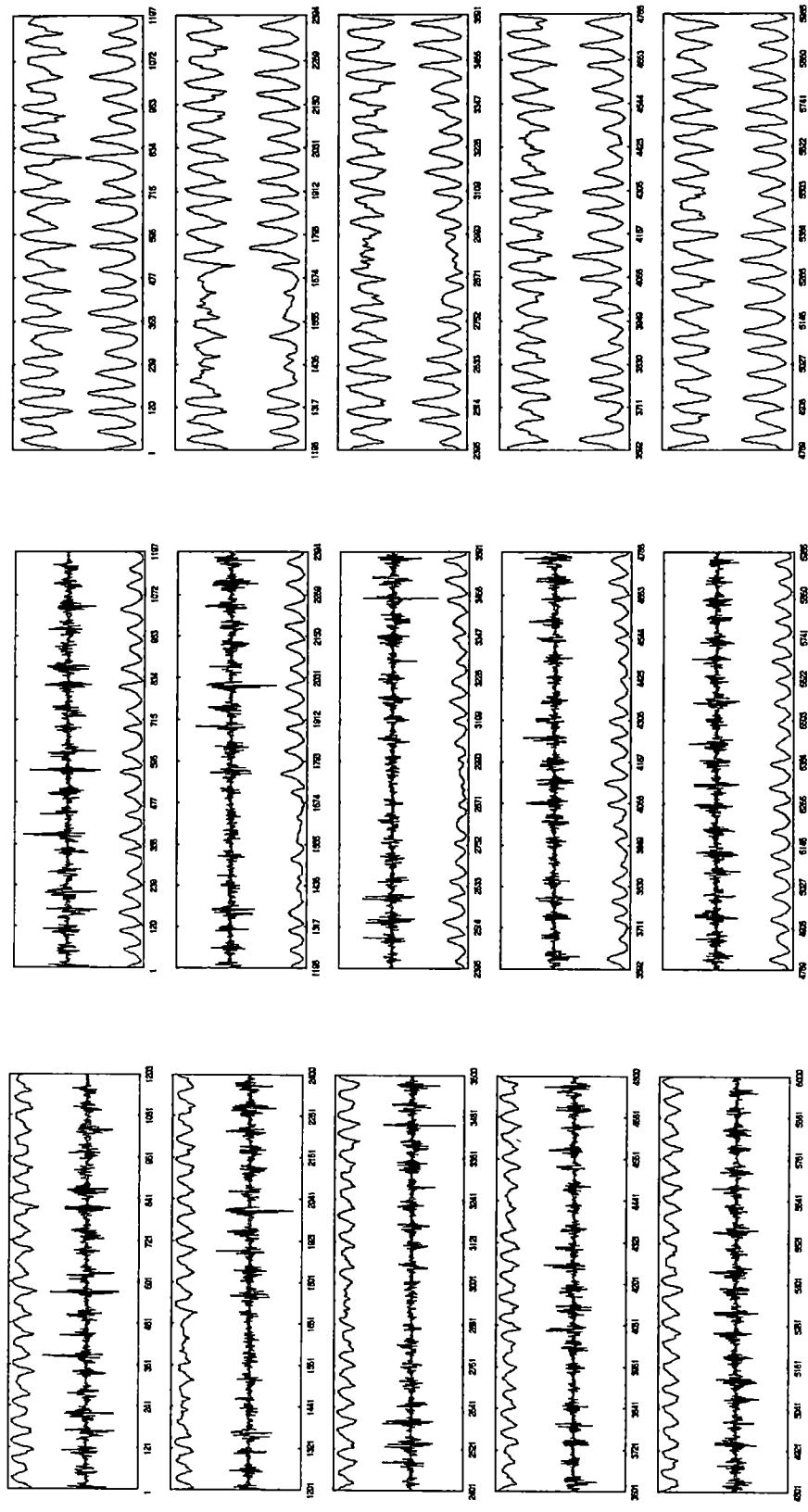
(a) Pressure (Upper Trace) and Raw Acoustic (Lower Trace)

(b) Raw Acoustic (Upper Trace) and RMS-1250 Acoustic (Lower Trace)

(c) Pressure (Upper Trace) and RMS-1250 Acoustic (Lower Trace)

Figure 6. RMS preprocessing of the acoustic signal with simultaneous pressure signal for 18x50 mesh stainless steel at U/U$_{mf}$ of 1.19.

due to a decrease in pressure as the bubbles traverse pass the pressure taps, whereas positive acoustic deviations correspond to an increase in vibrations as the result of the passage of the bubbles. On the other hand, positive pressure deviations occur when solid particles move pass the pressure taps following the passage of bubbles which results in an increase in pressure, whereas negative acoustic deviations are due to a decrease in vibrations after the passage of bubbles. Thus, this phase difference is an actual event and not an artifact of the low-pass or RMS-1250 filtering Figure 7 displays time series of the pressure, raw acoustic and RMF-filtered acoustic signals for glass particles (group D) at three different fluidizing velocities of U/U_{mf} of 1.11, 1.16, and 1.81 At U/U_{mf} of 1.01 and 1.16, the fluidization states are fairly similar and periodic, whereas at $U/U mf$ of 1.81 it is rather complicated Figure 8 presents the time series for 18x50 mesh stainless steel particles at U/U_{mf} of 1 07, 1.54, and 3.44. At U/U_{mf} of 1.07, the bed is slugging, and the pressure and acoustic signals are very similar and fairly regular. Breaking of slugs is observed at U/U_{mf} of 1.54 where the signals start to fluctuate irregularly For U/U_{mf} of 3.44, turbulent behavior of violent mixing of bubbles and slugs is observed in the bed Both signals reflect this increased complexity Figure 9 illustrates time-series segments of 35x100 mesh stainless steel particles at U/U_{mf} of 1 11, 2.54, and 13.18 Occasionally bubbling is observed near the minimum fluidization velocity at U/U_{mf} of 1 11 At U/U_{mf} of 2.54, the bed starts to enter slugging condition where the pressure and acoustic signals appear to be periodic but vary in amplitude, reflecting variation of bubble sizes Near turbulent velocity at U/U_{mf} of 13.18, the time series for pressure and acoustic signals show mixing of bubbles and slugs in the bed Figure 10 shows time-series of BB particles at U/U_{mf} of 1.17, 1.49, and 1.86. The fluidization regimes for U/U_{mf} of

34
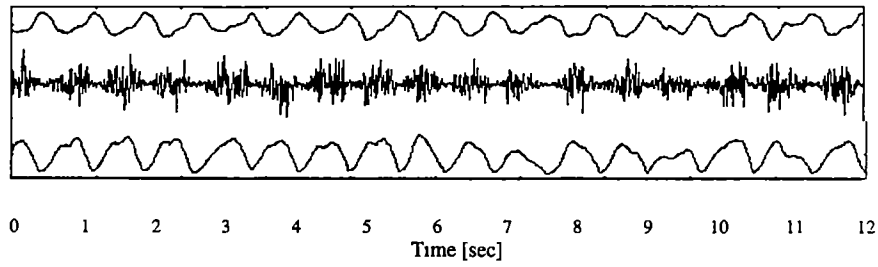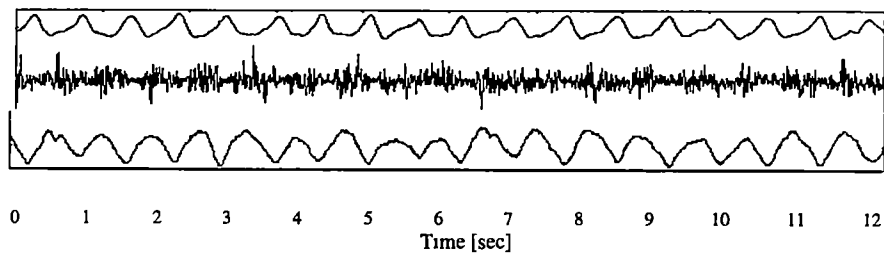
(a) $U/U_{mf} = 1.11$

(b) $U/U_{mf} = 1.16$
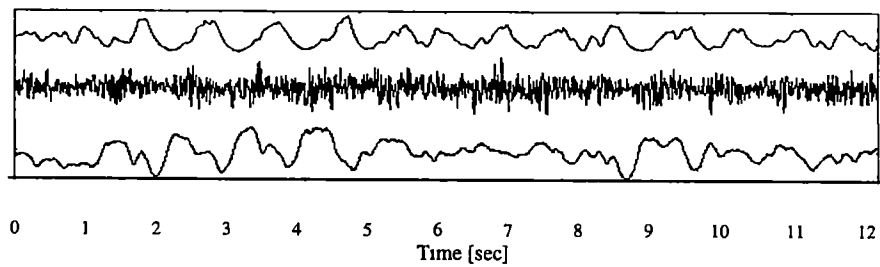
(c) $U/U_{mf} = 1.81$

Pressure (Upper trace)	Acoustic (Middle Trace)	RMS-1250 Acoustic (Lower Trace)

Figure 7. Representative time series of the pressure, acoustic and RMS-filtered acoustic signals for glass particles at U/U_{mf} of 1.11, 1.16, and 1.81

35
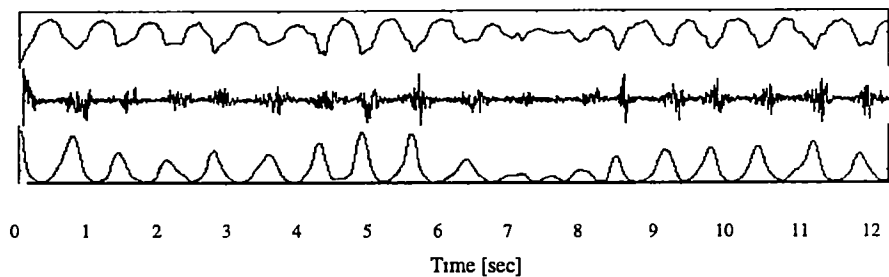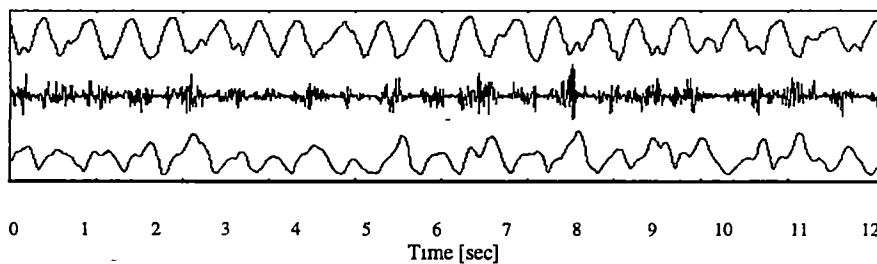
(a) $U/U_{mf} = 1.07$

(b) $U/U_{mf} = 1.54$
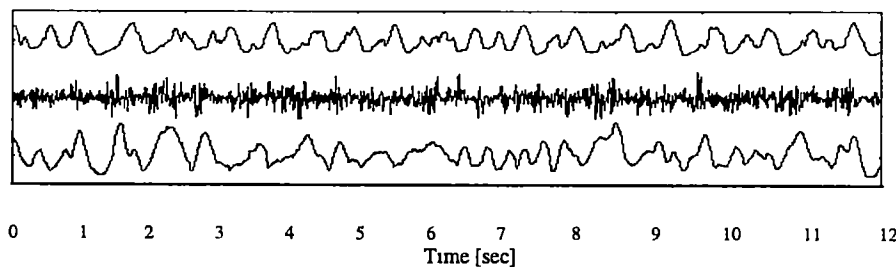
(c) $U/U_{mf} = 3.44$

| Pressure (Upper trace) | Acoustic (Middle Trace) | RMS-1250 Acoustic (Lower Trace) |

Figure 8. Representative time series of the pressure, acoustic and RMS-filtered acoustic signals for 18x50 mesh Stainless steel at U/U_{mf} of 1.07, 1.54, and 3.44.

0   1   2   3   4   5   6   7   8   9   10   11   12
Time [sec]

(a) U/U$_{mf}$ = 1.11

0   1   2   3   4   5   6   7   8   9   10   11   12
Time [sec]

(b) U/U$_{mf}$ = 2.54

0   1   2   3   4   5   6   7   8   9   10   11   12
Time [sec]
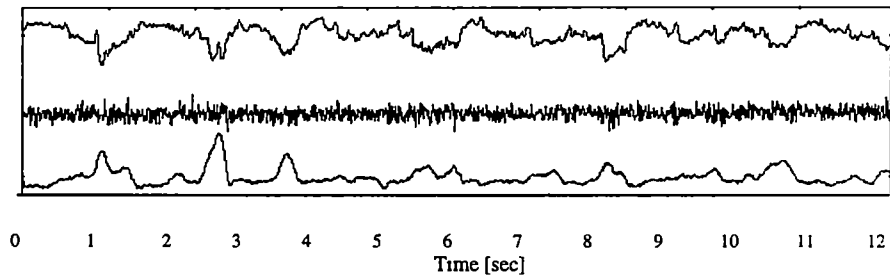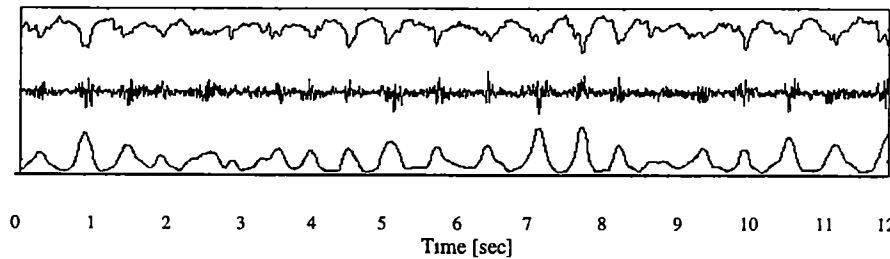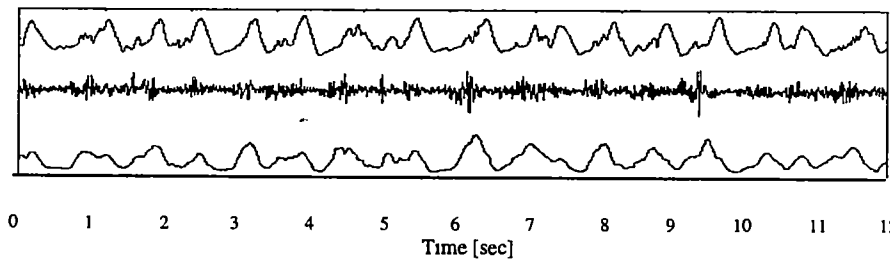
(c) U/U$_{mf}$ = 13.18

| Pressure (Upper trace) | Acoustic (Middle Trace) | RMS-1250 Acoustic (Lower Trace) |

Figure 9. Representative time series of the pressure, acoustic and RMS-filtered acoustic signals for 35x100 mesh Stainless steel at U/U$_{mf}$ of 1.11, 2.54, and 13.18.
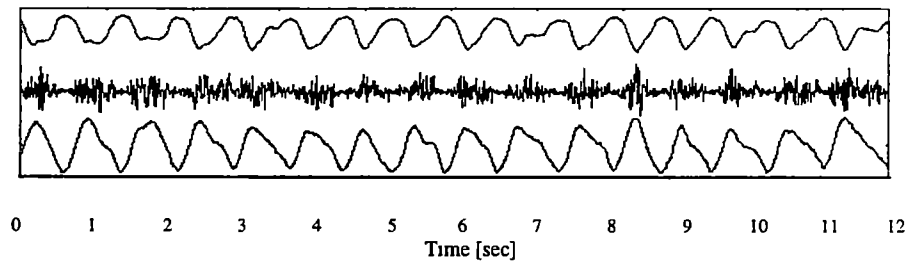
(a) U/U$_{mf}$ = 1.17
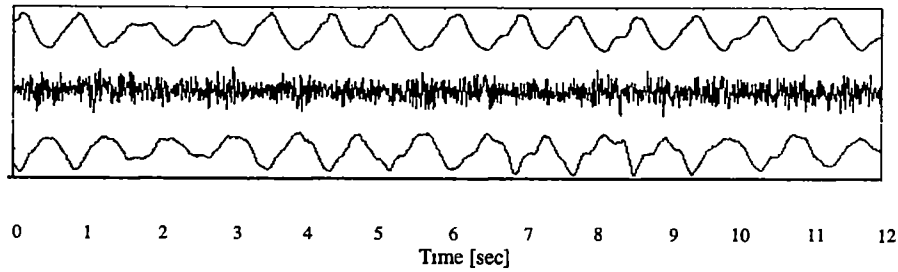
(b) U/U$_{mf}$ = 1.49
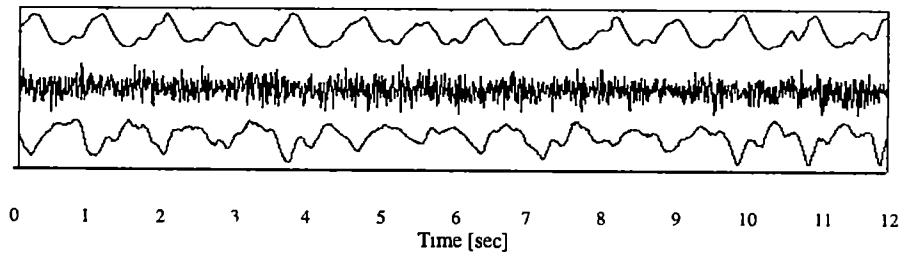
(c) U/U$_{mf}$ = 1.86

| Pressure (Upper trace) | Acoustic (Middle Trace) | RMS-1250 Acoustic (Lower Trace) |

Figure 10. Representative time series of the pressure, acoustic and RMS-filtered acoustic signals for BB particles at U/U$_{mf}$ of 1.17, 1.49, and 1.86.

1 17 and 1.49 are similar and periodic due to the stable slugging in the fluidized bed When the bed approaches turbulent velocity at U/U_{mf} of 1.86, the time series becomes less regular and is rather different than the other two fluidization states Hereafter, unless otherwise specified, the term "filtered acoustic signal" refers to the RMS-filtered acoustic signal.

4.2   FOURIER POWER SPECTRUM

Power spectral density (PSD) plots for the pressure and RMS-filtered acoustic signals for four different fluidizing materials are shown in Figures 11 – 14 Five consecutive, nonoverlapping blocks with 1024 data points are averaged to generate an overall PSD composite for each fluidizing velocity. Representative power spectra are selected to distinguish four fluidization conditions (i.e., near minimum fluidization, developing slugs, slugging, and breaking slugs) for each fluidizing material. Complete PSD results for each fluidizing solid are shown in Appendix B. The overall PSD composite trends for pressure and RMS filtered acoustic signals are compared and discussed to determine the amount of information shared by both signals In this section, only the power spectra for the 35x100 mesh stainless steel particles are presented because similar results are observed for the other fluidizing solids.

The dominant frequencies of power spectra are within the range of 0 – 6 Hz for all fluidizing solids. Typically, dominant power peaks are in the range of 0 – 2 Hz at which large time-scale fluctuations such as slugging and large bubbling are observed in the bed Power peaks in 2 – 6 Hz region indicate small time-scale fluctuations, including particle

39
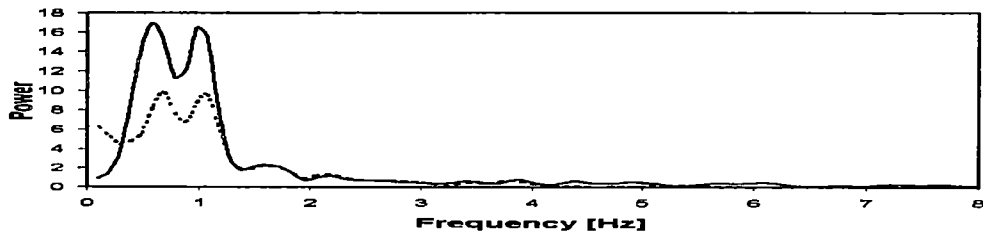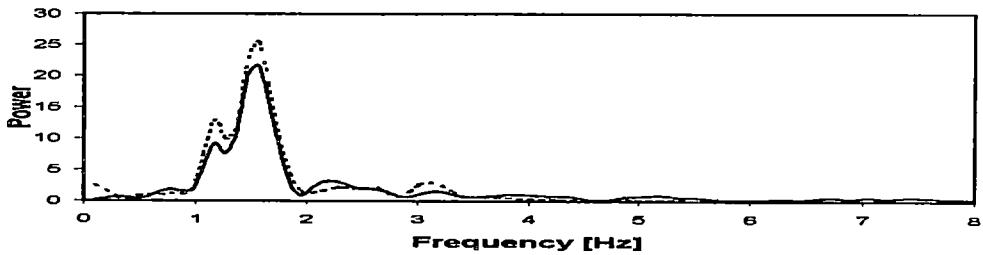
(a) $U/U_{mf} = 1.11$

(b) $U/U_{mf} = 1.42$

(c) $U/U_{mf} = 2.03$

(d) $U/U_{mf} = 7.61$

----- RMS filtered acoustic signal   —— Pressure signal
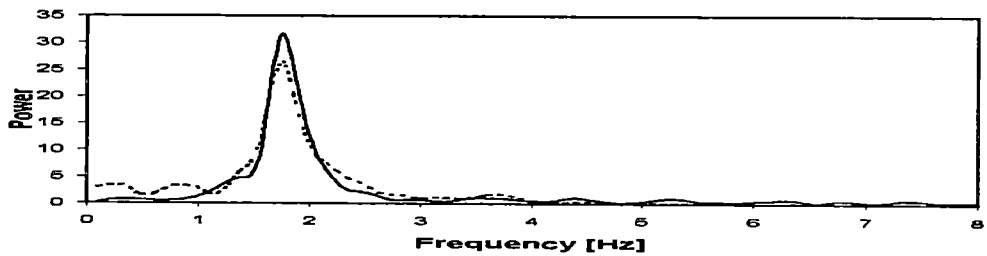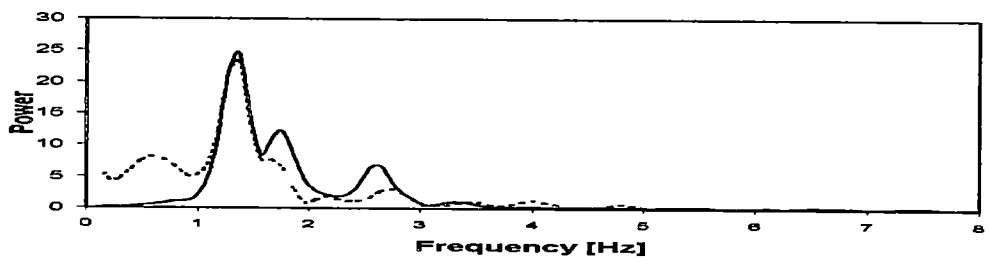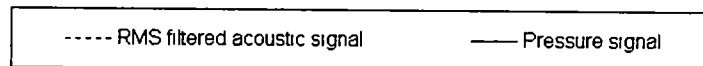
Figure 11. Fourier power spectra of pressure and RMS-filtered acoustic signals for 35x100 mesh stainless steel at four different fluidization states.
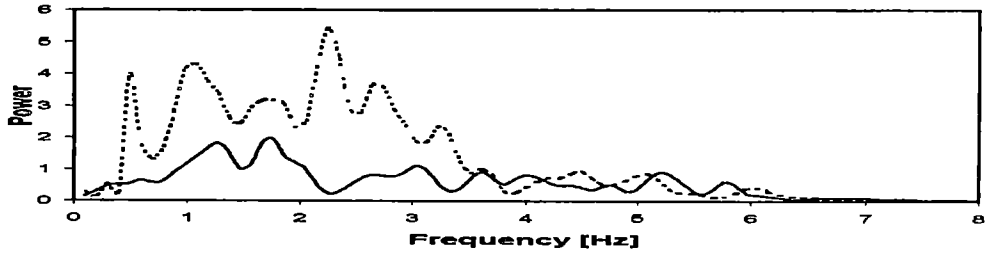
(a) $U/U_{mf} = 1.01$
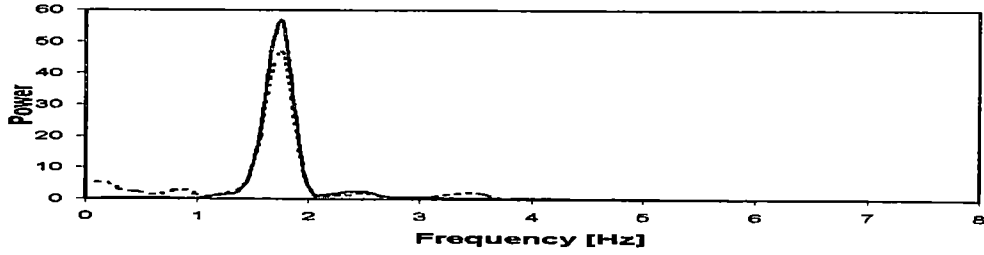
(b) $U/U_{mf} = 1.19$

(c) $U/U_{mf} = 1.31$

(d) $U/U_{mf} = 3.56$

- - - - - RMS filtered acoustic signal ——— Pressure signal
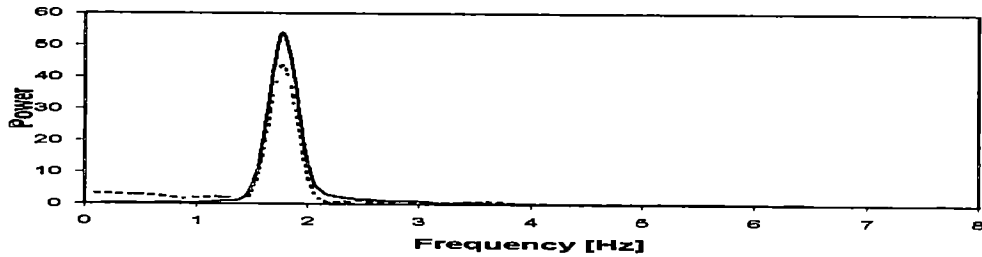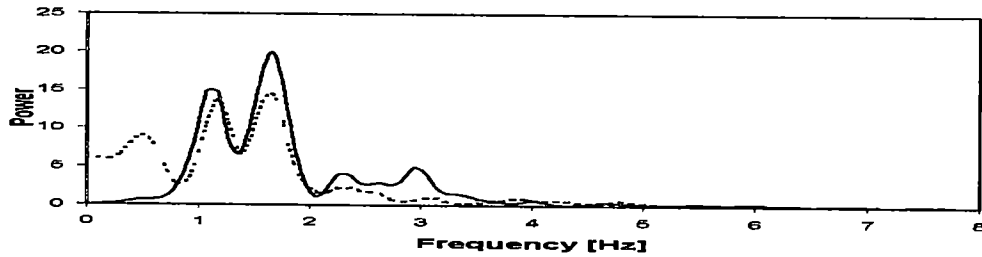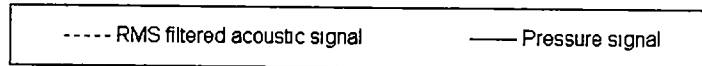
Figure 12. Fourier power spectra of pressure and RMS-filtered acoustic signals for

18x50 mesh stainless steel at four different fluidization states.

41
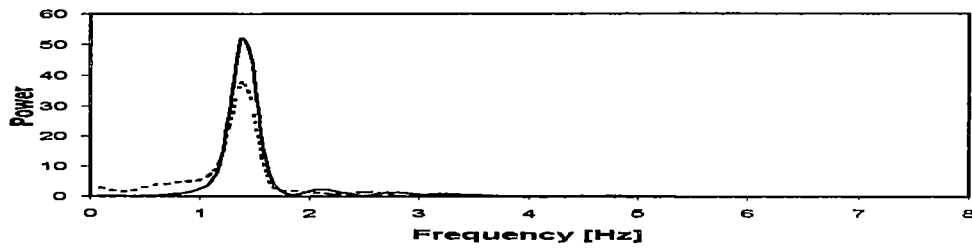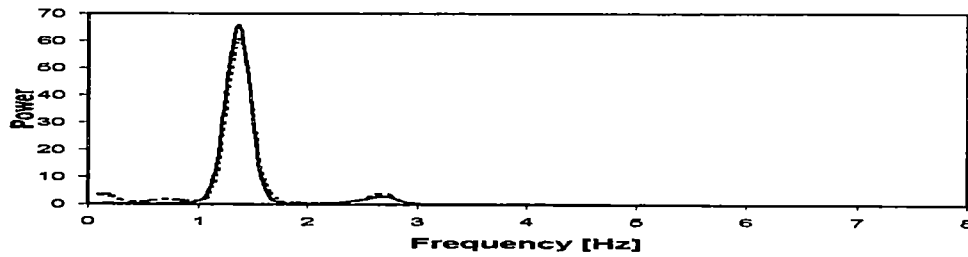
(a) U/U$_{mf}$ = 1.01

(b) U/U$_{mf}$ = 1.05

(c) U/U$_{mf}$ = 1.11

(d) U/U$_{mf}$ = 2.41

----- RMS filtered acoustic signal   —— Pressure signal
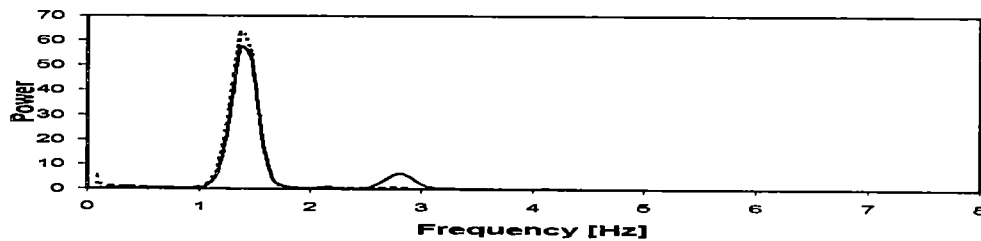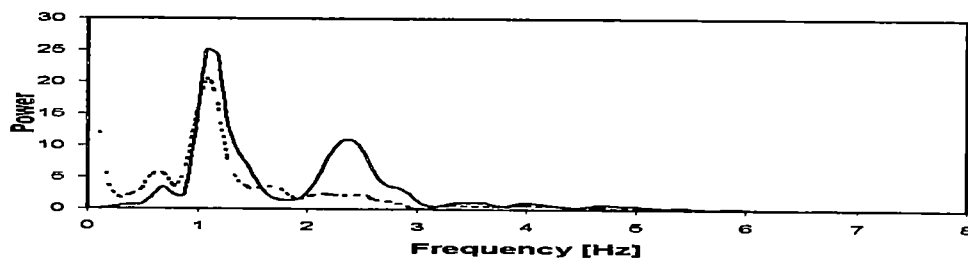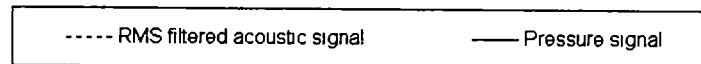
Figure 13. Fourier power spectra of pressure and RMS-filtered acoustic signals for glass particles at four different fluidization states.
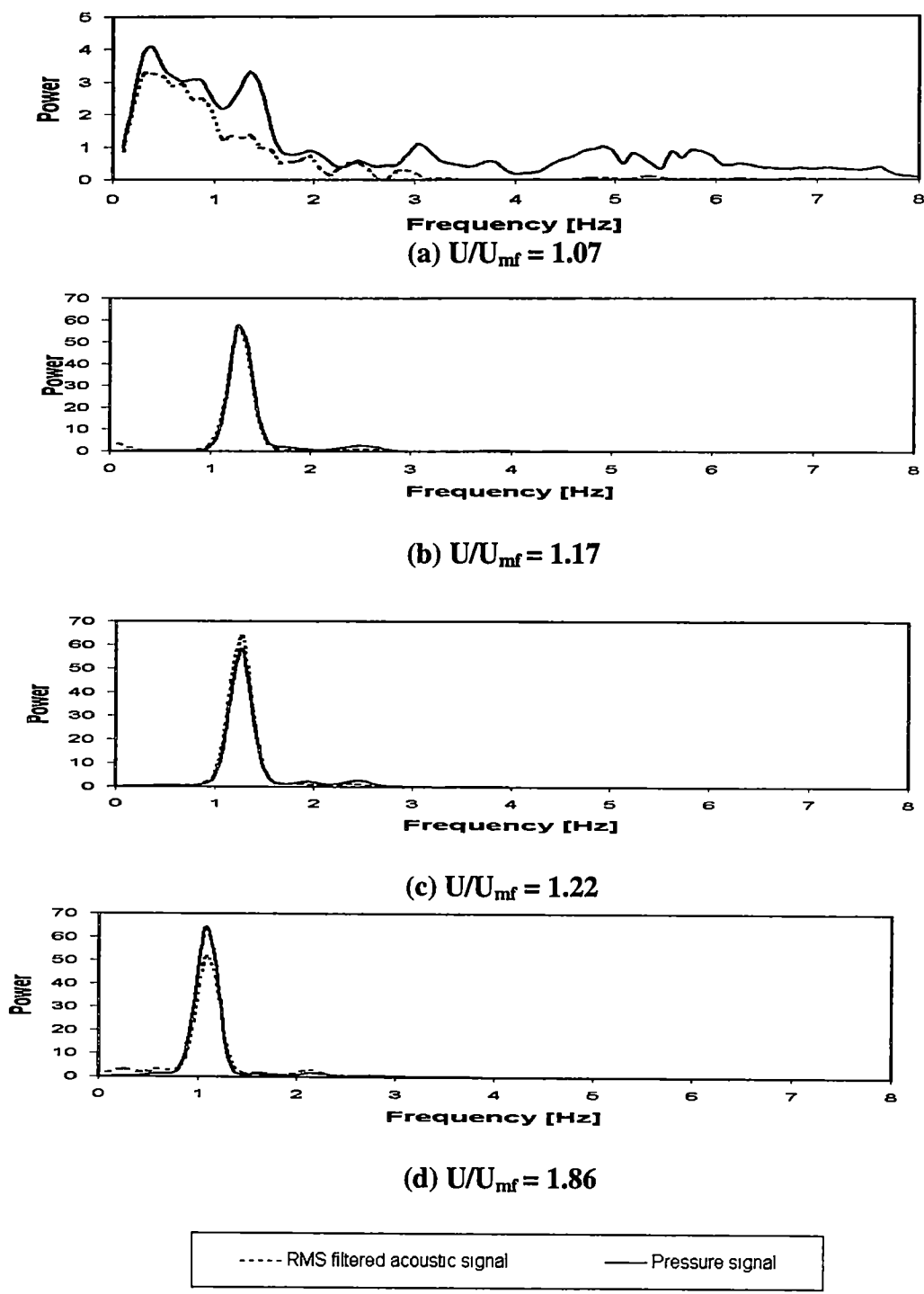
Figure 14. Fourier power spectra of pressure and RMS-filtered acoustic signals for BB particles at four different fluidization states.

fluttering or vibrating and small bubbling in the bed [Vasudevan, M., 1995, Skrzycke, D., 1993].

Figure 11 displays the power spectra for 35x100 stainless steel particles at U/Umf of 1.11, 1.42, 2.03, and 7.61. Near minimum fluidization (U/Umf = 1.11), the power spectra for the pressure and acoustic signals are similar and widely distributed among different frequencies. Two major peaks are observed at 0.6 and 1 2 Hz for both signals This phenomenon is due to the complexity of individual particle movements, irregular bubbling and occasionally slugging in the bed As flow is increased to the onset of slugging condition at U/U$_{mf}$ of 1.42, the power spectra for pressure and acoustic signals are observed to be less complicated with a narrower frequency band. Stronger dominant power spectra for both time series are noted in the 1 − 2 Hz region reflecting large time-scale oscillations in the bed. With further increase in flow rate to a regular slugging condition, a single dominant frequency can be easily revealed at 1 8 Hz in the pressure and acoustic signals. As fluidization velocity increases beyond the slugging regime, the frequency band becomes wider due to the complexity of violent mixing of bubbles and slugs in the near turbulent regime. At this flow rate, the acoustic and pressure signals share similar major peaks in the 1 − 3 Hz region However, some relatively weak frequency content is observed in the 0 − 1 Hz region in the acoustic signal, which indicates vibrations of the collapsing solids in the bed This phenomenon is more predominant in denser particles such as 18x50 and 35x100 mesh stainless steel at high velocities

In general, power spectra for the acoustic and pressure signals are observed to show similar features over all fluidization states Different patterns of frequencies are

observed in the power spectra reflecting the transition of fluidization regimes Broadband power peaks indicate the behavior of the bed near minimum fluidization velocity, whereas sharp power peaks are seen in slugging bed. Figure 12 shows the power spectra of 18x50 mesh stainless at different fluidizing velocities which are similar to those of 35x100 mesh stainless steel However, the power spectra of 18x50 mesh stainless steel in Figure 12a in the neighborhood of minimum fluidization velocity are very complex due to the occasional bed expansion. Power spectra again become broad-banded with further increase in the flow rates beyond the slugging regime These transitions of power spectra describe the behavior of the bed from complex to nearly regular and then back to more complex oscillations.

4.3 CROSS-CORRELATION FUNCTION

Cross-correlation is used to evaluate the degree of correlation between the acoustic and pressure signals. Figures 15 – 18 show cross-correlation for each fluidizing solid at four distinct fluidization regimes: near minimum fluidization, developing slugs, slugging, and breaking slugs Since there are similar features among these figures, only the cross-correlation for 35x100 mesh stainless steel is discussed in detail, allowing similar interpretations to be made for other fluidizing solids. Note that the cross-correlation is calculated using pressure signal (reference) and RMS-filtered acoustic signal (test) The maximum correlation value is negative due to the anti-correlation or phase difference between the pressure and acoustic signals. Strong correlation implies higher correlation values and compact correlation observed in the figure, whereas weak
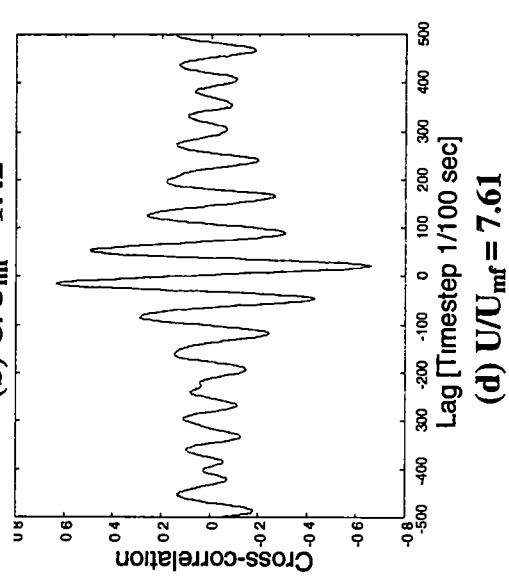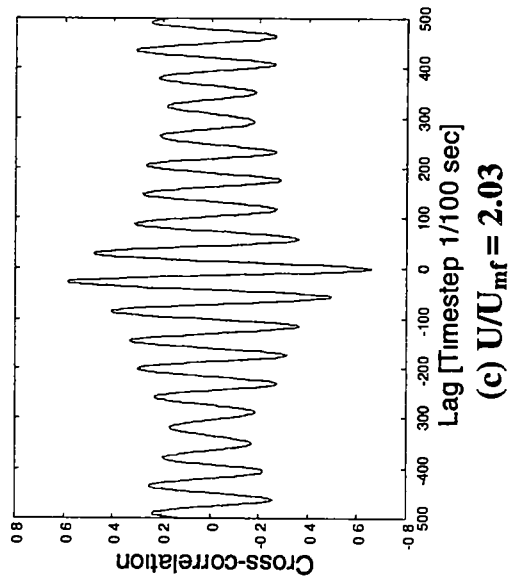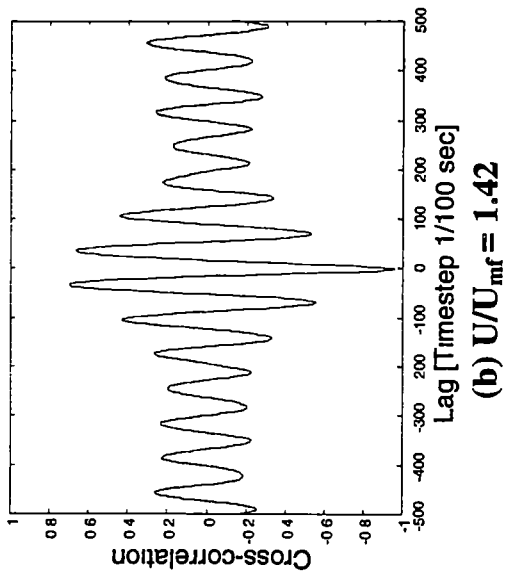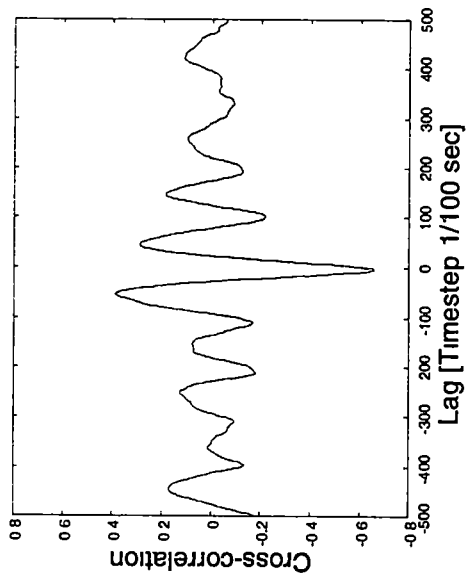
Figure 15. Cross-correlation for 35x100 mesh stainless steel at four different fluidization states.
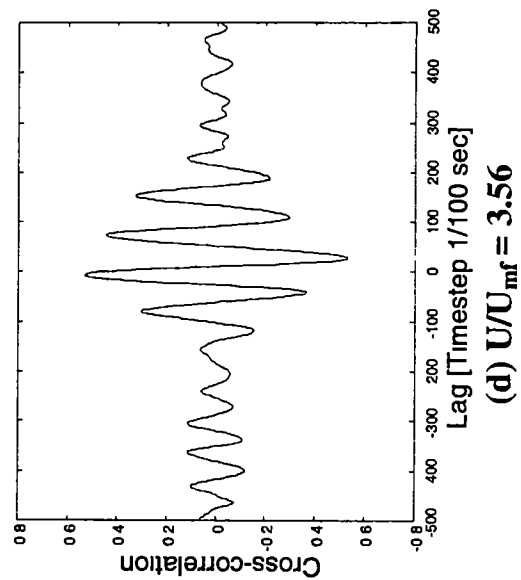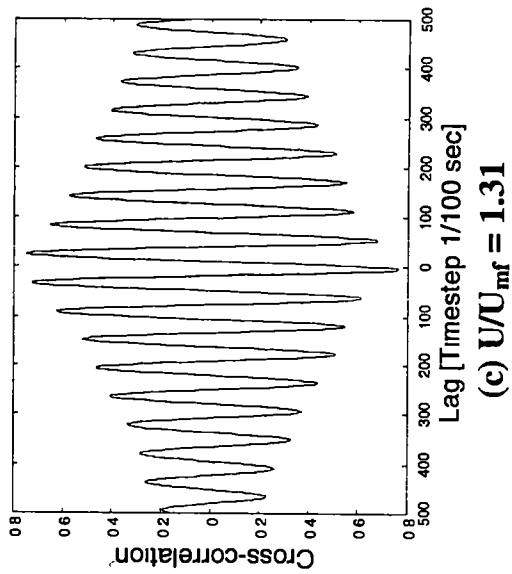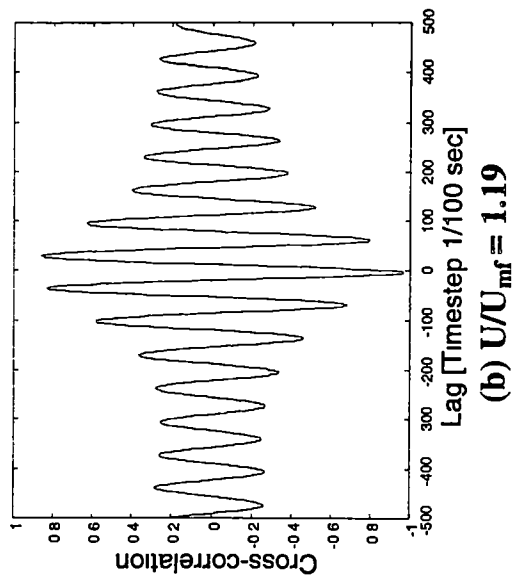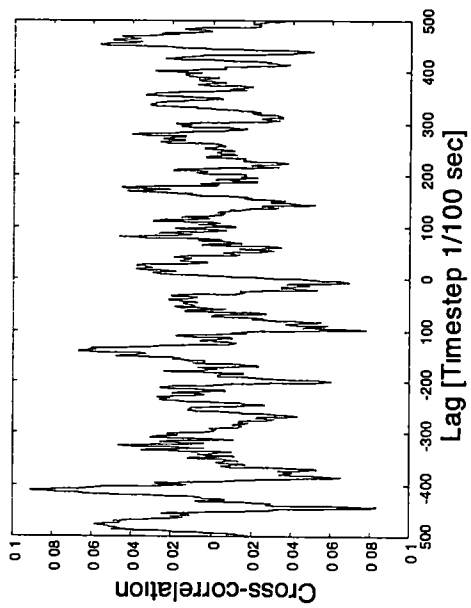
Figure 16. Cross-correlation for 18x50 mesh stainless steel at four different fluidization states.

47
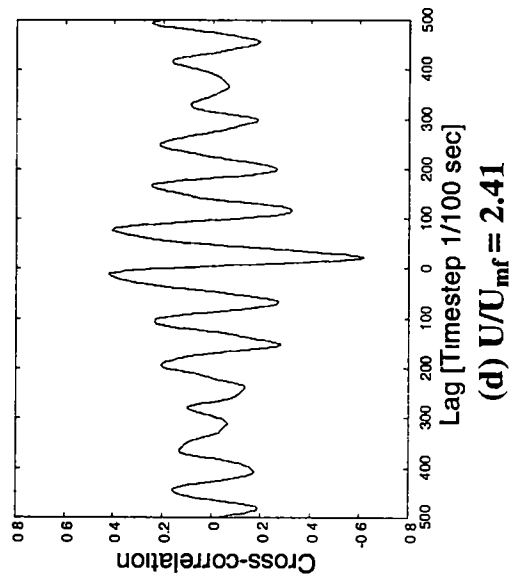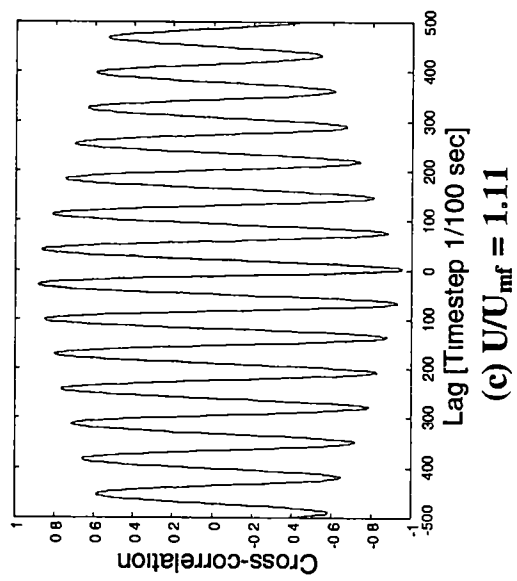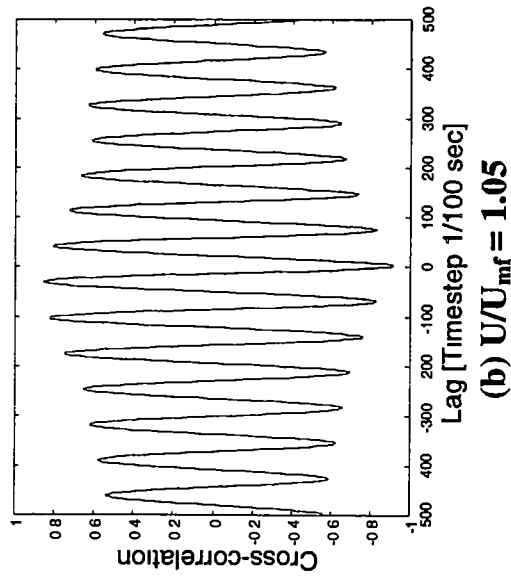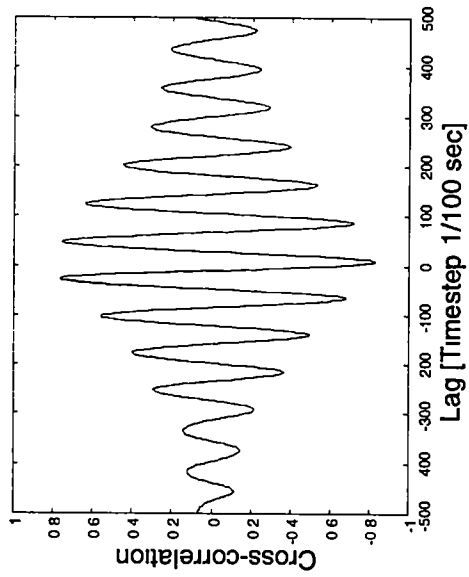
Figure 17. Cross-correlation for glass particles at four different fluidization states.

48
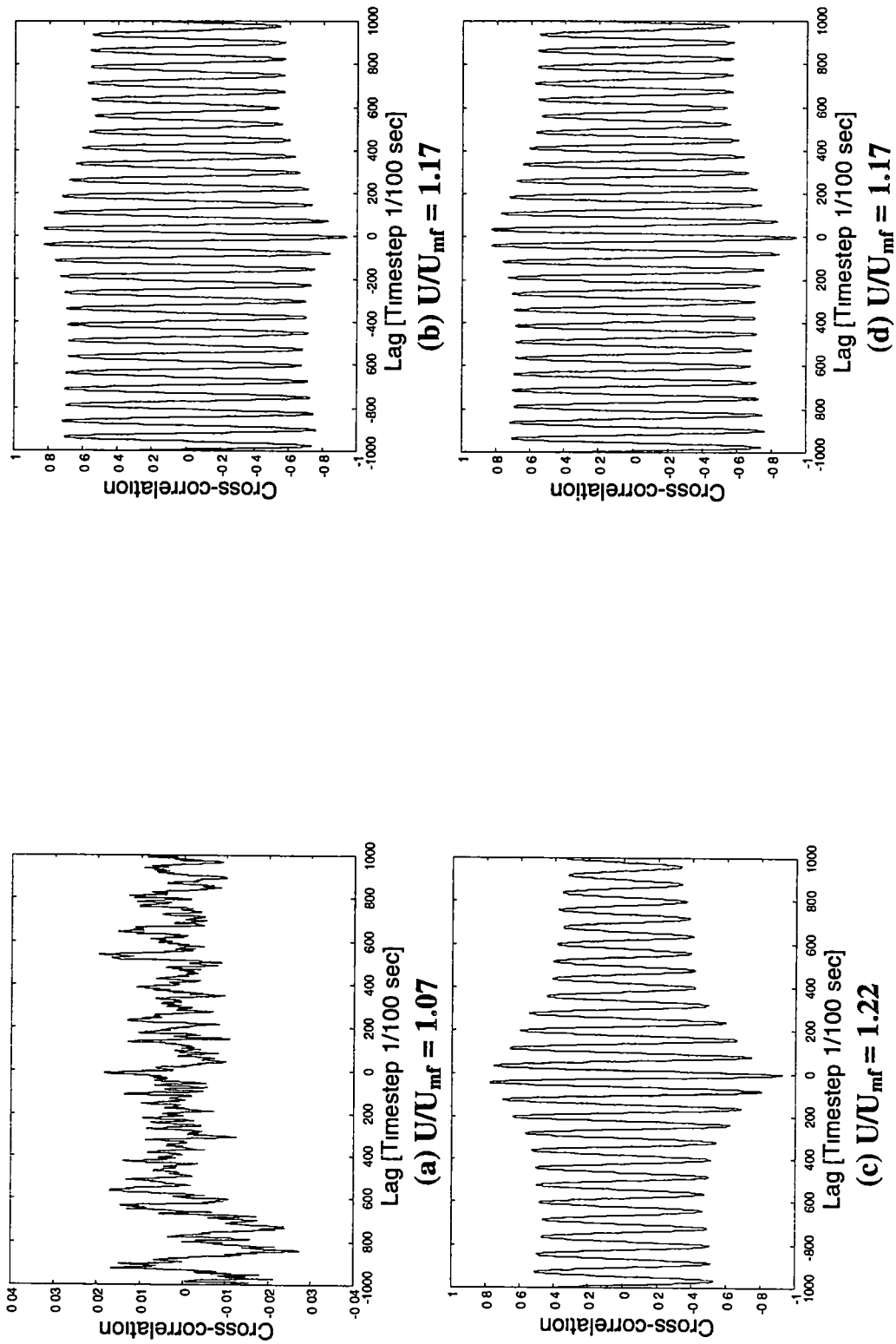
Figure 18. Cross-correlation for BB particles at four different fluidization states.

(a) $U/U_{mf} = 1.07$

(b) $U/U_{mf} = 1.17$

(c) $U/U_{mf} = 1.22$

(d) $U/U_{mf} = 1.17$

correlation reflects lower correlation values from the figure. Complete cross-correlation results for four fluidizing solids are shown in the Appendix.

Figure 15 presents cross-correlations for 35x100 mesh stainless steel at U/U_{mf} of 1.11, 1.42, 2.03, and 7.61. Note that each function is plotted on a different scale to view the structure in low amplitude functions Near minimum fluidization ($U/U_{mf} = 1$ 11), the cross-correlation between the acoustic and pressure signals is relatively low due to the complexity of individual particle movements in the bed, and each sensor measures different events such as occasional slugging, bubbling, and bed expansion In the developing of slugs and slugging regimes ($U/U_{mf} = 1.42$ and $U/U_{mf} = 2.03$, respectively), strong correlation is observed between the acoustic and pressure signals, indicating that both signals are periodic and very similar to each other. As the fluidization velocity increases beyond slugging, the cross-correlation is weakened by the presence of large bubbles and slugs With further increases in flow, the cross-correlation between both signals is greatly reduced by the complexity of irregular and violent mixing in the bed

Similar observations are shown in all other figures. Visible transitions are observed at which the degree of correlation changes from weak to strong and then to weak corresponding to complex behavior near minimum fluidization velocity to regular in slugging condition and then to complex behavior in the breaking slug regime However, the cross-correlation of 18x50 mesh stainless steel (Figure 16a) and BB particles (Figure 18a) are very complicated due to the occasionally bed expansion in the near minimum fluidization.

4.4   CORRELATION DIMENSION

Correlation dimension is used to estimate the complexity of the system behavior using the maximum-likelihood method described in Chapter 3   This technique is found useful for observing the trends over a wide range of fluidizing velocity, specifically to transitions in the fluidization regime.   For instance, high dimensionality reflects high complexity of the system behavior such as occurs near minimum fluidization or near the transition to turbulence, whereas low dimensionality indicates stable and regular system behavior such as slugging.

Correlation dimension values are calculated and plotted against U/U_{mf} for four different fluidizing solids in Figures 19 – 22. The plots generated from the pressure and acoustic signals are then compared and discussed. Near minimum fluidization, the bed behavior is extremely complicated due to individual particle movements and occasional bubbling in the bed. This fluidization regime results in high dimension values observed in both acoustic and pressure signals for all fluidizing solids. When the flow rate is increased to the slugging regime, the dimension decreases to a minimum value for pressure and acoustic signals due to the low degree of complexity in the system   For instance, the minimum dimension values for glass (Figure 21) and BBs (Figure 22) are observed at U/U_{mf} of 1 12 and U/U_{mf} of 1.22, respectively With an increase in flow rate, the bed becomes progressively disordered and complex, as seen by an increase in the dimension This trend is seen for both acoustic and pressure signals

The overall dimension trends from this study are similar to those obtained from M. Vasudevan and Dean Skrzycke However, the dimensions for the acoustic signal are
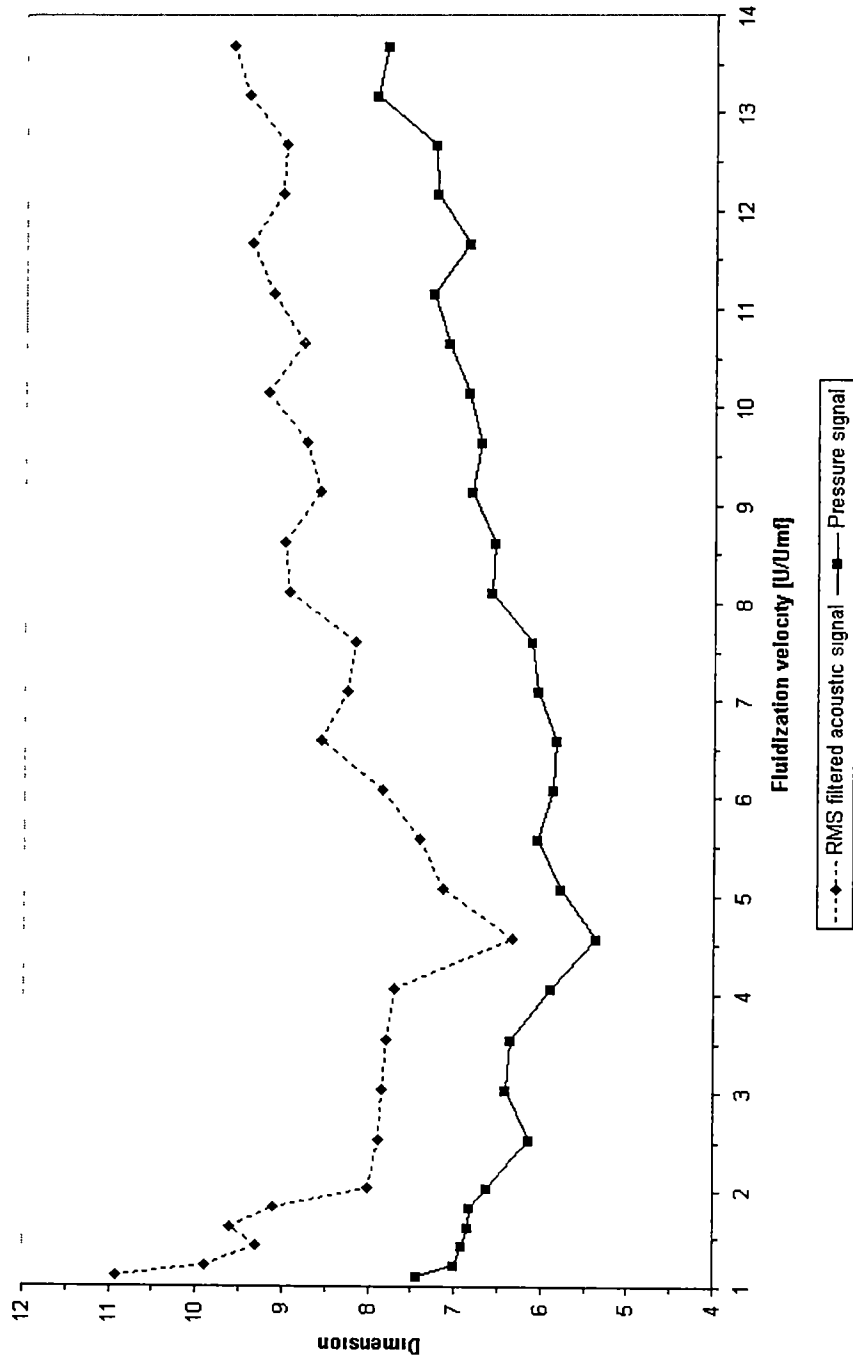
Figure 19. Variation of dimension based on pressure and RMS filtered acoustic signals for 35x100 stainless steel over a velocity range of U/U$_{mf}$ = 1.11 to 13.69

52
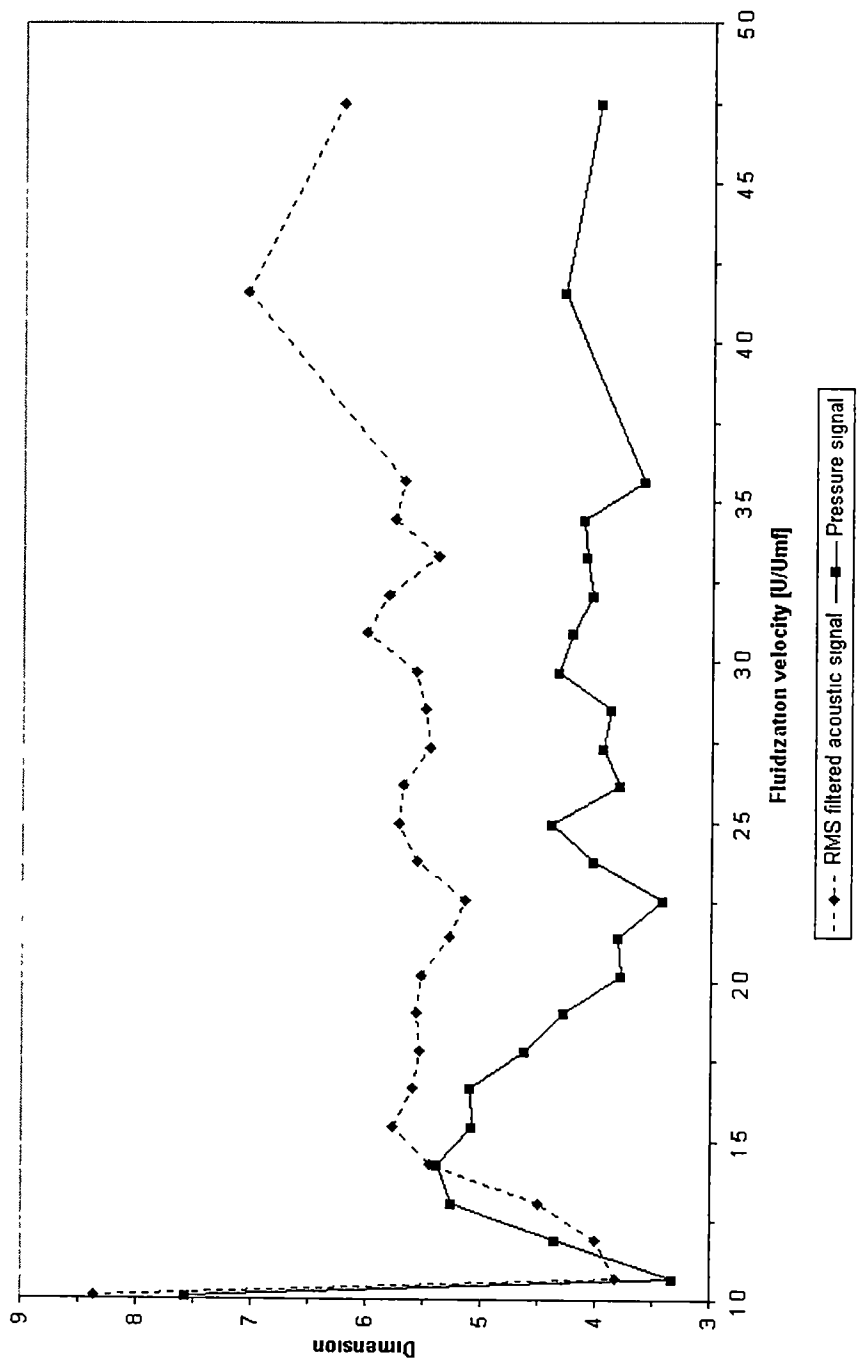
Figure 20. Variation of dimension based on pressure and RMS filtered acoustic signals for 18x50 stainless steel over a velocity range of $U/U_{mf} = 1.01$ to 4.75
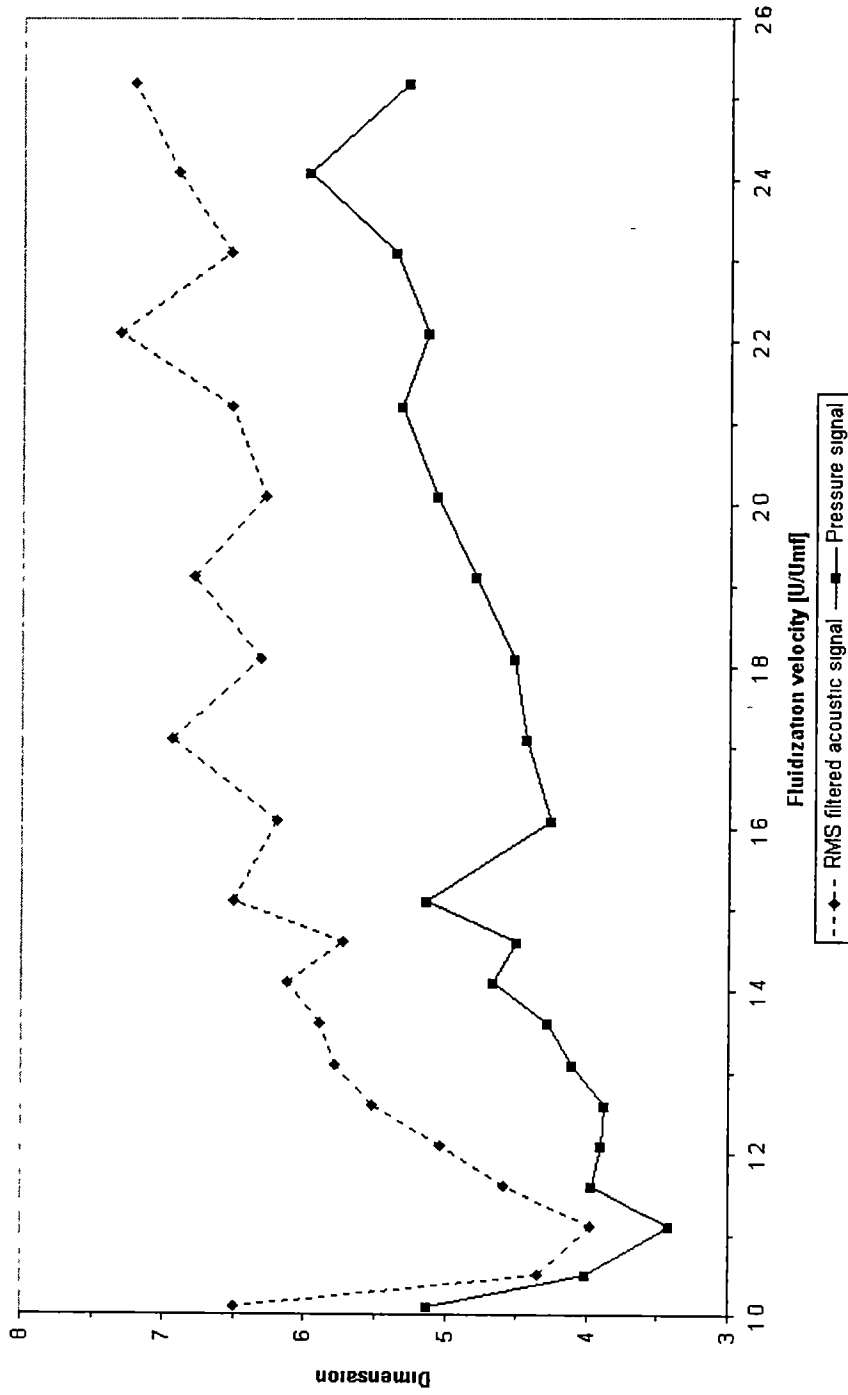
Figure 21. Variation of dimension based on pressure and RMS filtered acoustic signals for glass particles over a velocity range of U/U_{mf} = 1.01 to 2.52
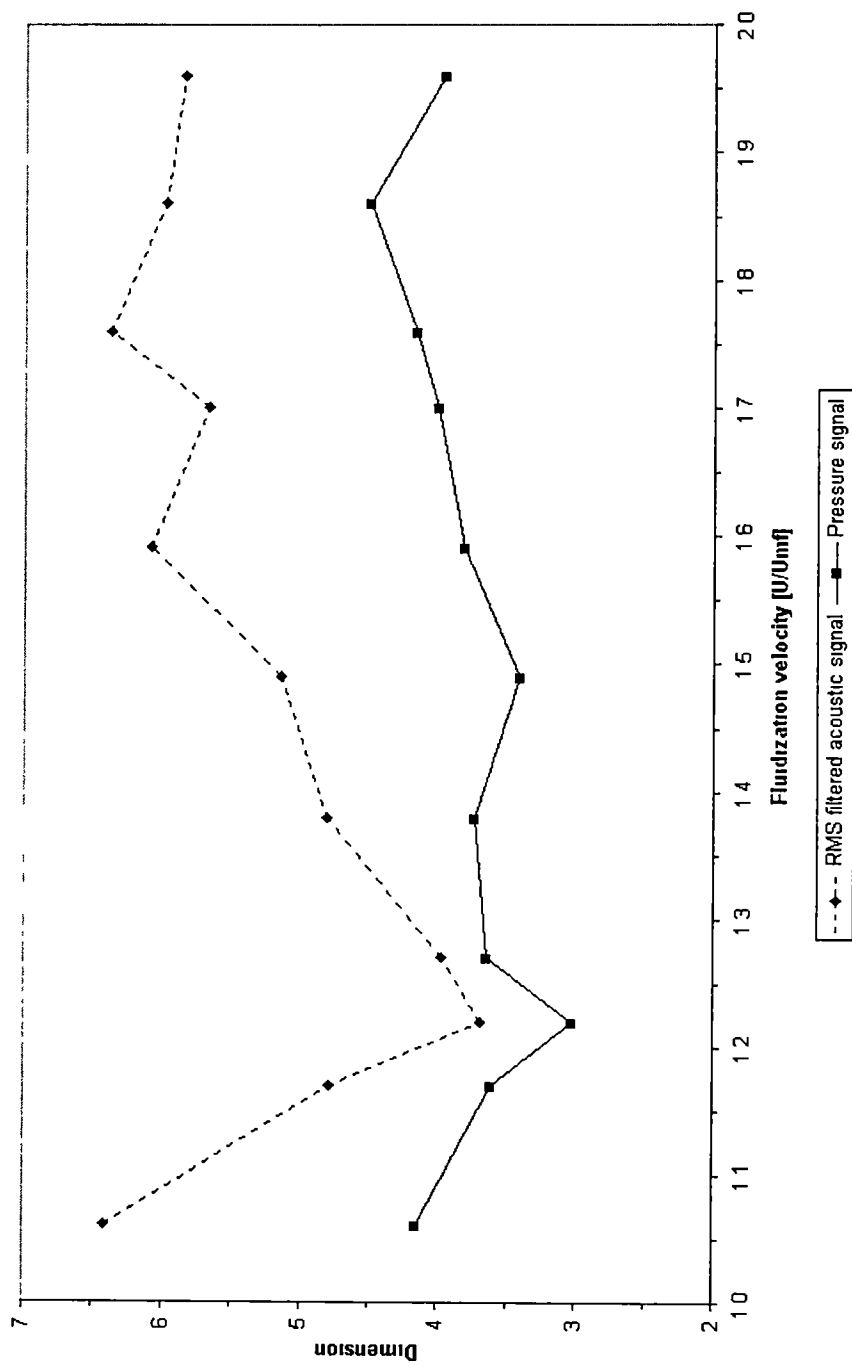
Figure 22. Variation of dimension based on pressure and RMS filtered acoustic signals for BB particles over a velocity range of U/U_{mf} = 1.06 to 1.96

always higher than those for the pressure signals This implies that the overall acoustic signals obtained from the piezoelectric accelerometer are more complex due to the vibration and movement of the fluidized bed. In general, transitions of the bed from a complex to regular and back to complex behaviors over the velocity ranges are observed by corresponding variations in dimensions.

4.5   KOLMOGOROV ENTROPY

Kolmogorov entropy measures the degree of predictability in the signal. The maximum likelihood estimator of Kolmogorov entropy outlined in Chapter 3 provides information about the system behavior by mapping the overall dynamical trends over a wide velocity range. In Figures 23 – 26 entropy is plotted against flow rate for each fluidizing solid. The entropy curves generated from the acoustic and pressure signals are compared in each figure. Discussion here however, is limited to result from 35x100 mesh stainless steel, which has common features that are shared with other fluidizing solids.

Figure 23 presents entropy values for acoustic and pressure signals for 35x100 stainless steel particles Transitions of fluidization regimes can be identified by the variation of entropy curve over fluidizing velocities. At U/U_{mf} of 1.11 to 2.03, the slope of the curve is negative and steepest corresponding to the bubbling regime in the system Developing slug regime is observed at U/U_{mf} between 2.03 and 4.56   At U/U_{mf} of 4 56, minimum entropy values for acoustic and pressure signals are observed and the bed is in regular slugging regime   With further increase in flow rate from U/U_{mf} of 4 56 to
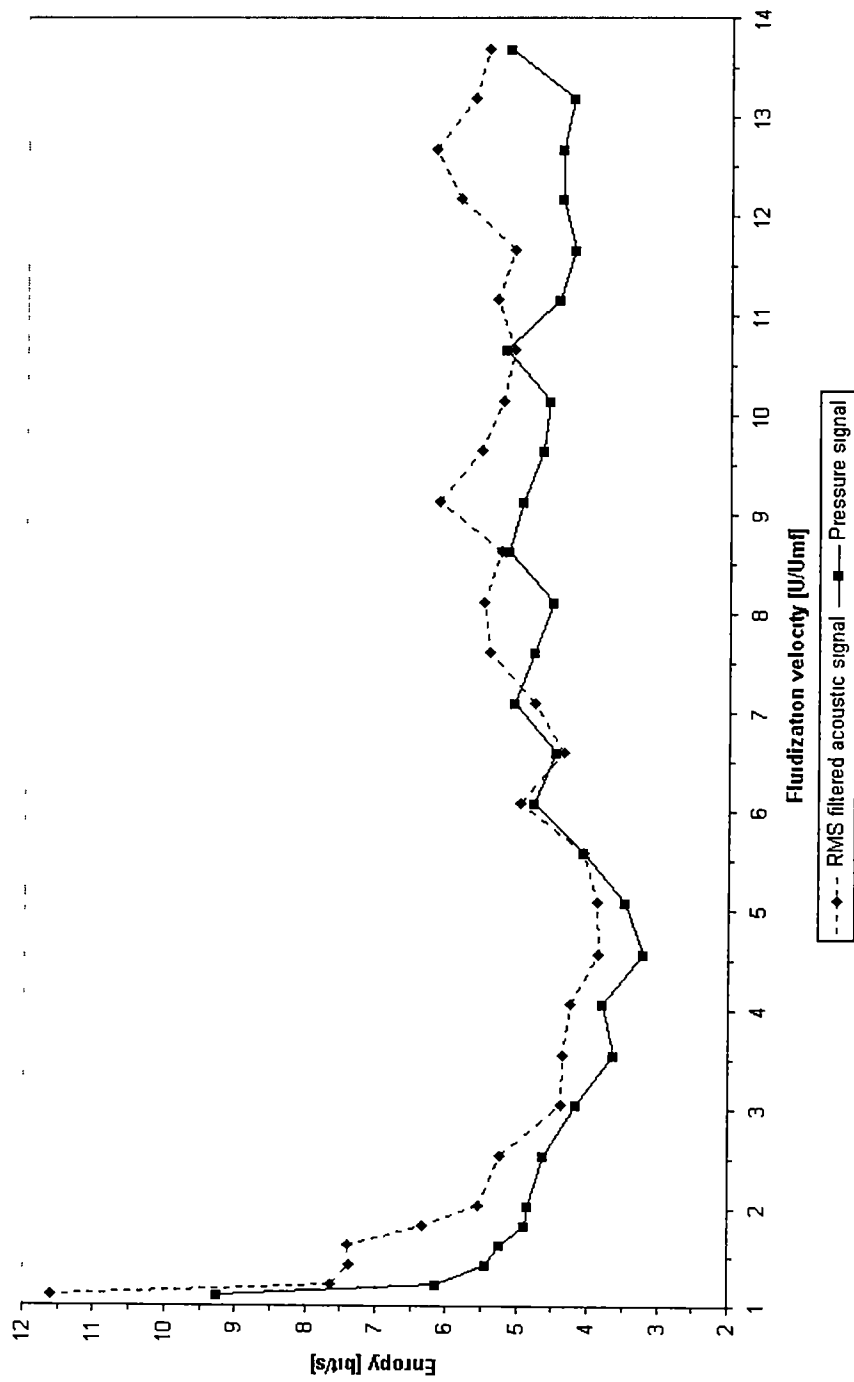
Figure 23. Variation of entropy based on pressure and RMS filtered acoustic signals for 35x100 stainless steel over a velocity range of U/U_{mf} = 1.11 to 13.69
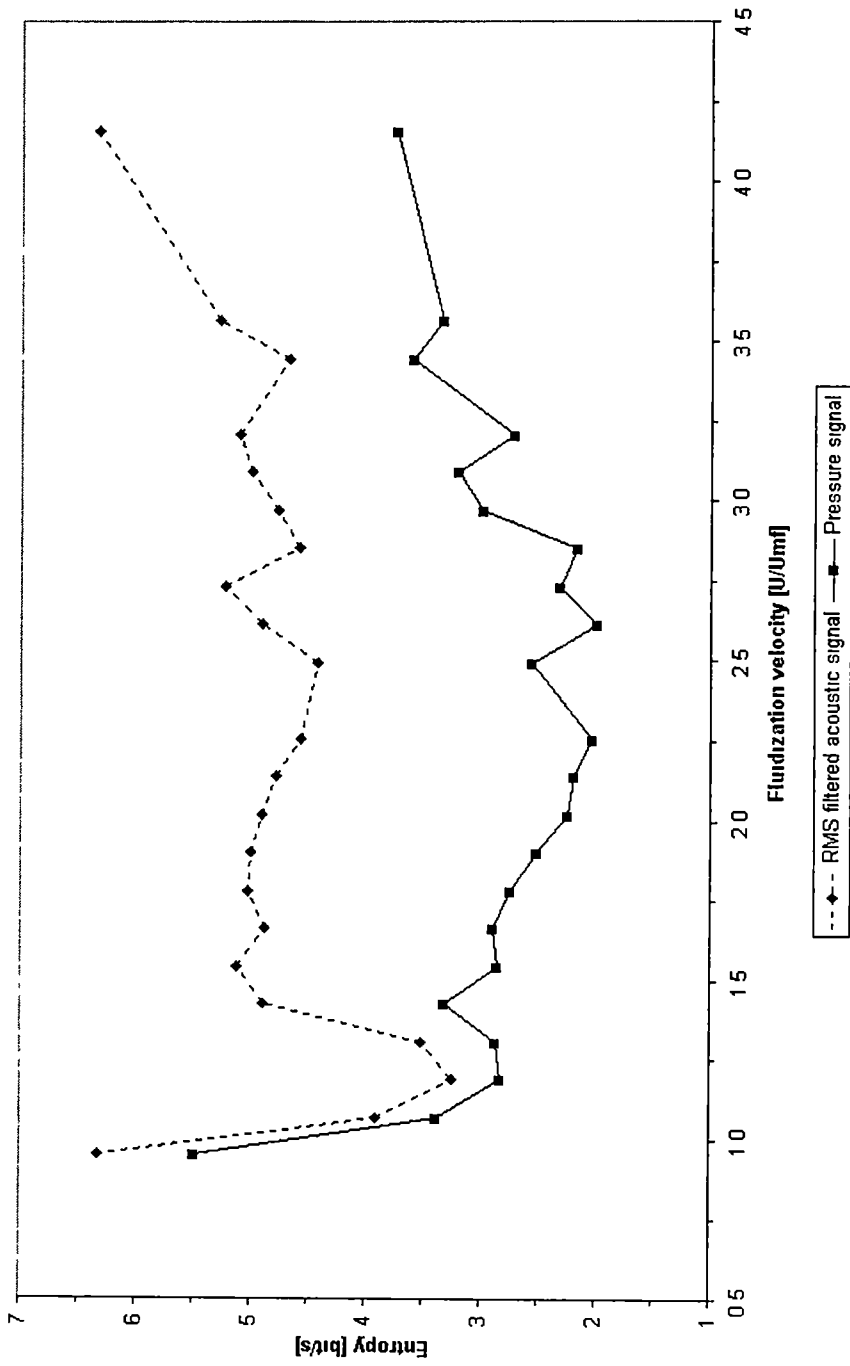
Figure 24. Variation of entropy based on pressure and RMS filtered acoustic signals for 18x50 stainless steel over a velocity range of $U/U_{mf} = 1.01$ to 4.75
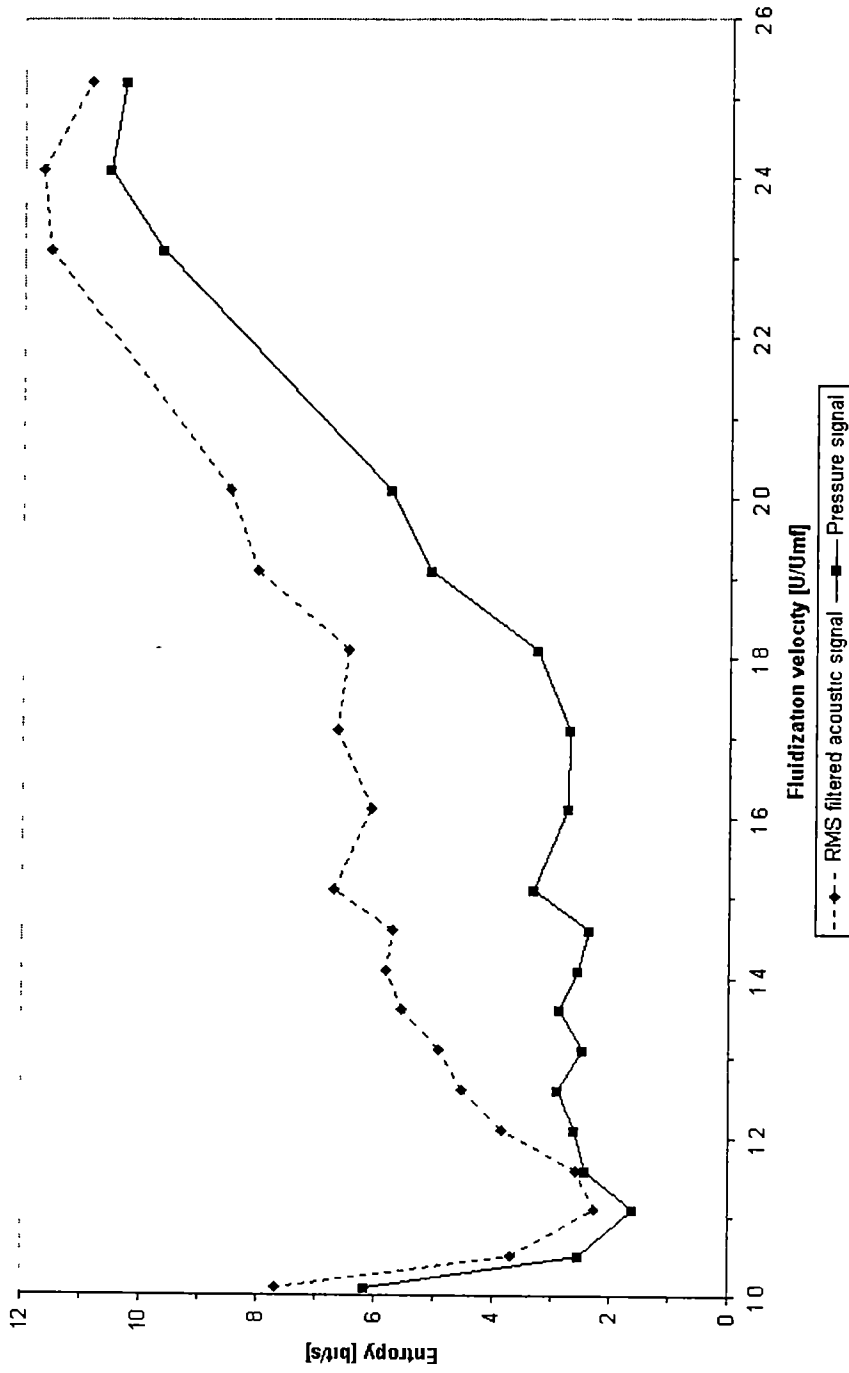
Figure 25. Variation of entropy based on pressure and RMS filtered acoustic signals for glass particles over a velocity range of $U/U_{mf} = 1.01$ to 2.52
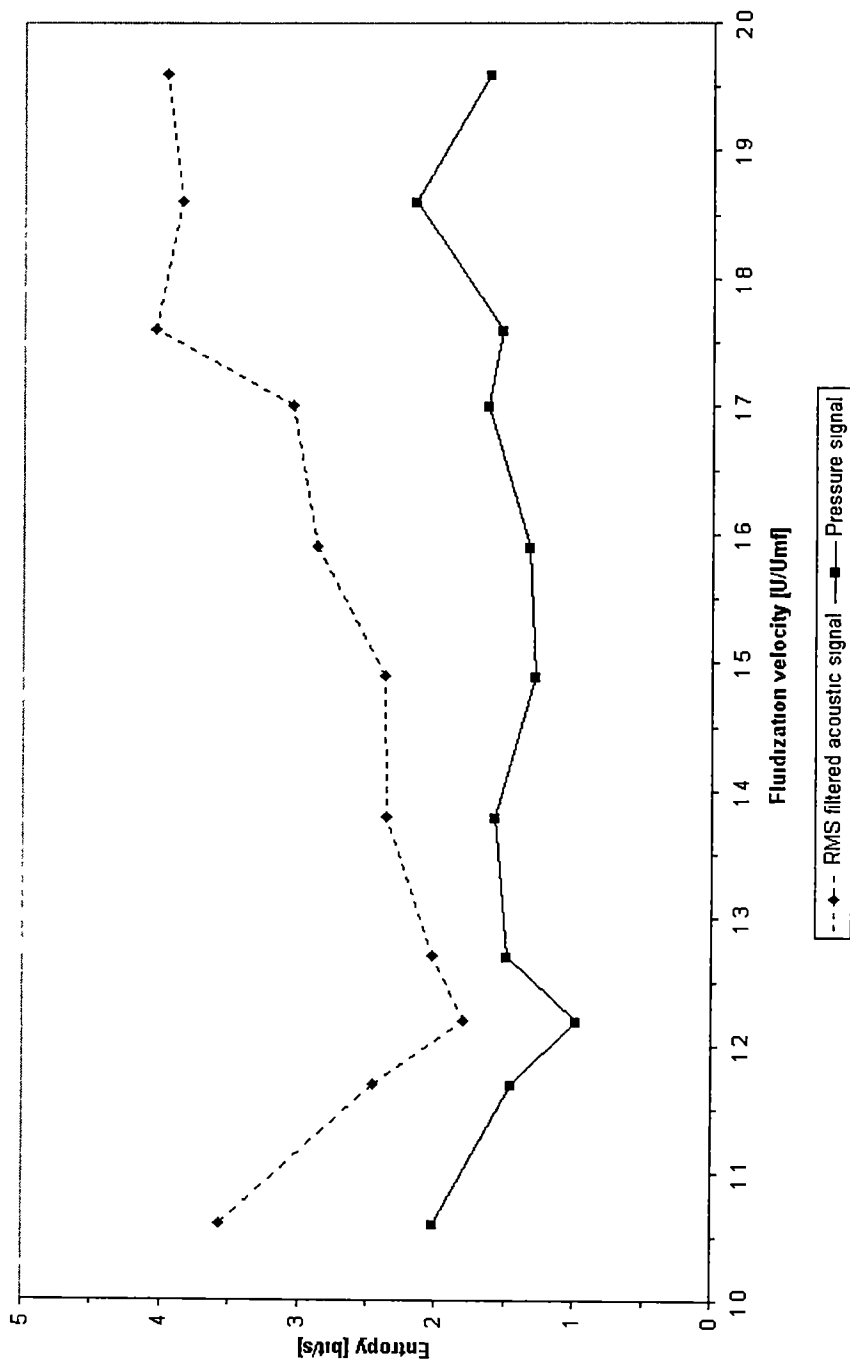
Figure 26. Variation of entropy based on pressure and RMS filtered acoustic signals for BB particles over a velocity range of $U/U_{mf} = 1.06$ to 1.96

13.69, the bed becomes increasingly disordered and the entropy curves gradually increase for both signals. The entropy curves for 18x50 mesh stainless steel (Figure 24) and BB (Figure 26) exhibit trends similar to those of the 35x100 stainless steel. However, the entropy curve for glass reaches a peak and then drops off as shown in Figure 25, possibly indicating a transition to turbulence. This phenomenon is seen for both acoustic and pressure signals for glass particles.

Based on these results, both acoustic and pressure signals provide information about the system behavior similar to that obtained from the entropy curves. Transitions of fluidization regimes can be observed from the entropy curves for both the acoustic and pressure signals. However, the acoustic signals exhibit higher entropy than the pressure signals, possibly due to the bed vibration.

CHAPTER 5

CONCLUSIONS AND RECOMMENDATIONS

Based on the results obtained from the Group B and D particles in a laboratory-scale fluidized bed, it appears that significant information about the bed dynamics can be obtained from acoustic sensors. Using simple pre-processing of acoustic signals with RMS filtering, the fluidization dynamics can be monitored by measuring and extracting the low-frequency acoustic-intensity modulation. Linear and nonlinear analysis of the pressure and filtered acoustic signals are observed to share significant amount of information characterizing various fluidization regimes associated with near minimum fluidization, developing slugs, slugging, and breaking slugs.

Results of the correlation dimension and Kolmogorov entropy show that acoustic signal have higher complexity than the pressure signal. It is suspected that the piezoelectric accelerometer used here is measuring both global particle movements and the lateral bed vibration caused by the collapsing solids. An ill-chosen RMS filter could retain significant dynamic information which is not very useful for evaluating fluidization state. Therefore, it is suggested that further study concerning different software and hardware filtering techniques may be useful for producing better acoustic fluid-bed diagnostics

In this study, only one piezoelectric accelerometer mounted at a fixed location is used to obtain acoustic signals from the laboratory-scale fluidized bed. A single piezoelectric accelerometer is capable of measuring the global bed dynamics such as bubbling and slugging. However, the dynamic behavior of commercial fluidized bed

62

tends to produce more complicated results due to its large-scale vessel Uneven bubbling and slugging at different locations could result in incomplete measurements if only one piezoelectric accelerometer is employed to acquire signals. Therefore, it is thought that multiple piezoelectric accelerometers located at different elevation and different location on the circumference of the bed may be useful to measure the local and global behavior of the bed.

From these results, piezoelectric accelerometers are demonstrated to be useful for monitoring the dynamic behavior of a laboratory-scale fluidized bed This technique becomes more valuable especially in hazardous systems where nonintrusive measurement is an advantage Such monitoring capability shows great promise of being a valuable supplemental diagnostic tool for detecting anomalous or undesirable behavior such as defluidization and solid agglomeration in commercial fluidized bed reactors and combustors.

REFERENCES

REFERENCES

Burgess, J.C. (1998) Practical Consideration in Signal Processing. Chapter 82 in **Handbook of Acoustics**, M.J. Crocker, ed , *John Wiley & Sons*

Finney, C.E.A., Daw, C.S , Halow, J.S (1998). Measuring Slugging Bed Dynamics with Acoustic Sensors, *KONA Power and Particle*, No. 16, pp 125-135

Halstensen, M., de Silva, S., Esbensen, K. (1998) Acoustic Monitoring of Pneumatic Transport Lines· From Noise to Information, *KONA*, No. 16, pp 170-177

Hou, R., Hunt, A., Williams, R.A (1999). Acoustic Monitoring of Pipeline Flows Particulate Slurries, *Power Technology*, Vol. 106, No 1-2, pp 30-36

Geldart, D (1986) **Gas Fluidization Technology**, *Wiley-Interscience*

Grassberger, P , and Procaccia, I (1983a) Measuring the Strangeness of Strange Attractors, *Physica D*, Vol 9, pp. 189-208.

Grassberger, P., and Procaccia, I (1983b). Estimation of the Kolmogorov Entropy From a Chaotic Signal, *Physical Review A*, Vol 28, No 4, pp. 2591-2593

Kunni, D , and Levenspiel, O. (1969). **Fluidization Engineering**, *Robert E. Krieger Publishing Company, Inc*

Packard, N.H , Crutchfield, J.P , Farmer, J.D , and Shaw, R.S. (1980) Geometry From a Time Series, *Physical Review Letters*, Vol. 45, No. 9, pp 712-716

Pope, J (1998) Analyzers Chapter 107 in **Handbook of Acoustics** M.J. Crocker, ed , *John Wiley & Sons*

Schouten, J C., Takens, F., and Van den Bleek, C.M (1994a) Maximum-Likelihood Estimation of the Entropy of an Attractor, *Physical Review E*, Vol 49, No 1, pp 126-129

Schouten, J.C , Takens, F., and Van den Bleek, C.M (1994b) Estimation of the Dimension of a Noisy Attractor, *Physical Review E*, Vol 50, pp 1851-1861.

Schouten, J.C., Vander Stappen, M.L.M., and Van den Bleek (1996) Scale-Up of Chaotic Fluidized Bed Hydrodynamics, *Chemical Engineering Science*, Vol. 51, No. 10, pp. 1991-2000.

Skrzycke, D P., Nguyen, K., and Daw, C S (1993) Characterization of the Fluidization Behavior of Different Solid Types Based on Chaotic Time Series Analysis of Pressure Signals, *Proceedings of the 12th International Conference on Fluidized Bed Combustion*, L.N. Rubow (Ed.), ASME, New York, Vol 1, pp. 155-166

Skrzycke, D.P. (1993). Characterization of the Fluidization Behavior of Different Solid Types Based on Chaotic Time Series Analysis of Pressure Signals, M S. Thesis, University of Tennessee, 1993.

Stappen, M L M Vander (1996). Chaotic Hydrodynamics of Fluidized Beds, Ph D Dissertation, Technical University of Delft (Netherland), *Delft University Press*, 1996.

Takens, F. (1981). Detecting Strange Attractors in Turbulence, *Lecture Notes in Mathematics, Eds, D A Rand and L -S Young, Springer-Verlag*, Vol 898, New York, pp. 366-381.

Vasudevan, M. (1995). Characterization and Control of Slugging Behavior of Geldart's Group D Particles in a Laboratory Scale Fluidized Bed, M S Thesis, University of Tennessee.

APPENDICES

APPENDIX A
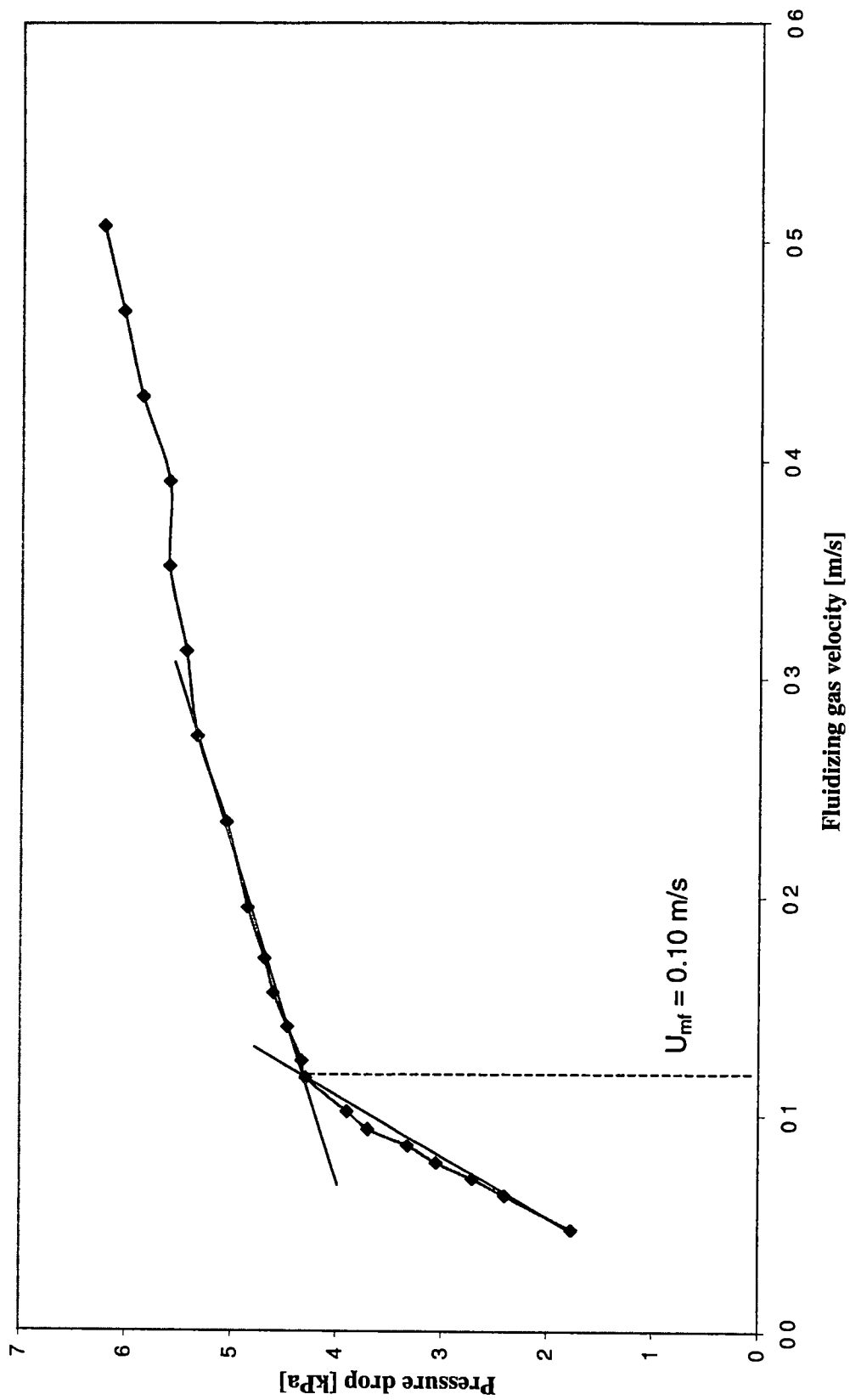
Figure A1. Minimum fluidization velocity for 35x100 mesh stainless steel

69
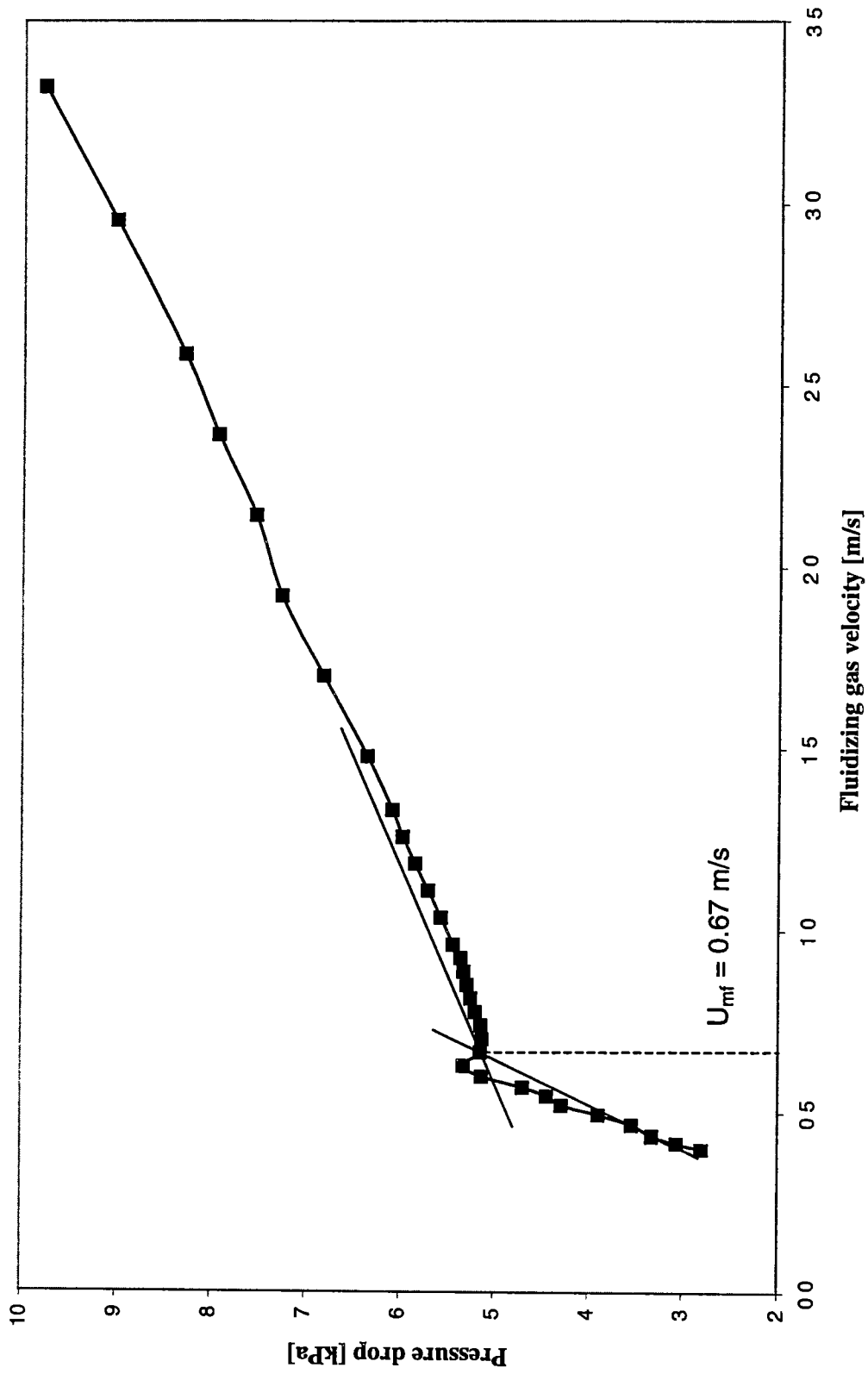
Figure A2. Minimum fluidization velocity for 18x50 mesh stainless steel

$U_{mf} = 0.67$ m/s

Fluidizing gas velocity [m/s]

Pressure drop [kPa]

70
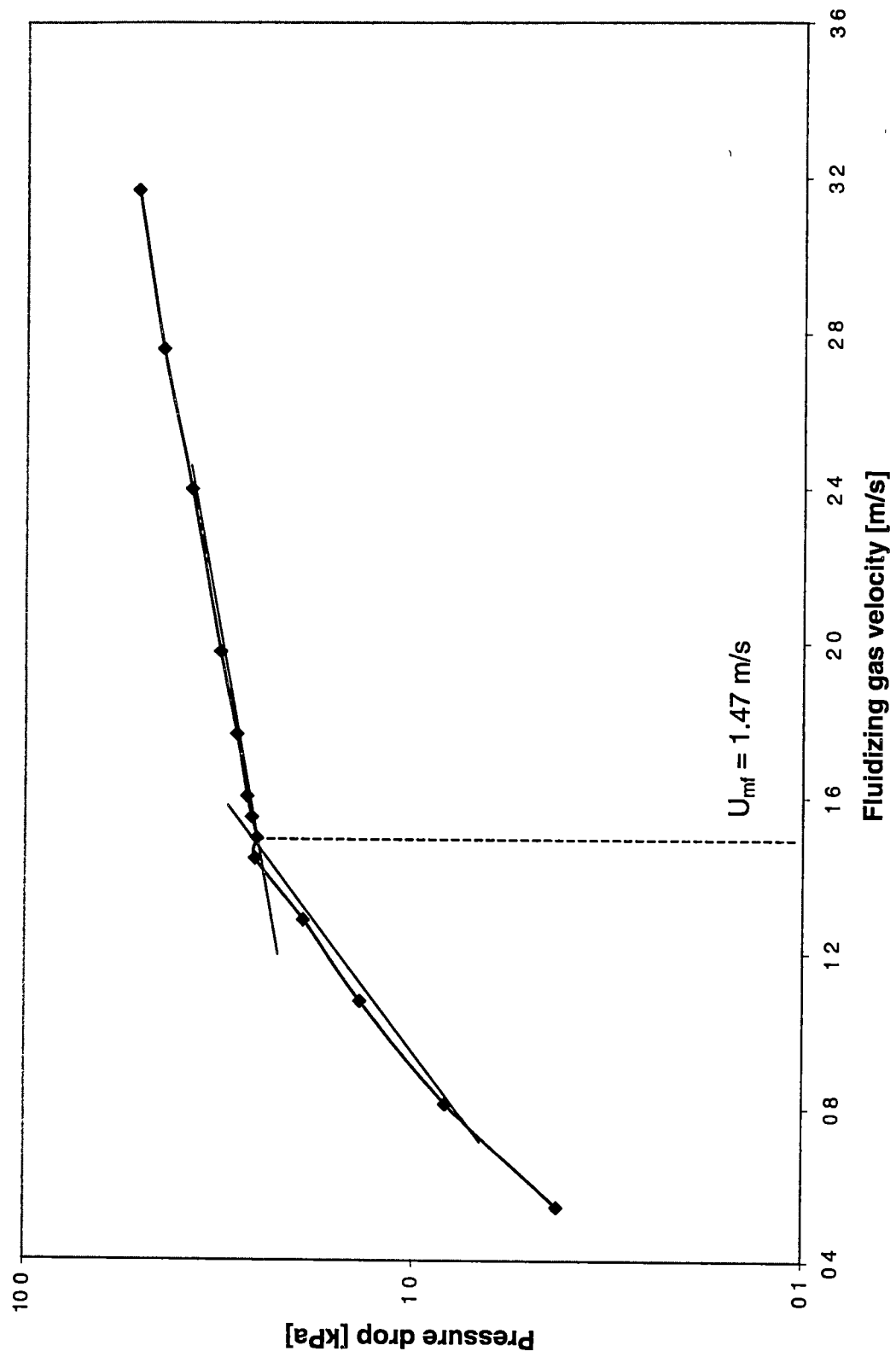
Figure A3. Minimum fluidization velocity for glass particles
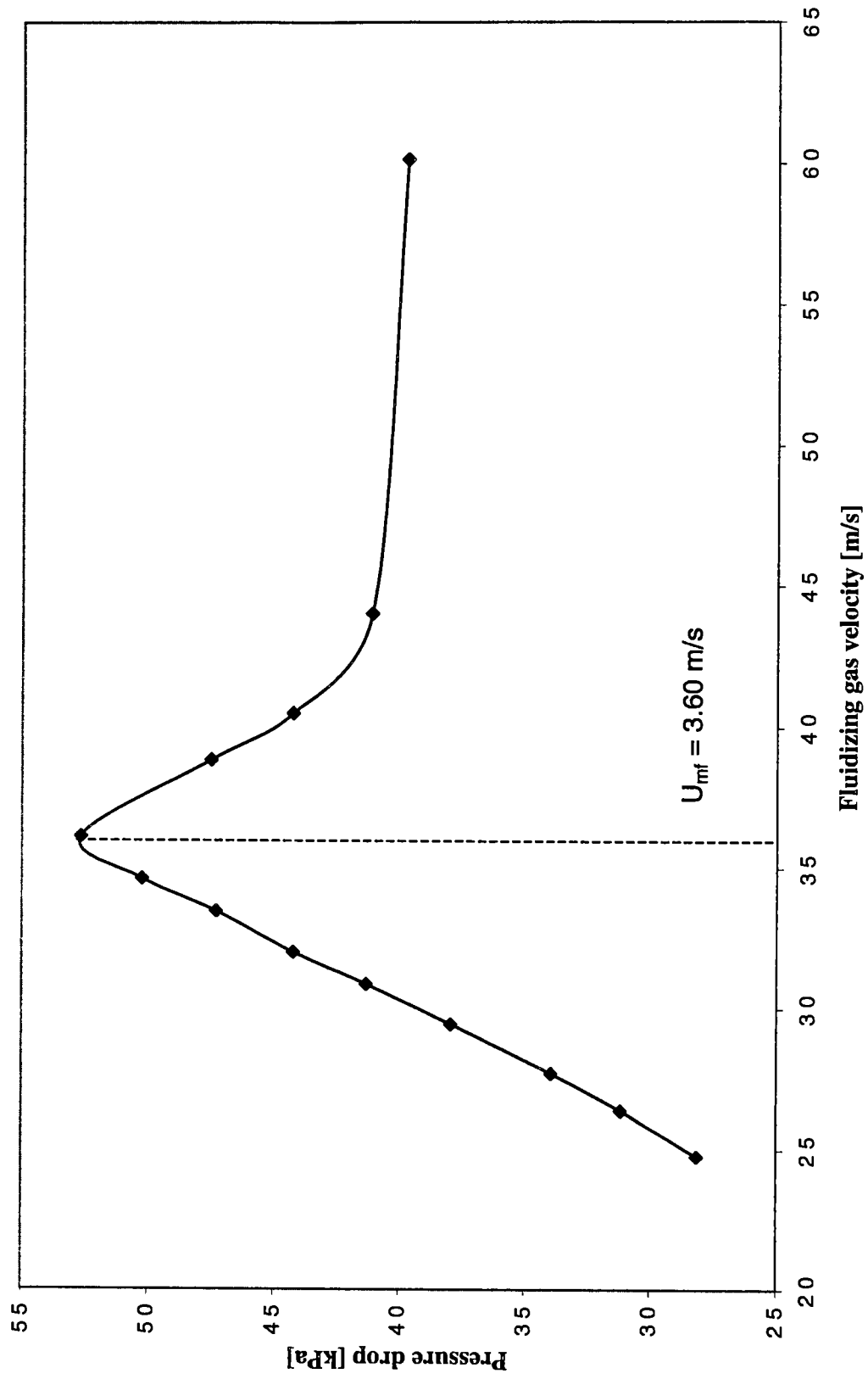
Figure A4. Minimum fluidization velocity for BB particles

$U_{mf} = 3.60$ m/s

APPENDIX B
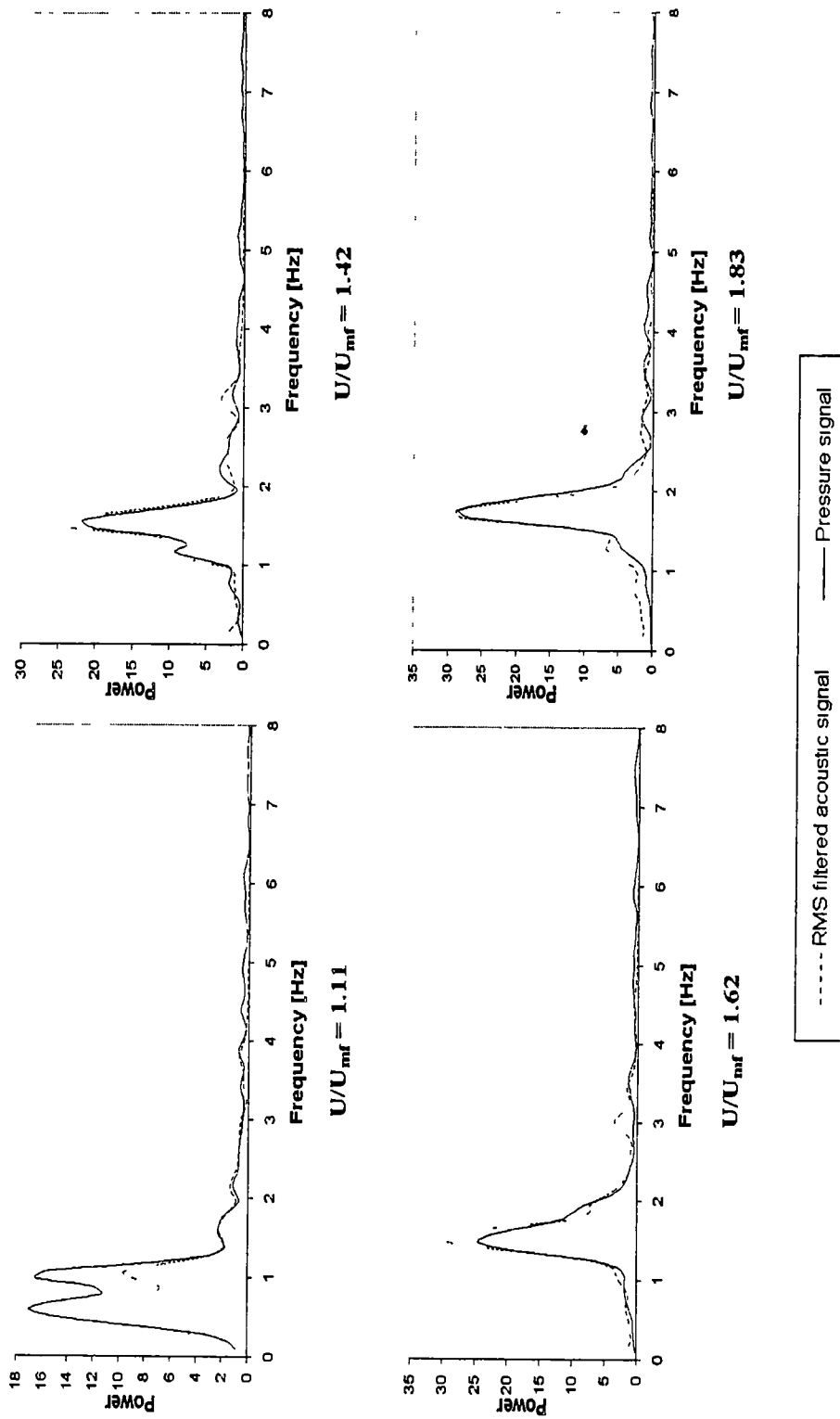
Figure B1. Fourier power spectra of acoustic and pressure signals for 35x100 mesh stainless steel over a velocity range of U/U$_{mf}$ = 1.11 to 1.83.
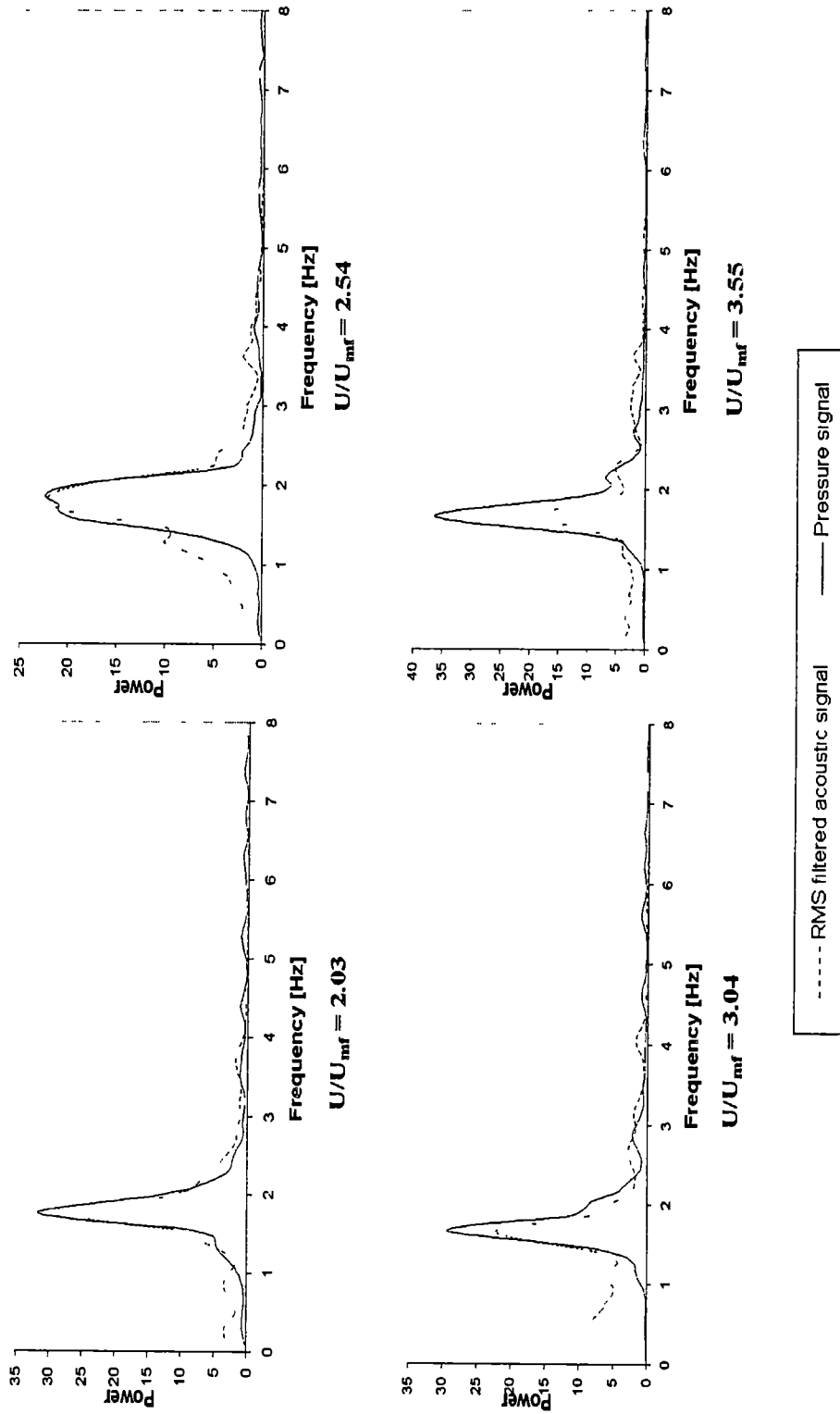
Figure B2. Fourier power spectra of acoustic and pressure signals for 35x100 mesh stainless steel over a velocity range of U/U$_{mf}$ = 2.03 to 3.55.
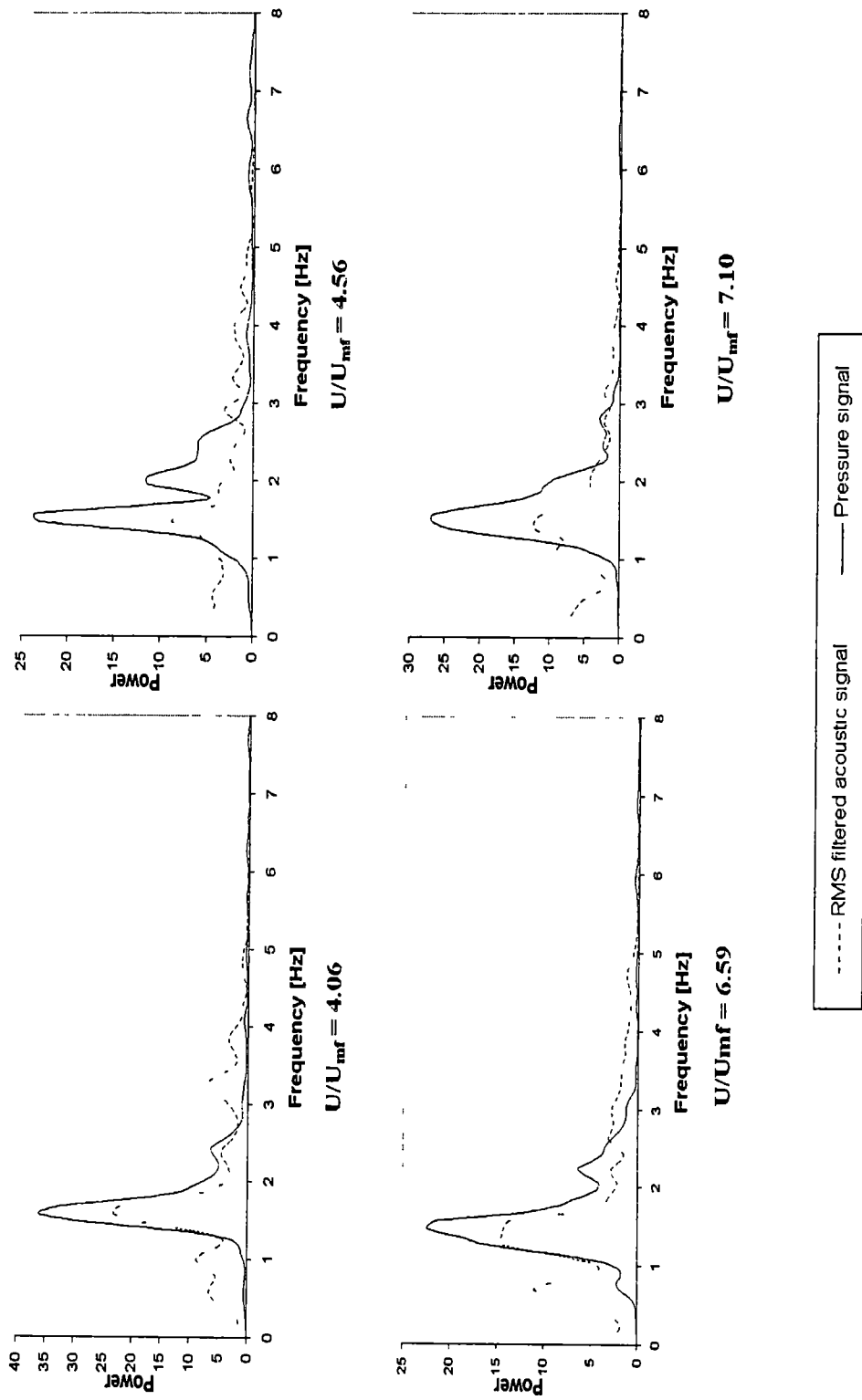
Figure B3. Fourier power spectra of acoustic and pressure signals for 35x100 mesh stainless steel over a velocity range of U/U_{mf} = 4.06 to 7.10.
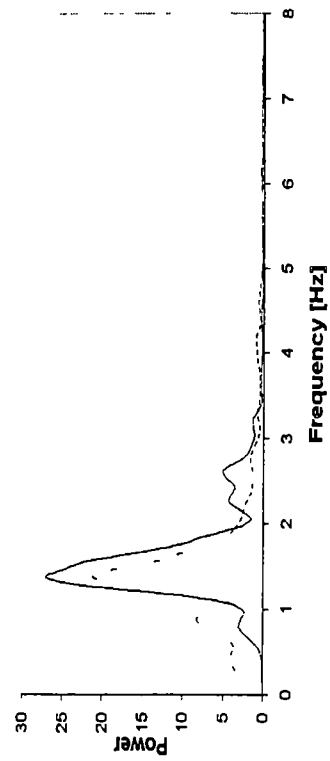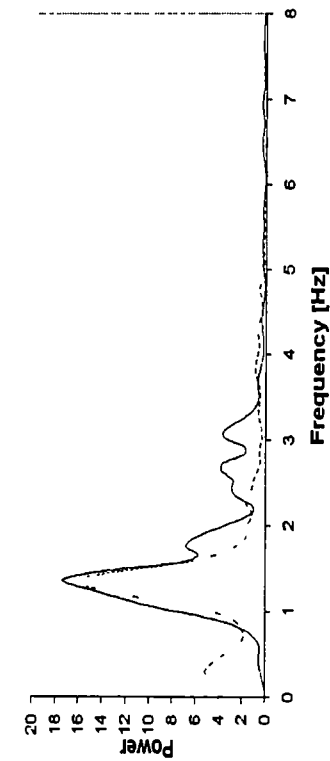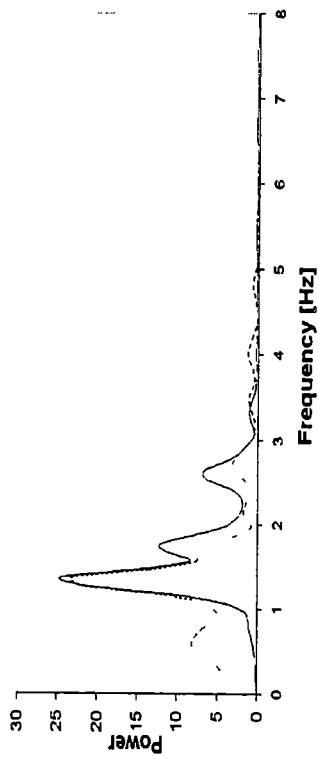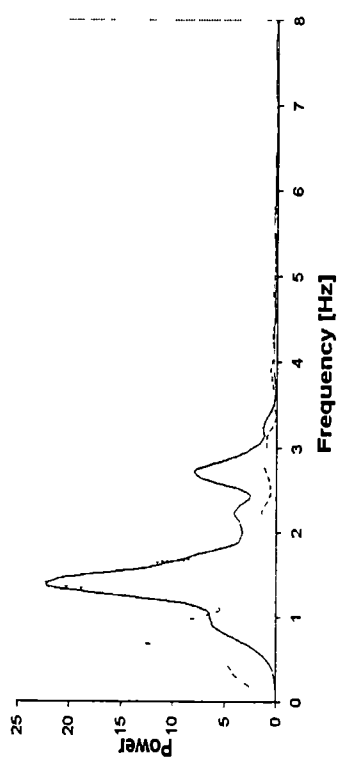
Figure B4. Fourier power spectra of acoustic and pressure signals for 35x100 mesh stainless steel over a velocity range of U/U_mf = 7.61 to 9.13.
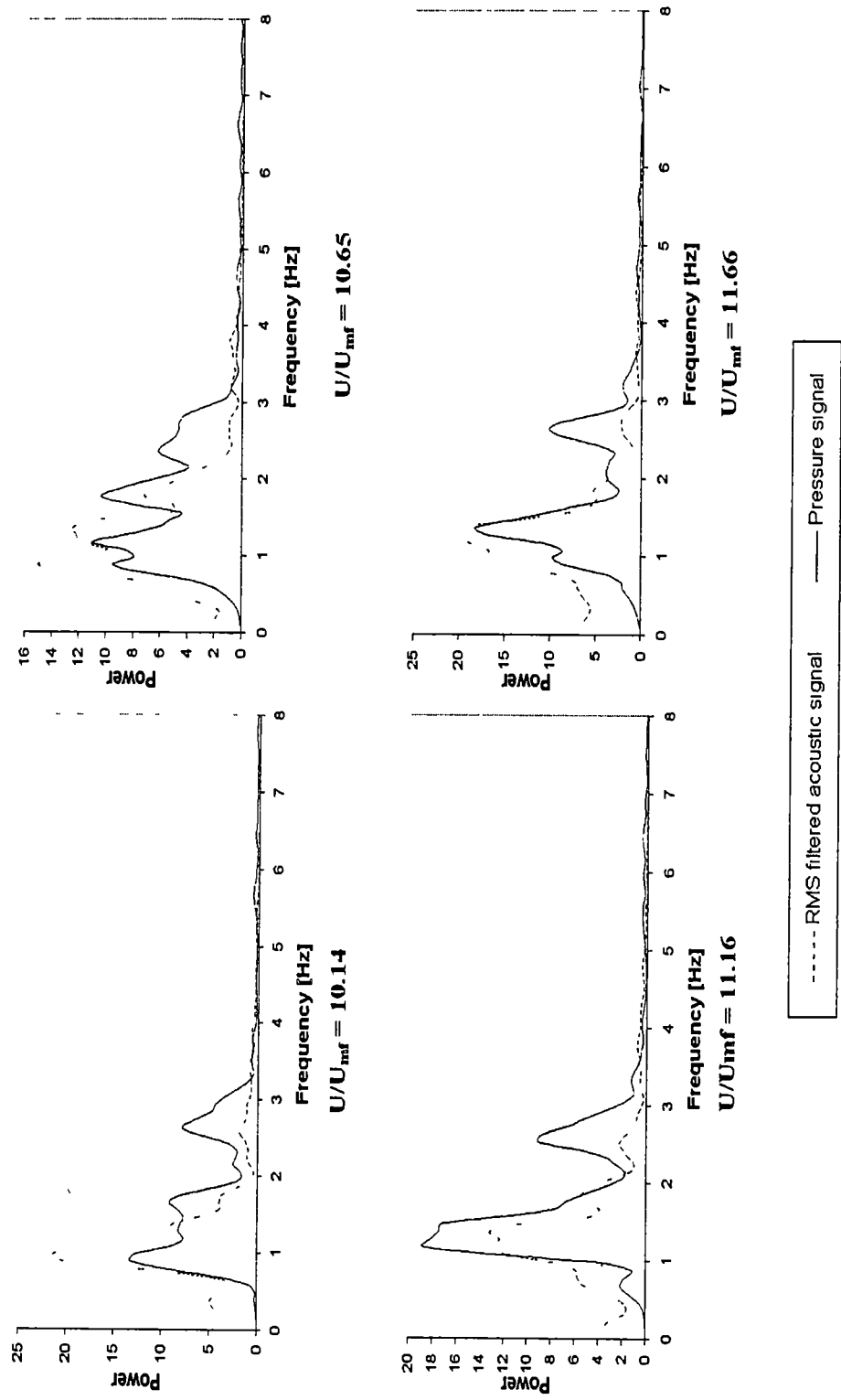
Figure B5. Fourier power spectra of acoustic and pressure signals for 35x100 mesh stainless steel over a velocity range of U/U_{mf} = 10.14 to 11.66.

78
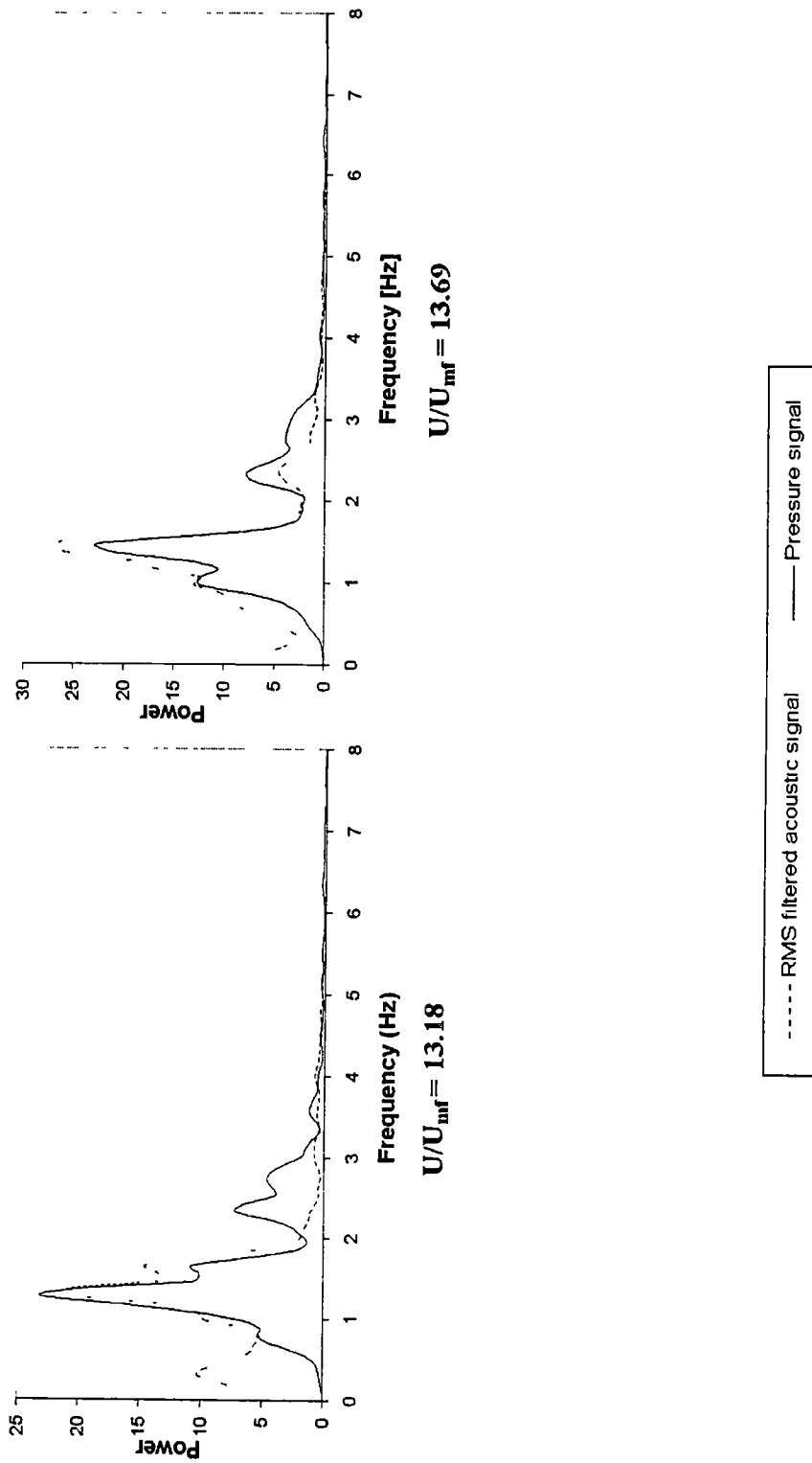
Figure B6. Fourier power spectra of acoustic and pressure signals for 35x100 mesh stainless steel over a velocity range of $U/U_{mf} = 13.18$ and 13.69.
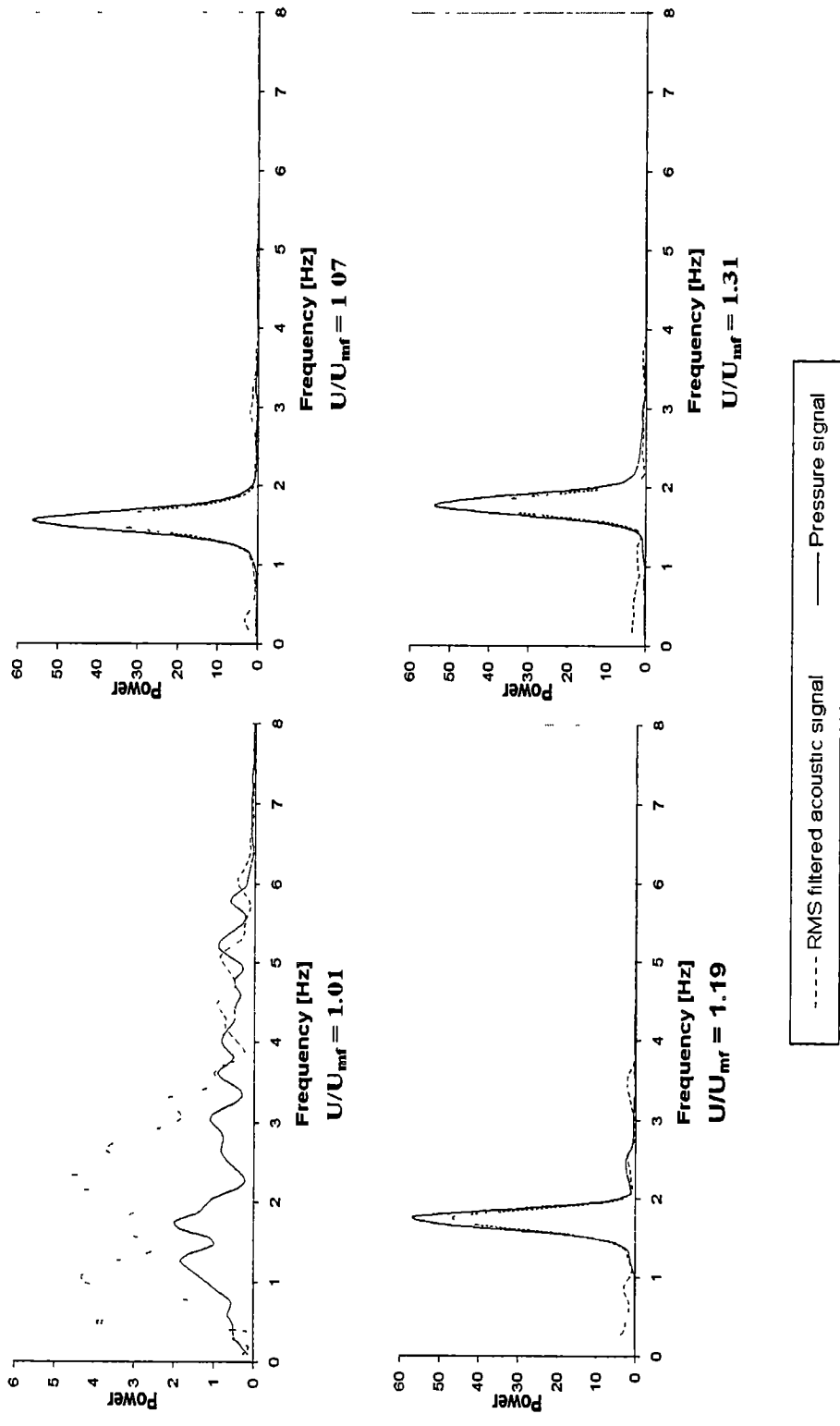
Figure B7. Fourier power spectra of acoustic and pressure signals for 18x50 mesh stainless steel over a velocity range of U/U$_{mf}$ = 1.01 to 1.31.
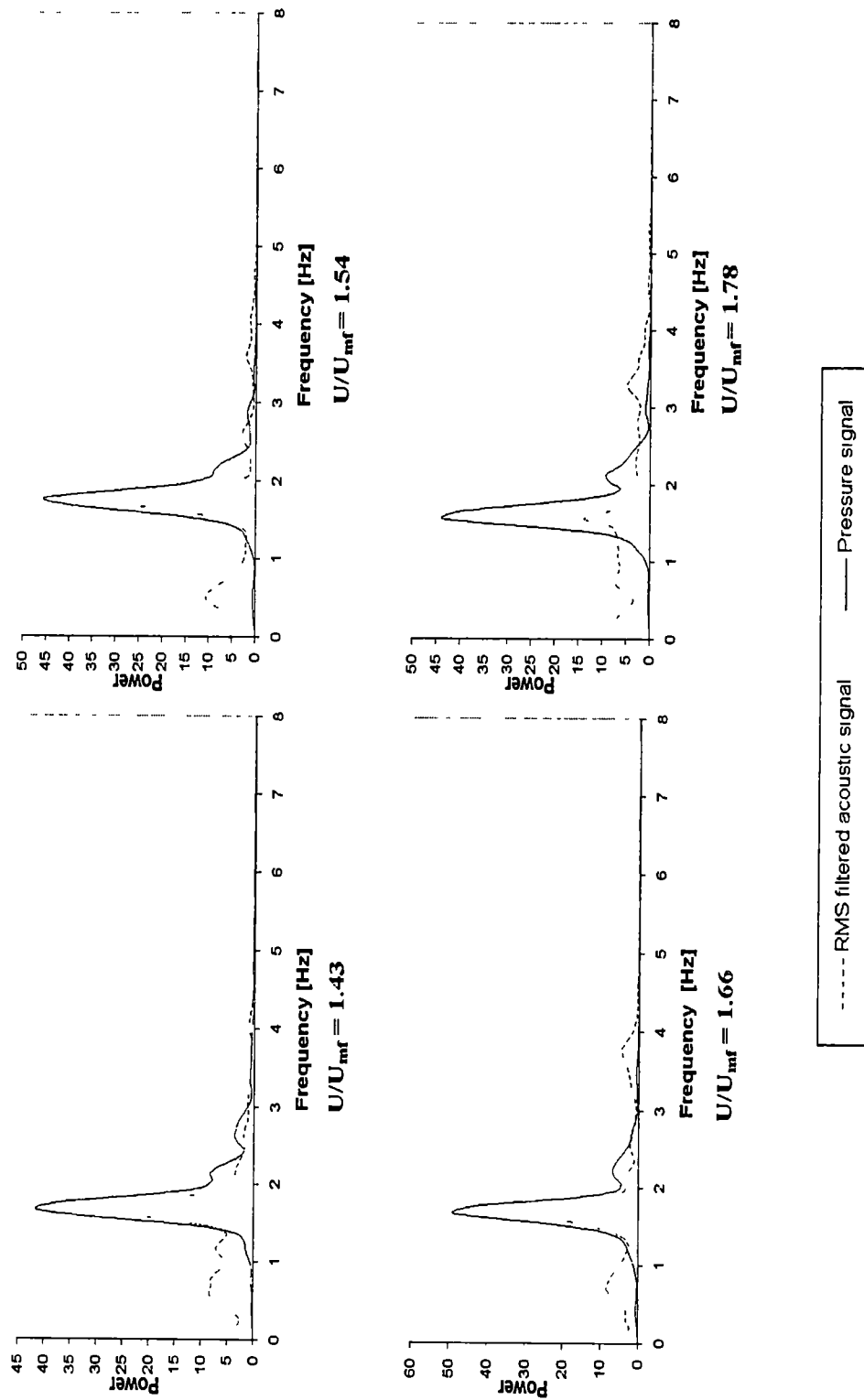
Figure B8. Fourier power spectra of acoustic and pressure signals for 18x50 mesh stainless steel over a velocity range of $U/U_{mf} = 1.43$ to 1.78.
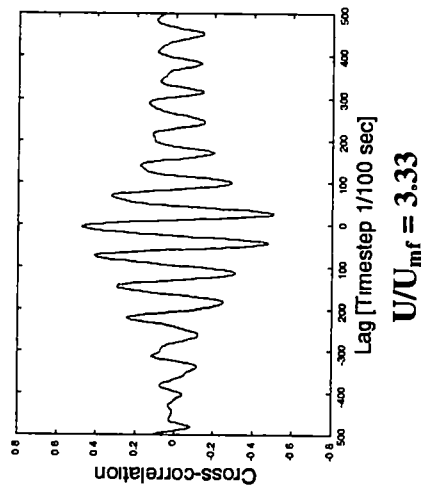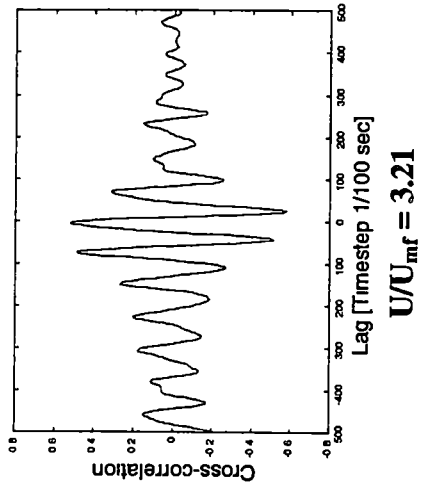
81
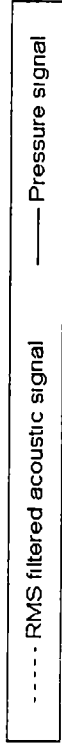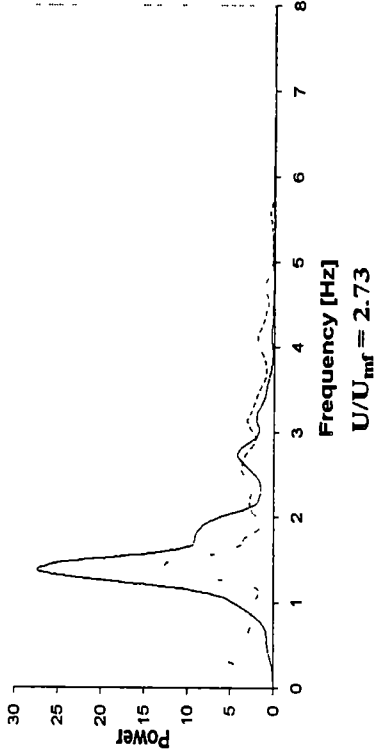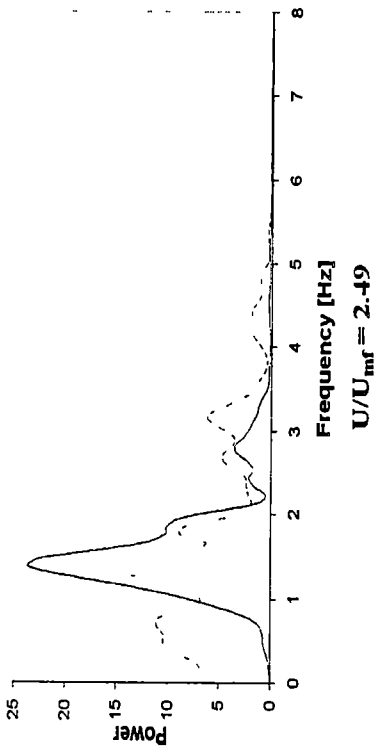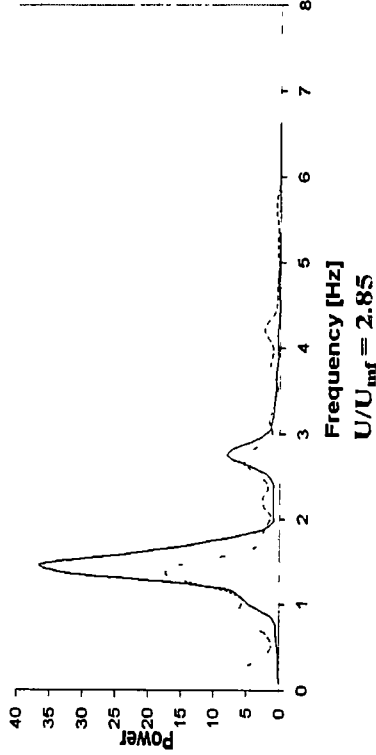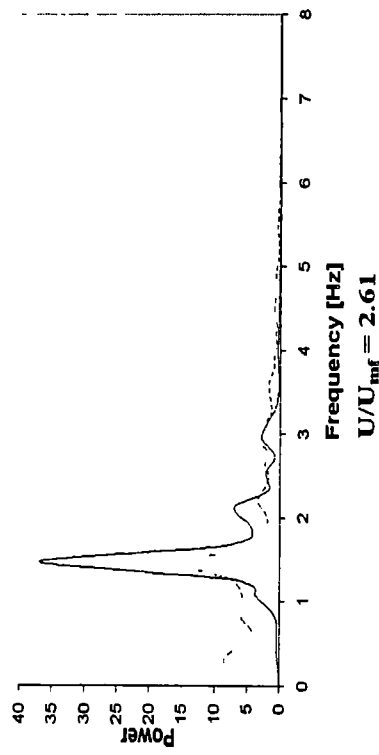
Figure B9. Fourier power spectra of acoustic and pressure signals for 18x50 mesh stainless steel over a velocity range of $U/U_{mf} = 2.49$ to 2.85.
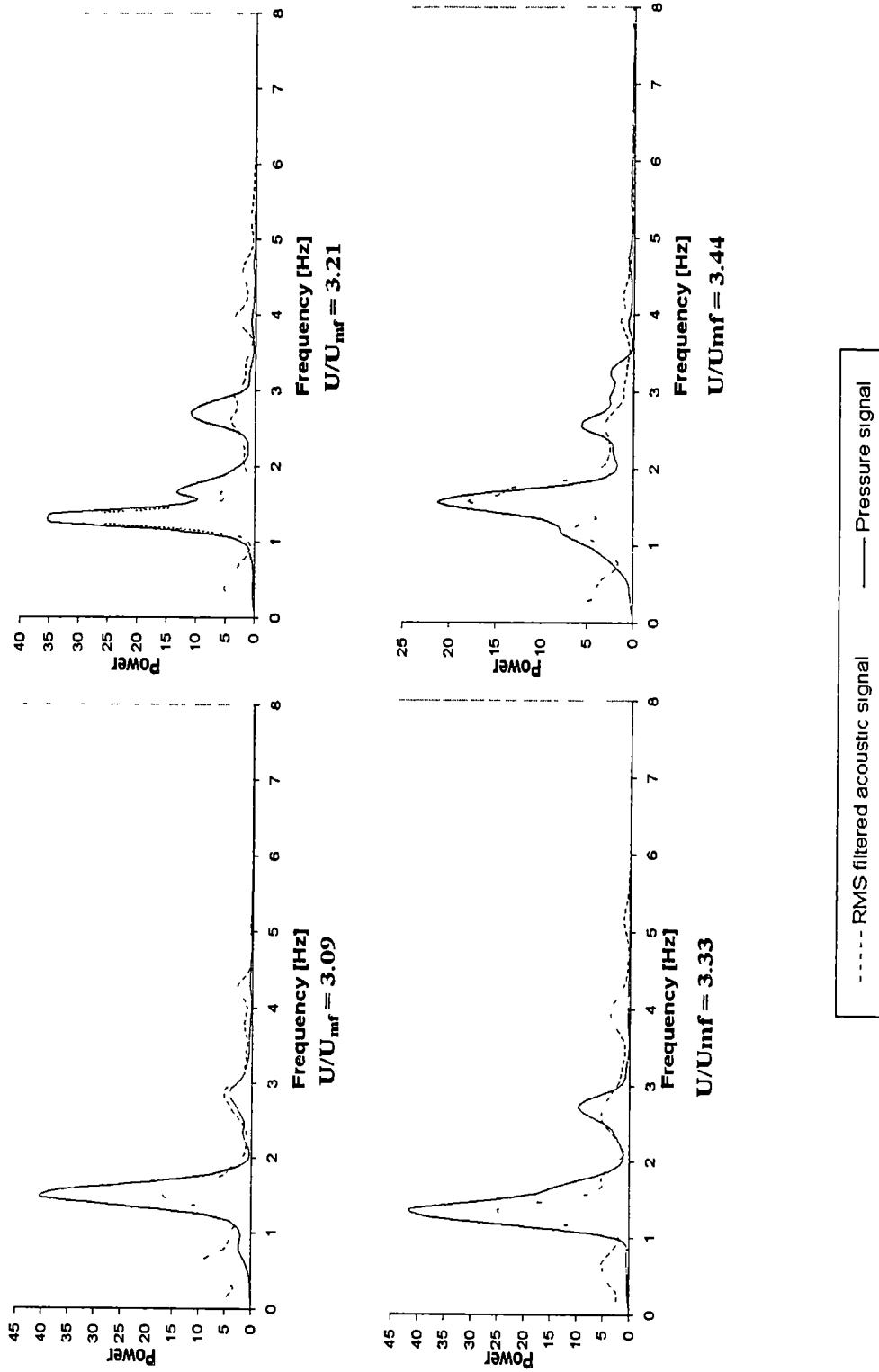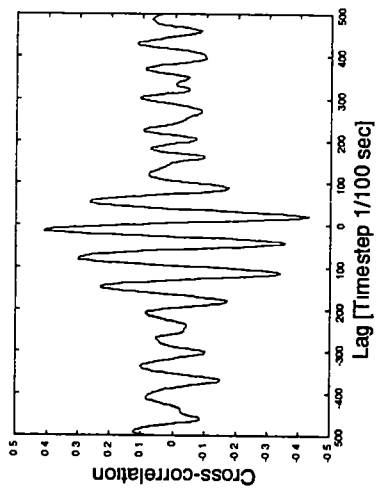
Figure B10. Fourier power spectra of acoustic and pressure signals for 18x50 mesh stainless steel over a velocity range of U/U_{mf} = 3.09 to 3.44.
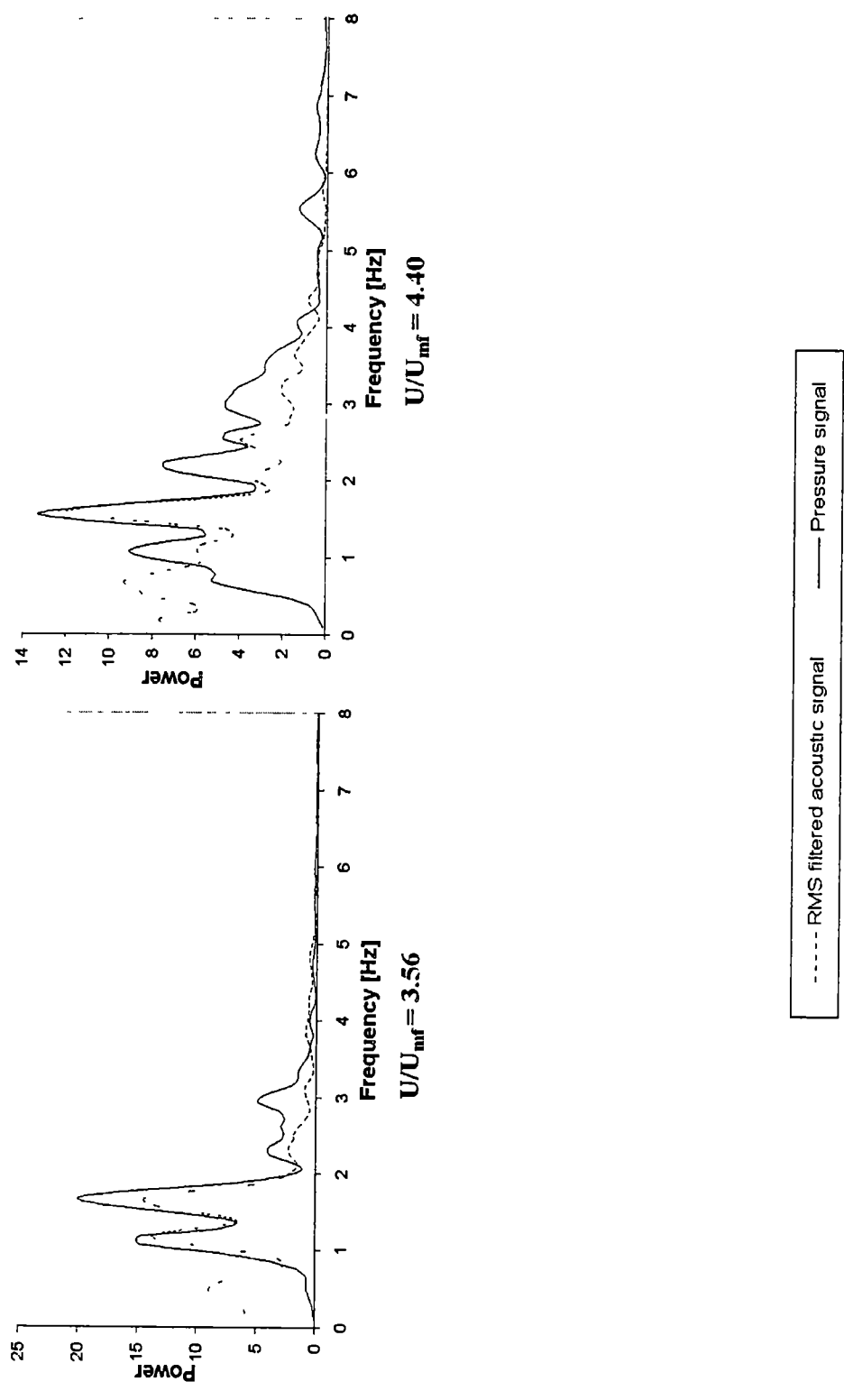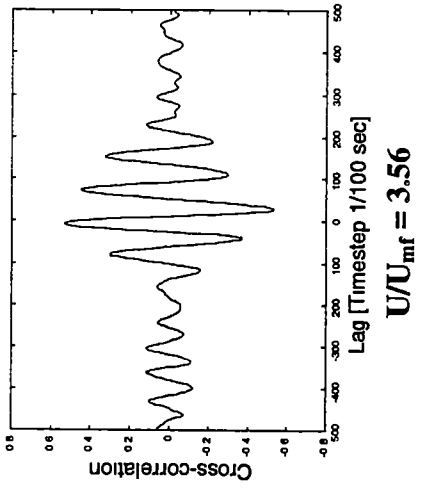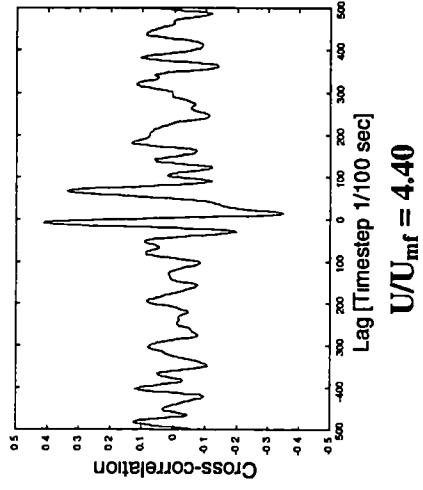
Figure B11. Fourier power spectra of acoustic and pressure signals for 18x50 mesh stainless steel over a velocity range of U/U_{mf} = 3.56 and 4.40.
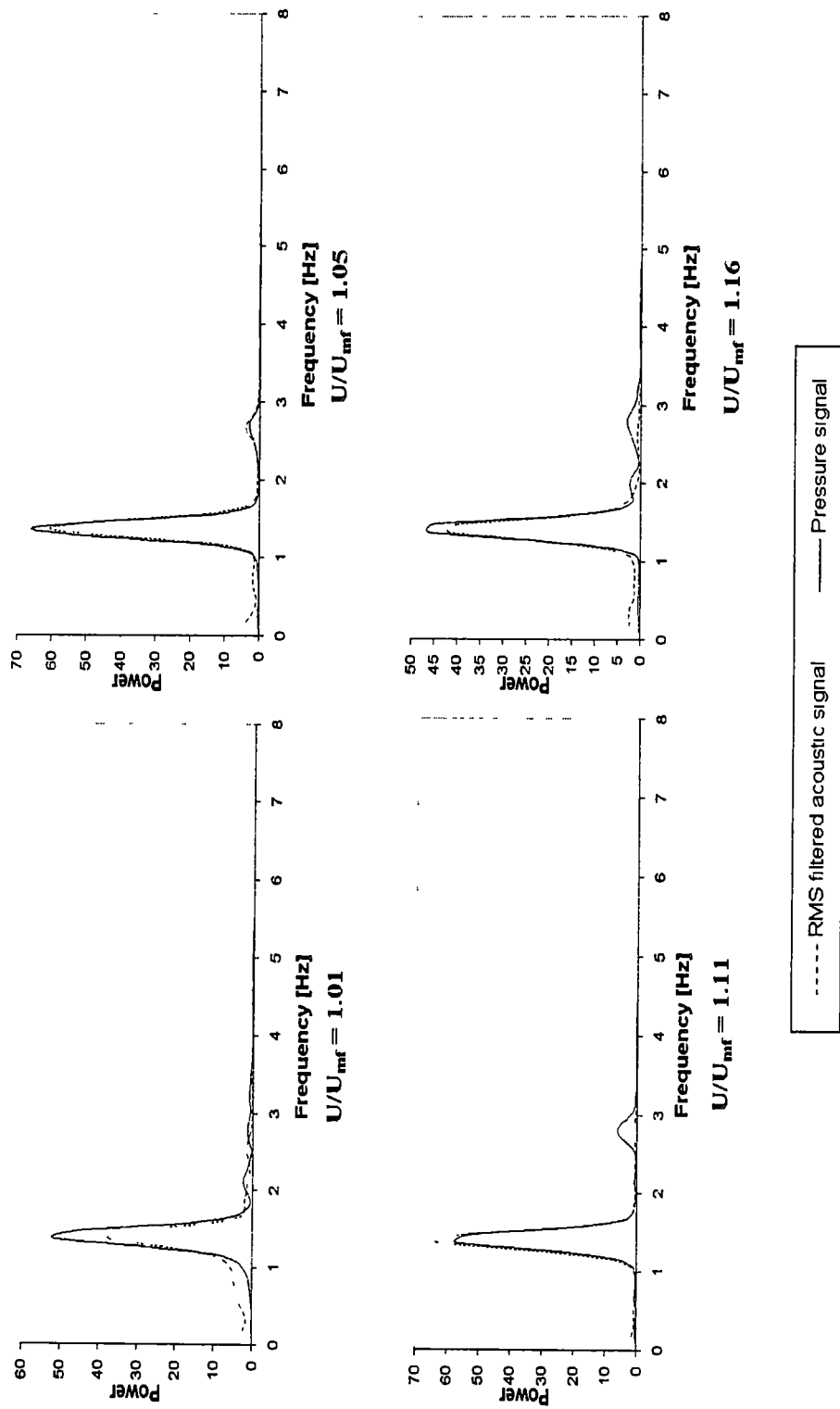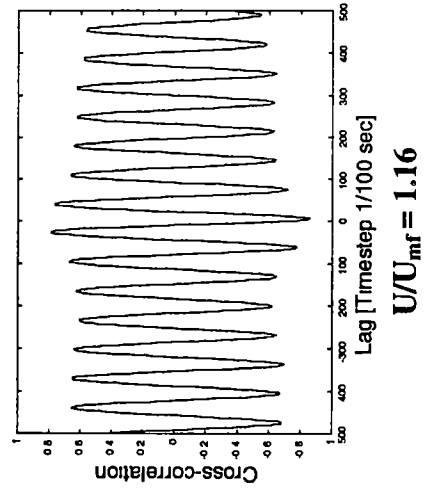
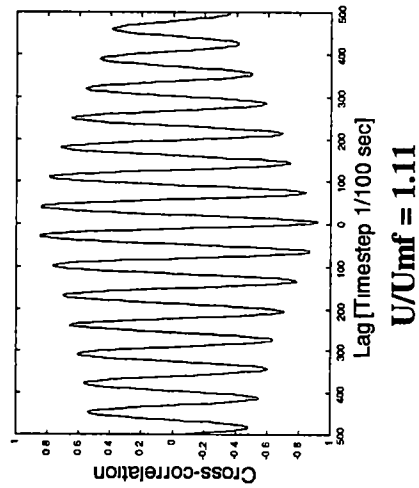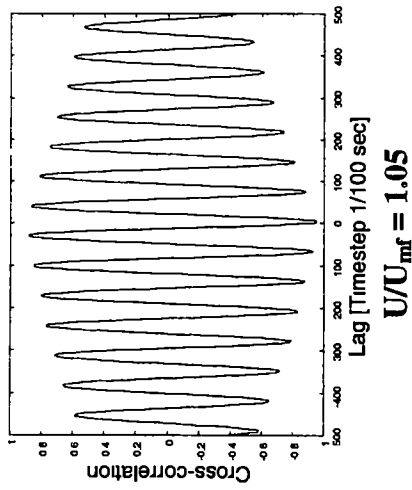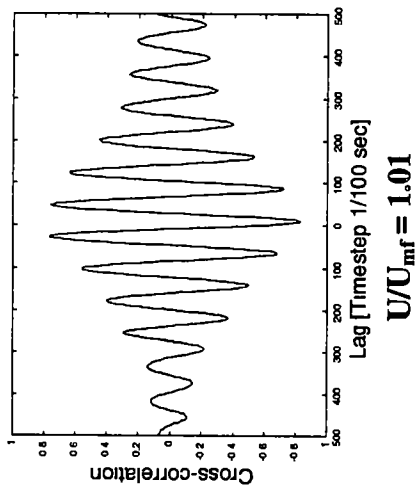**Figure B12.** Fourier power spectra of acoustic and pressure signals for glass particles over a velocity range of $U/U_{mf} = 1.01$ to 1.16.

85
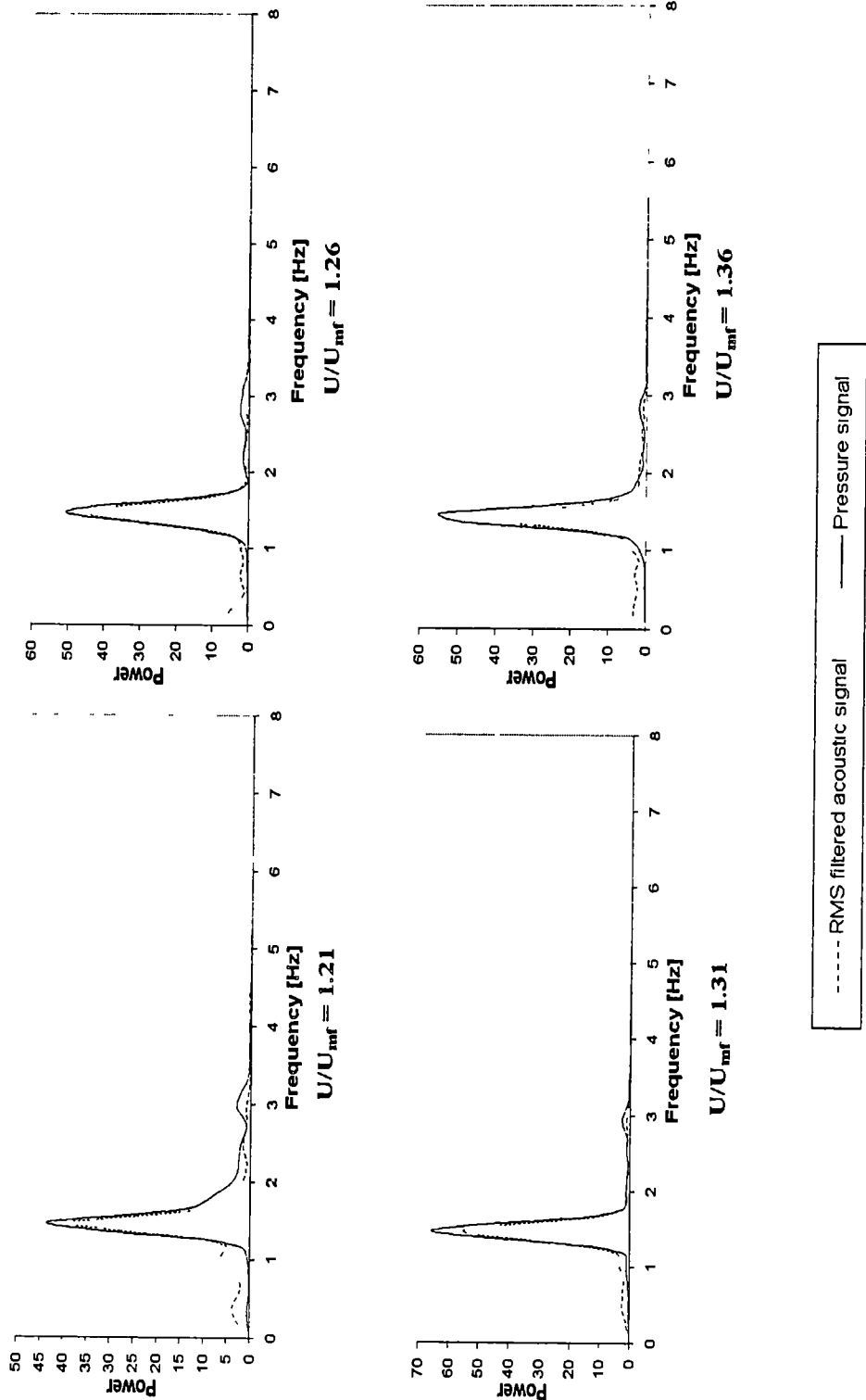
Figure B13. Fourier power spectra of acoustic and pressure signals for glass particles over a velocity range of $U/U_{mf} = 1.21$ to 1.36.
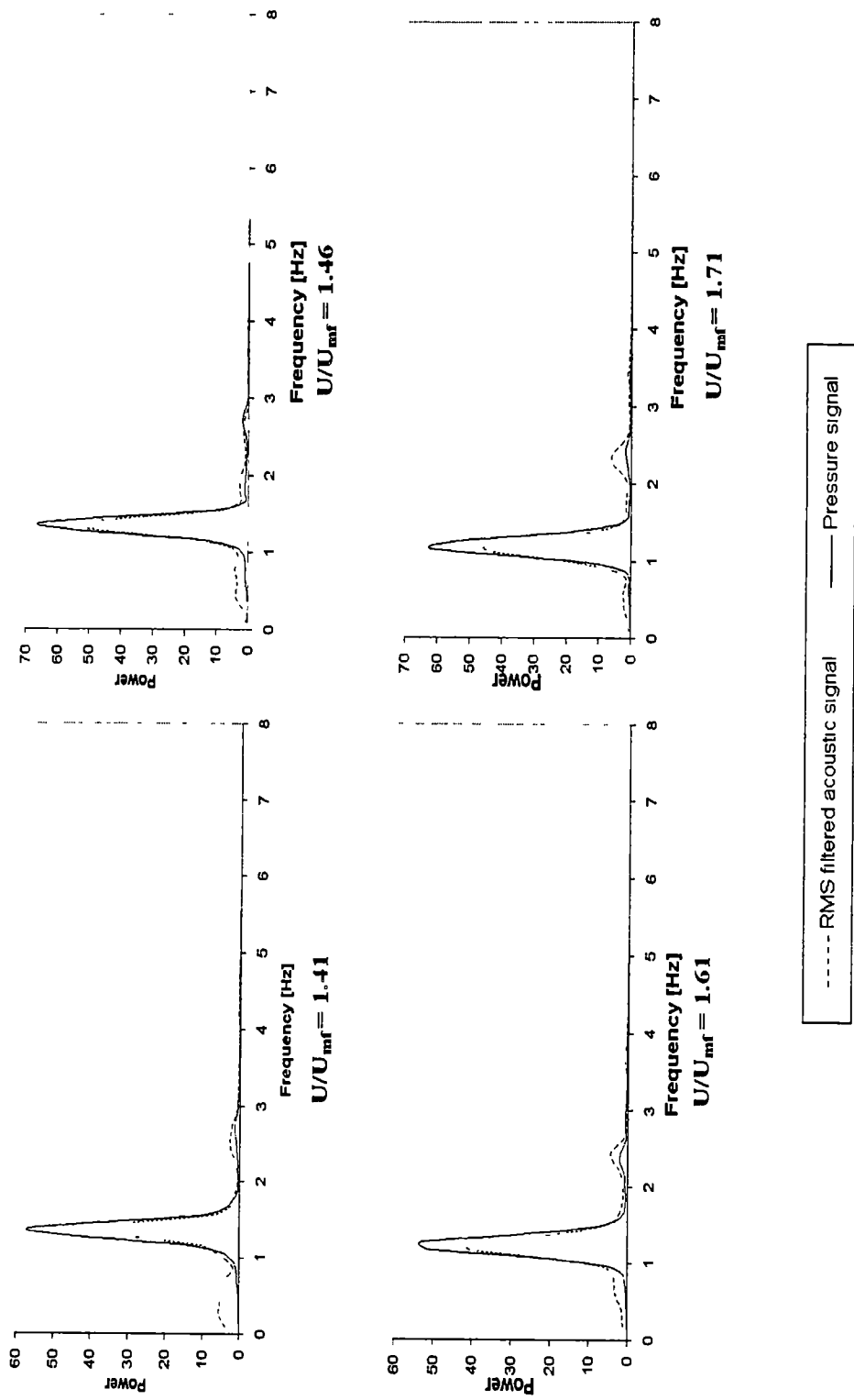
Figure B14. Fourier power spectra of acoustic and pressure signals for glass particles over a velocity range of U/U_{mf} = 1.41 to 1.71.
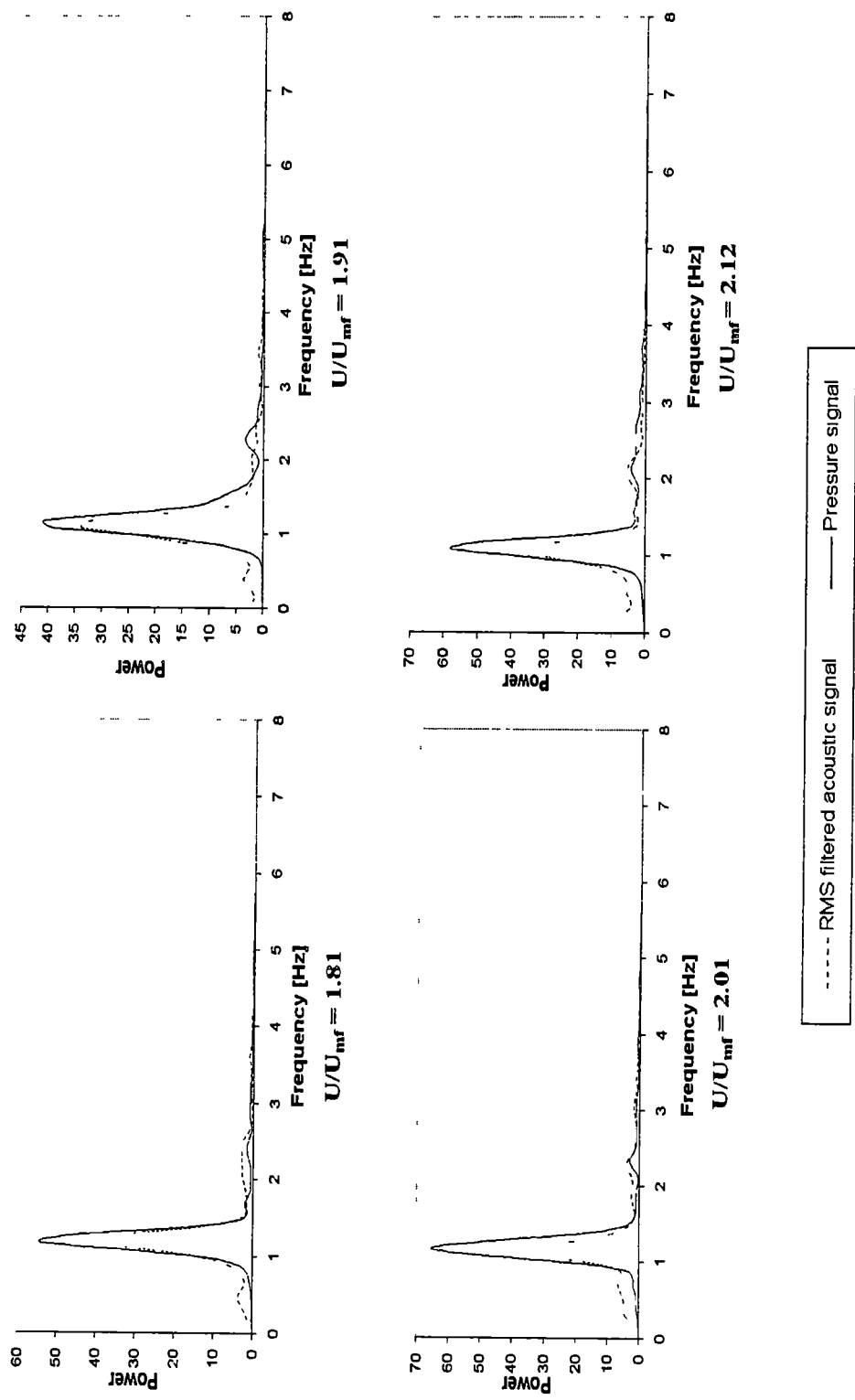
Figure B15. Fourier power spectra of acoustic and pressure signals for glass particles over a velocity range of U/U_{mf} = 1.81 to 2.12.

88
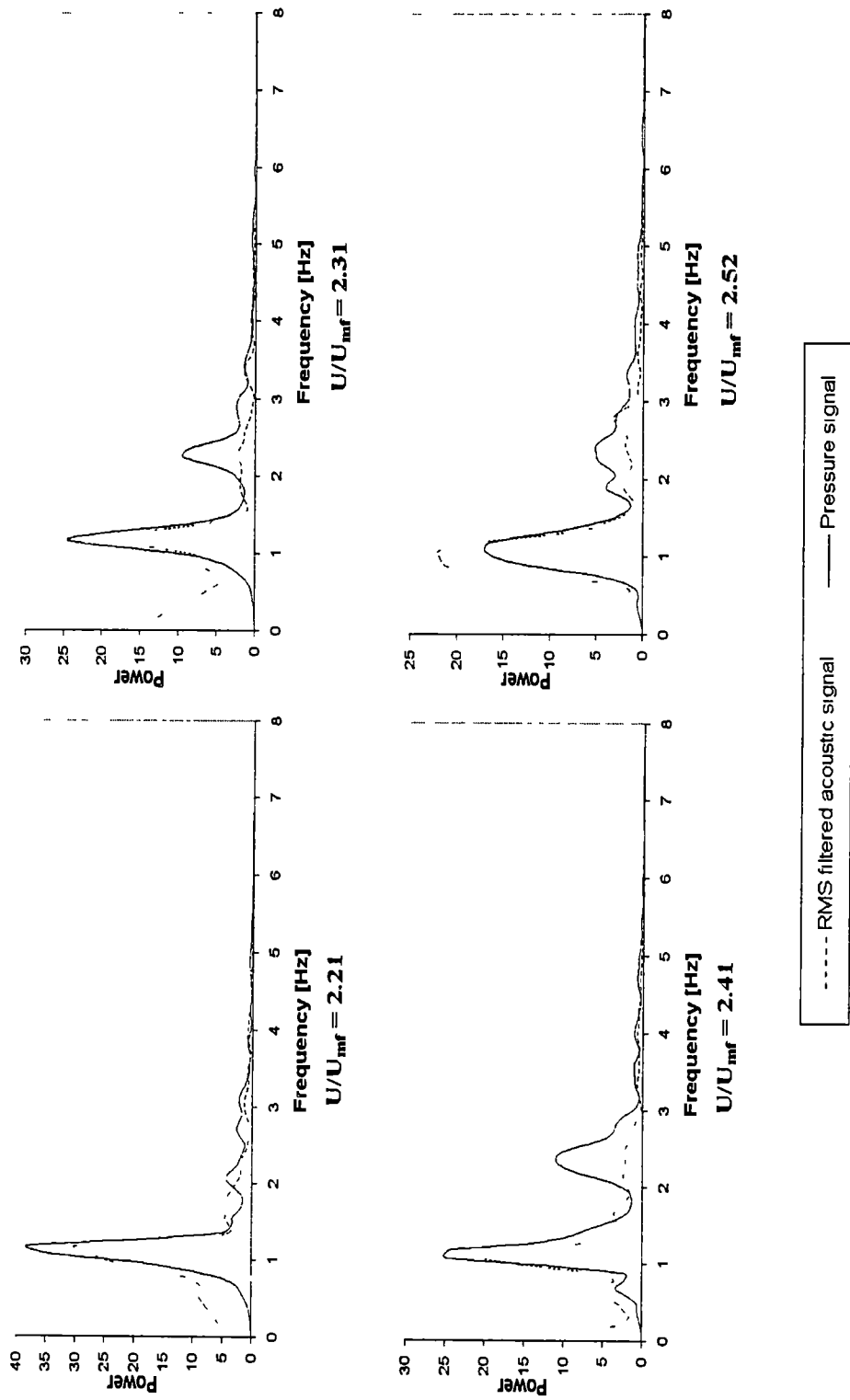
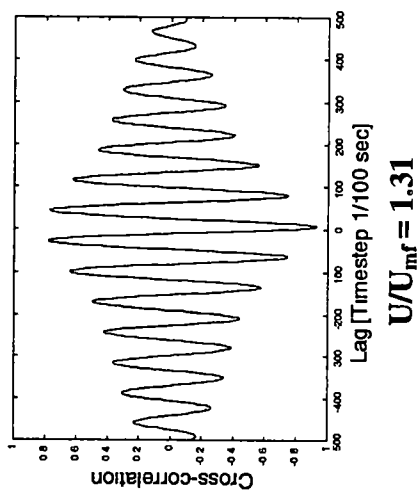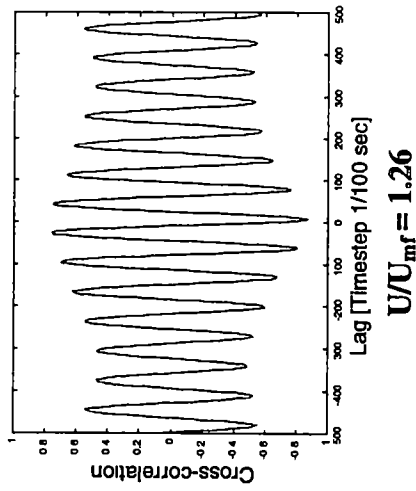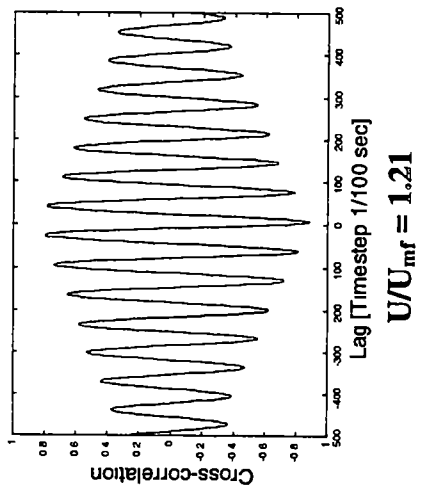Figure B16. Fourier power spectra of acoustic and pressure signals for glass particles over a velocity range of $U/U_{mf} = 2.21$ to 2.52.
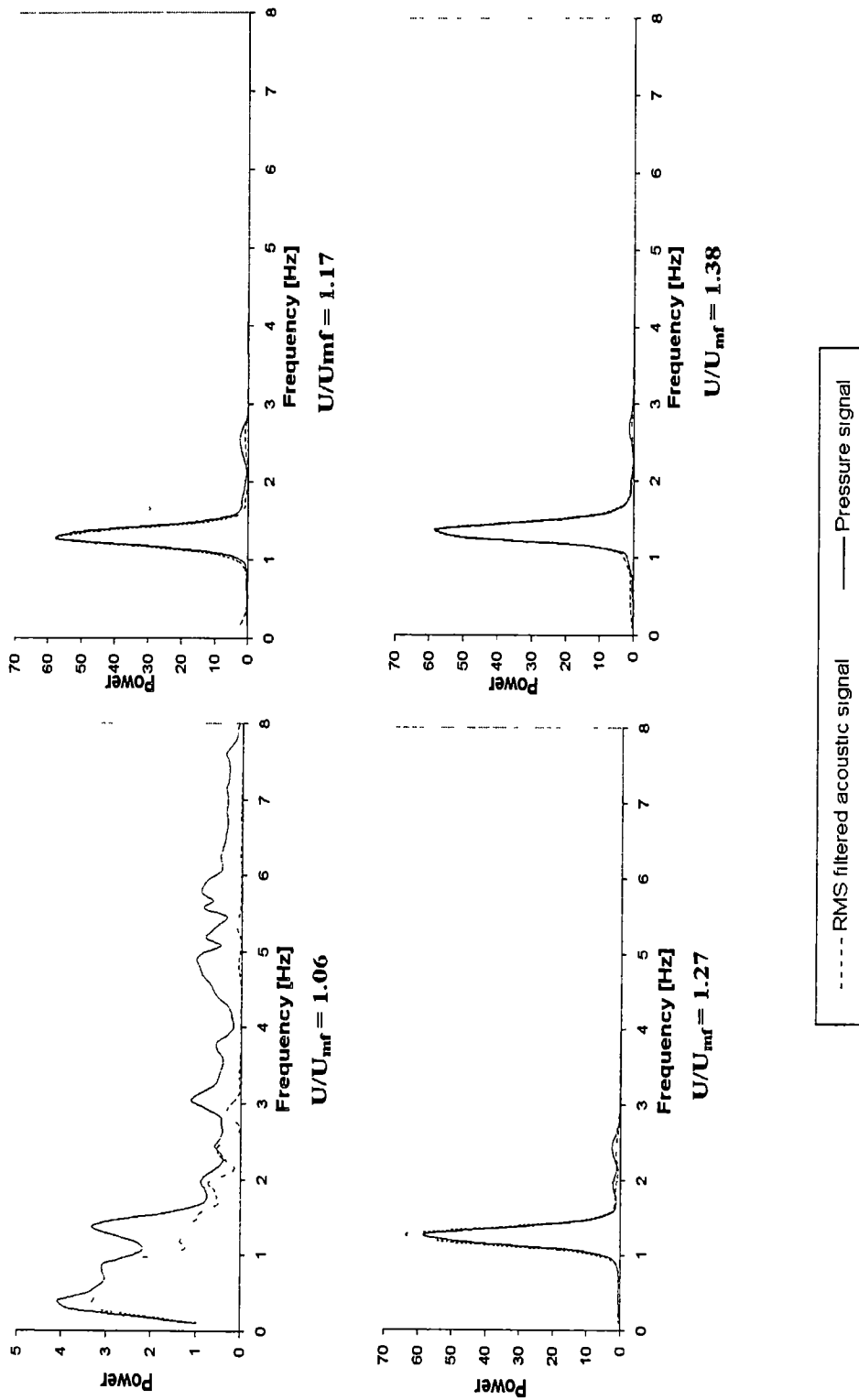
Figure B17. Fourier power spectra of acoustic and pressure signals for BB particles over a velocity range of $U/U_{mf} = 1.06$ to 1.38.
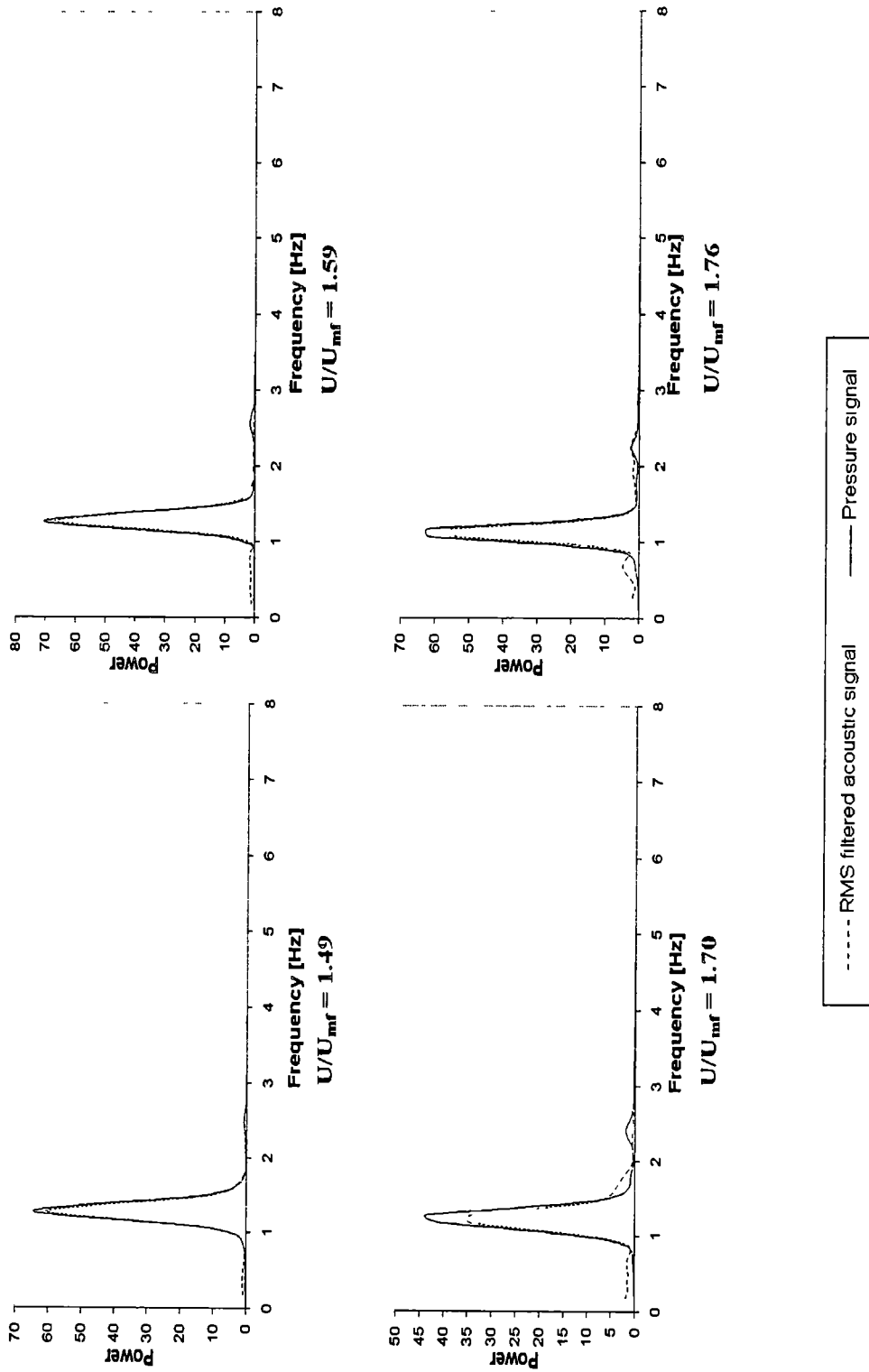
Figure B18. Fourier power spectra of acoustic and pressure signals for BB particles over a velocity range of U/U_{mf} = 1.49 to 1.76.
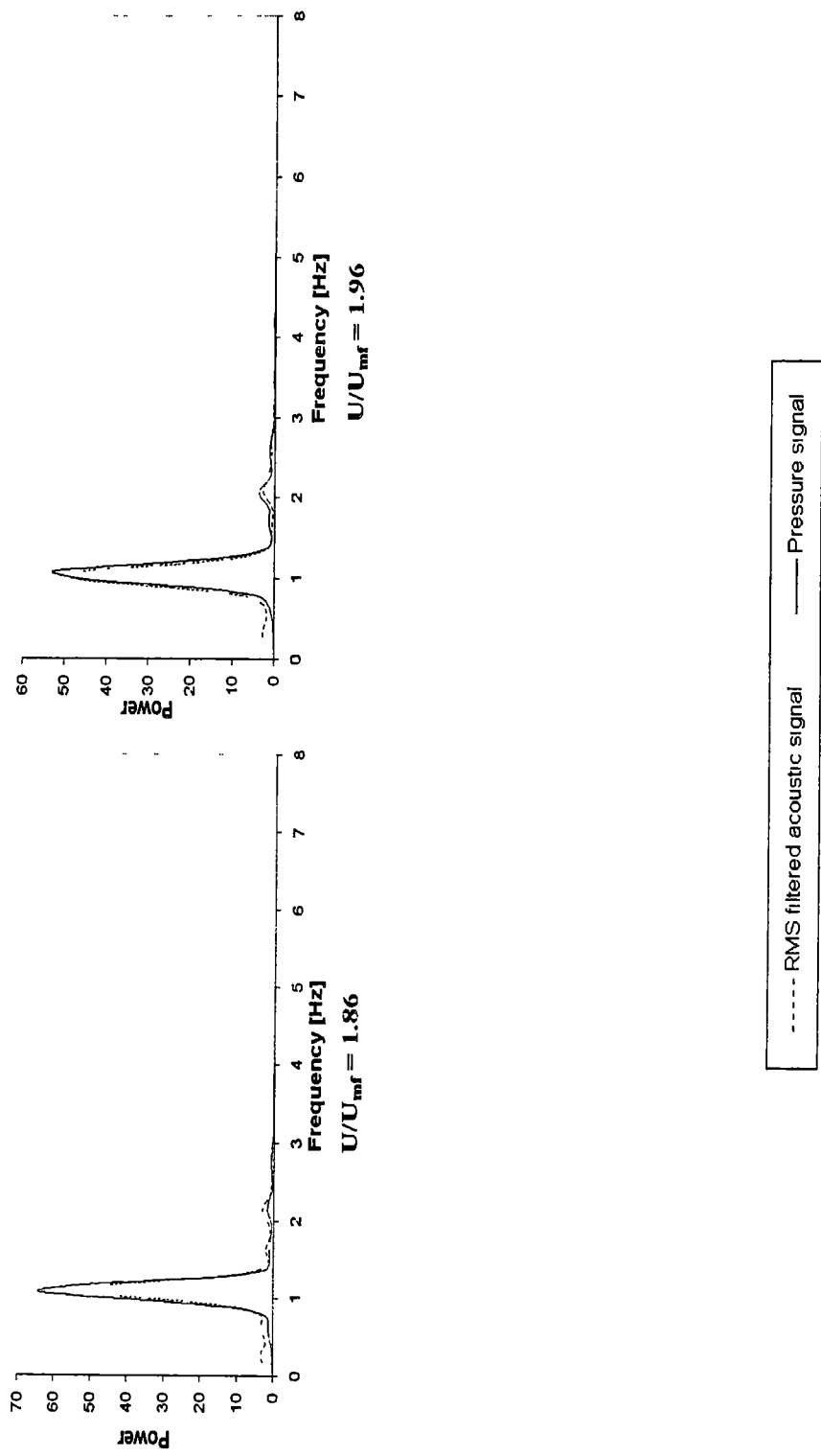
Figure B19. Fourier power spectra of acoustic and pressure signals for BB particles over a velocity range of U/U$_{mf}$ = 1.86 and 1.96.
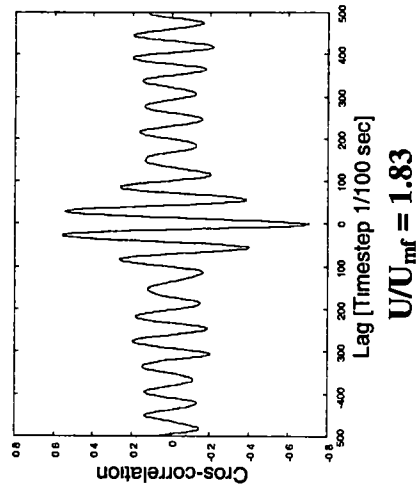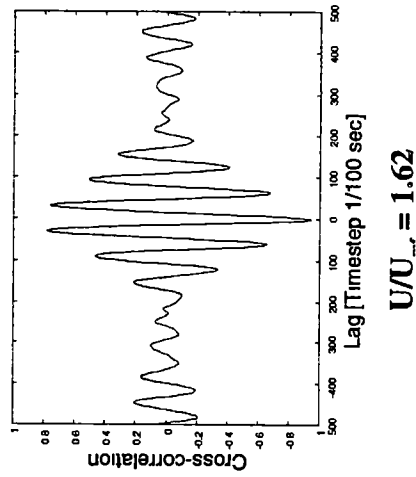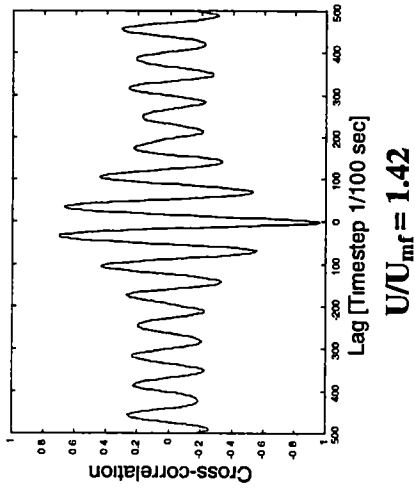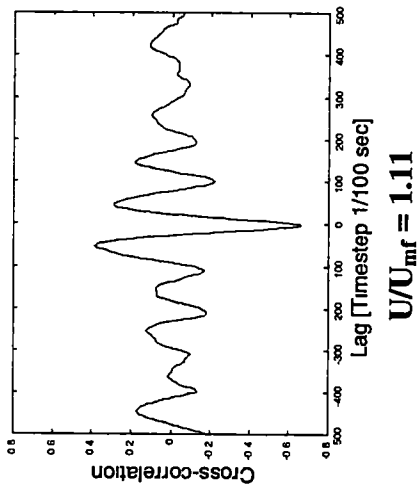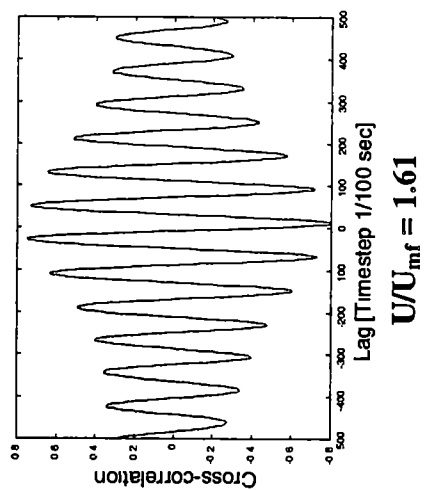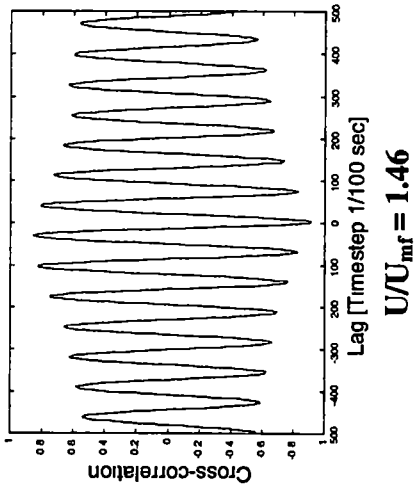
Figure B20. Cross-correlation of acoustic and pressure signals for 35x100 mesh stainless steel over a velocity range of U/U_{mf} = 1.11 to 1.83.

93
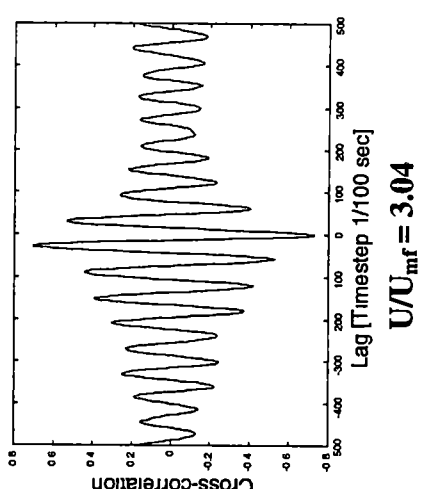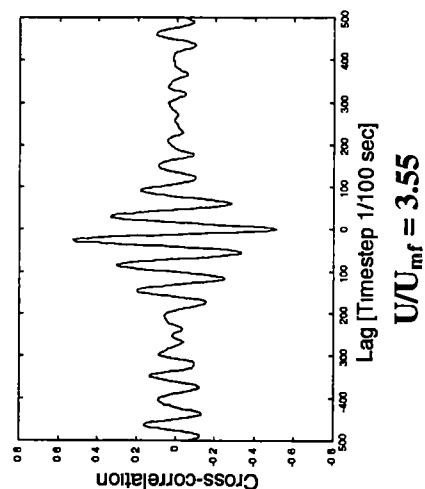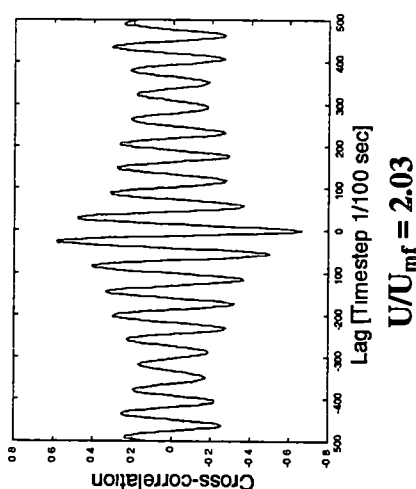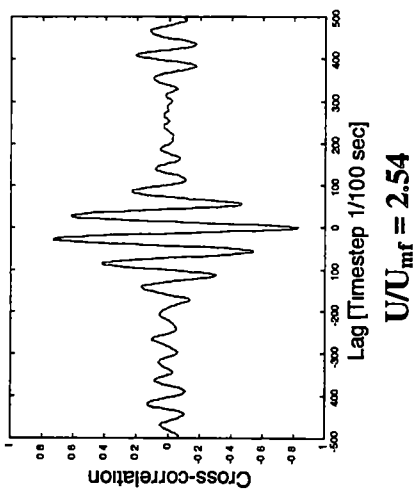
Figure B21. Cross-correlation of acoustic and pressure signals for 35x100 mesh stainless steel over a velocity range of U/U_{mf} = 2.03 to 3.55.

94
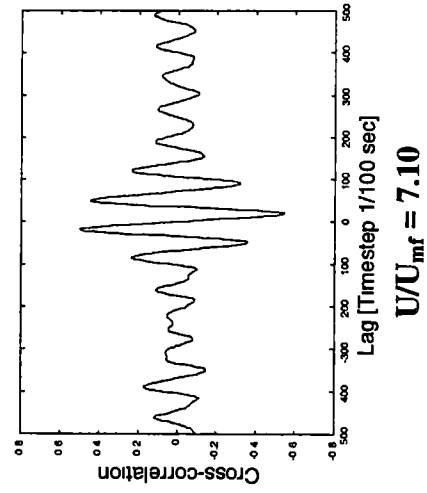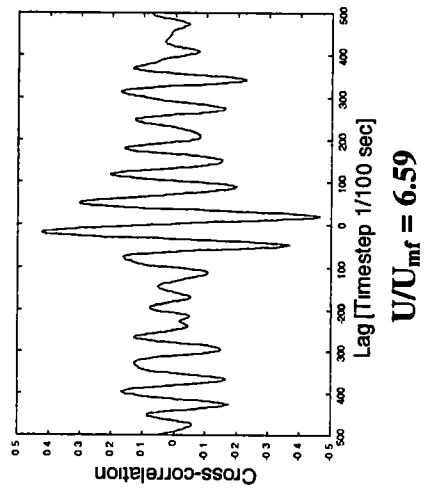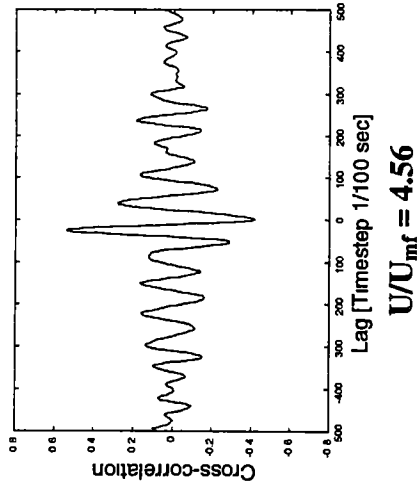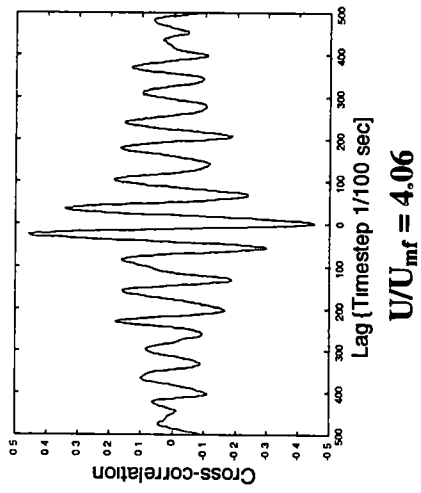
Figure B22. Cross-correlation of acoustic and pressure signals for 35x100 mesh stainless steel over a velocity range of U/U$_{mf}$ = 4.06 to 7.10.
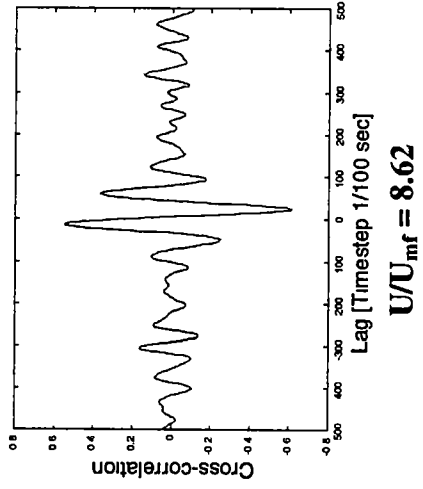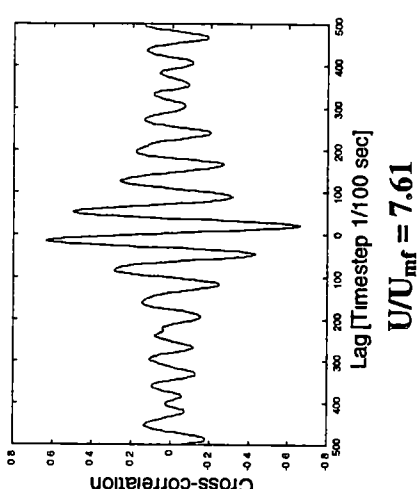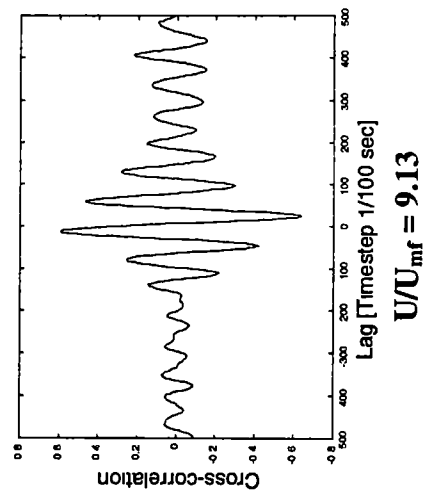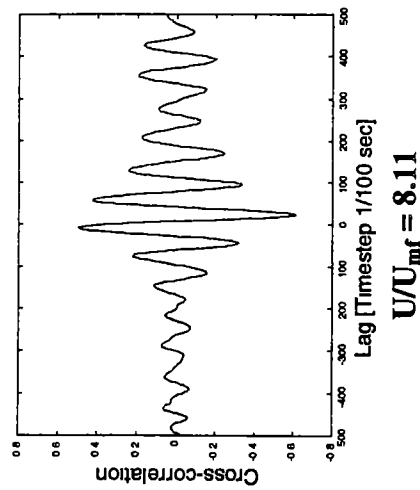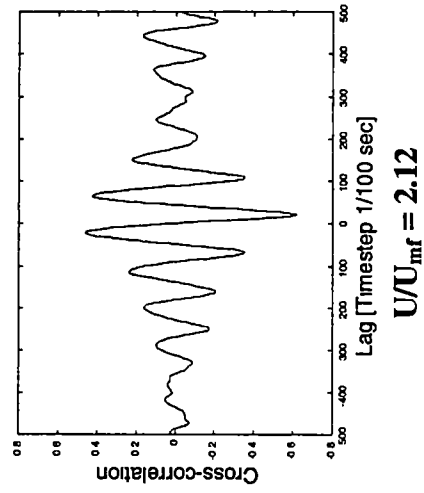
Figure B23. Cross-correlation of acoustic and pressure signals for 35x100 mesh stainless steel over a velocity range of $U/U_{mf} = 7.61$ to 9.13.
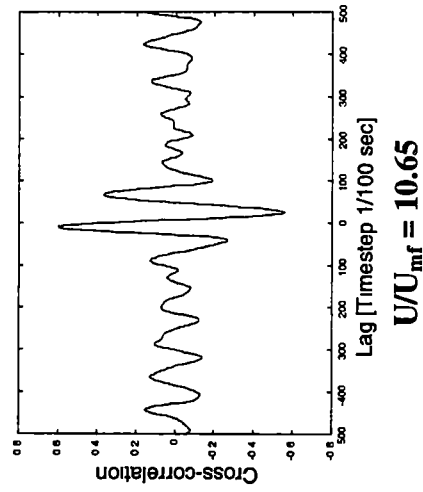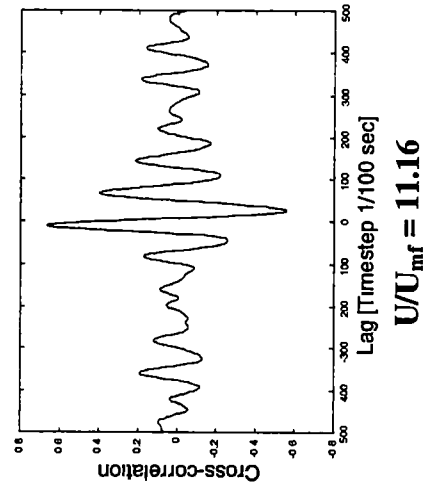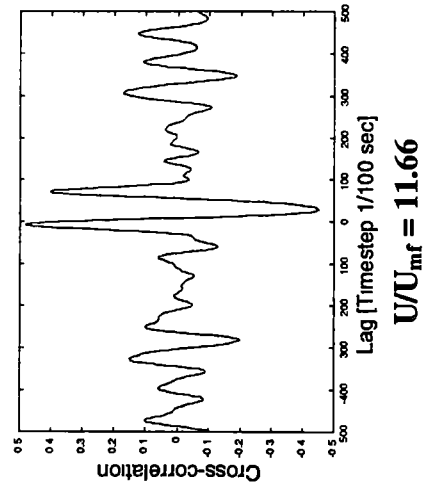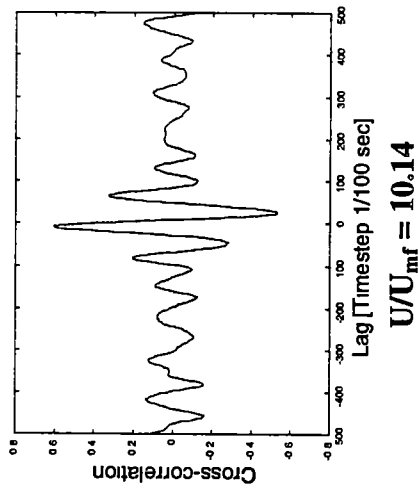
Figure B24. Cross-correlation of acoustic and pressure signals for 35x100 mesh stainless steel over a velocity range of $U/U_{mf} = 10.14$ to 11.66.
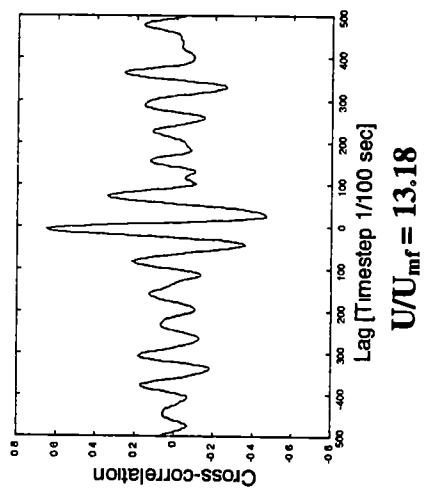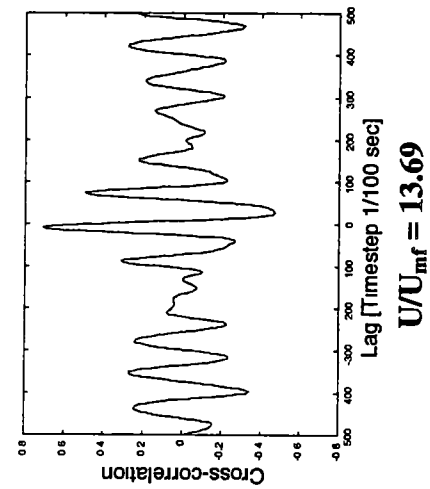
Figure B25. Cross-correlation of acoustic and pressure signals for 35x100 mesh stainless steel over a velocity range of U/U_{mf} = 13.18 and 13.69.
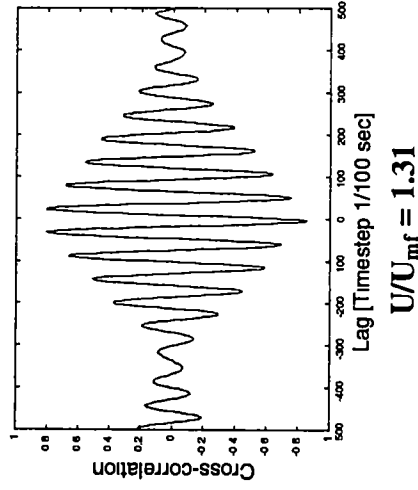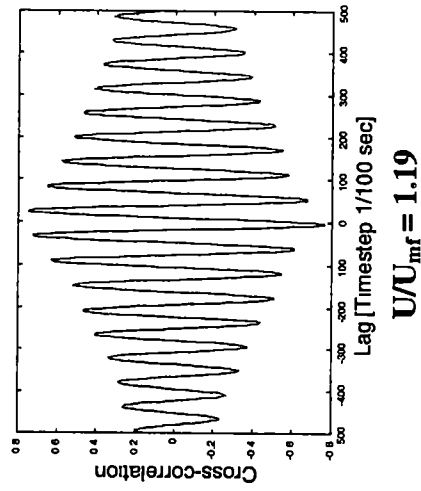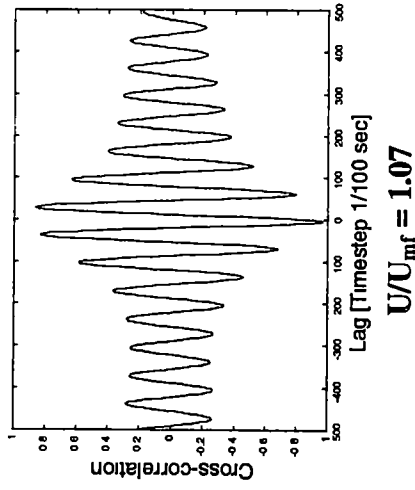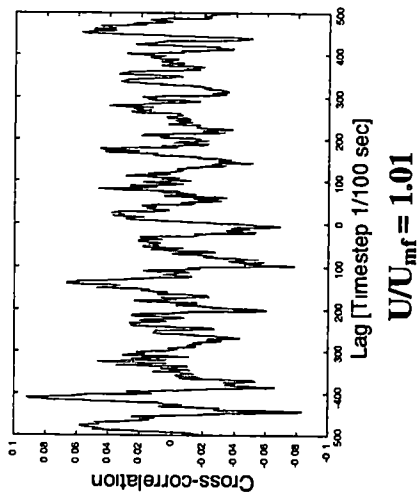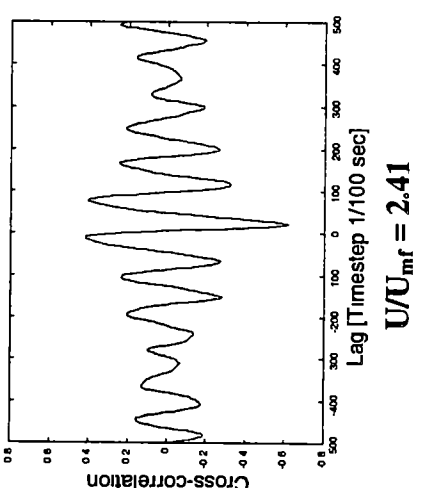
Figure B26. Cross-correlation of acoustic and pressure signals for 18x50 mesh stainless steel over a velocity range of U/U_{mf} = 1.01 to 1.31.
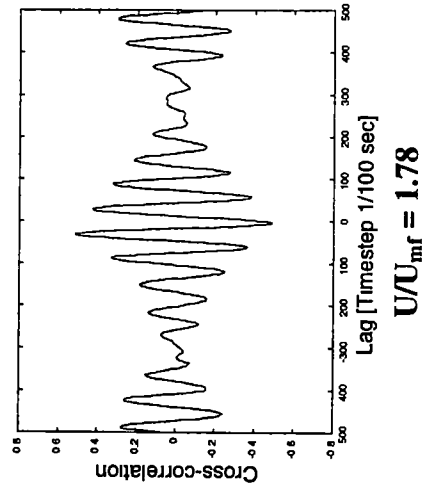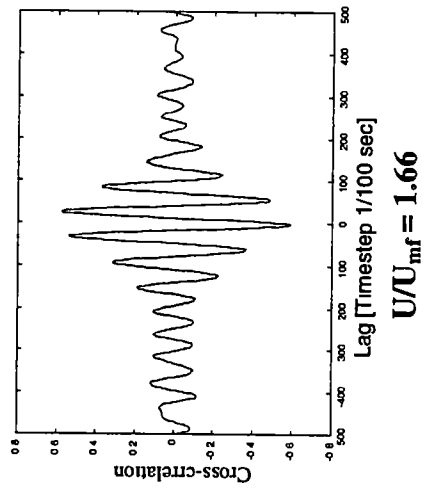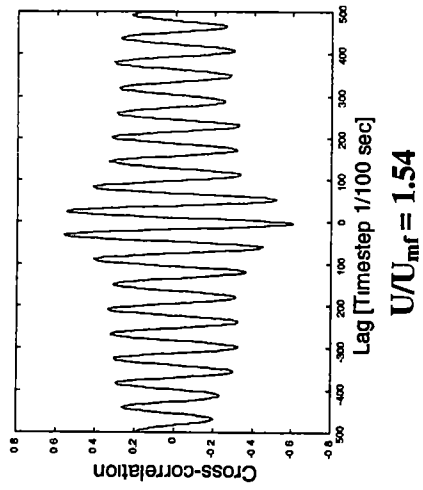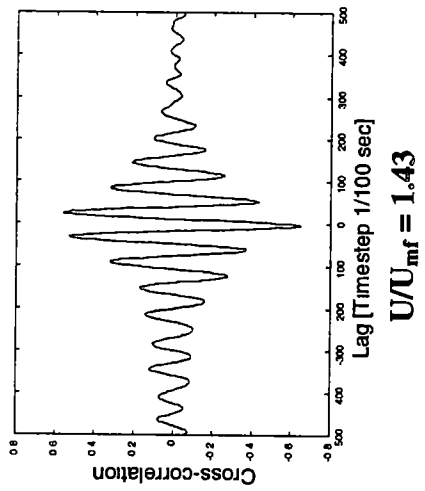
Figure B27. Cross-correlation of acoustic and pressure signals for 18x50 mesh stainless steel over a velocity range of $U/U_{mf} = 1.43$ to 1.78.
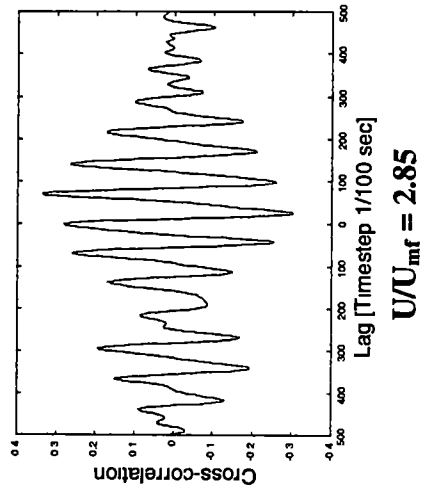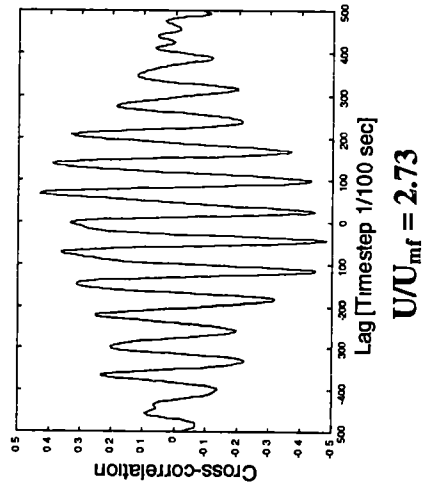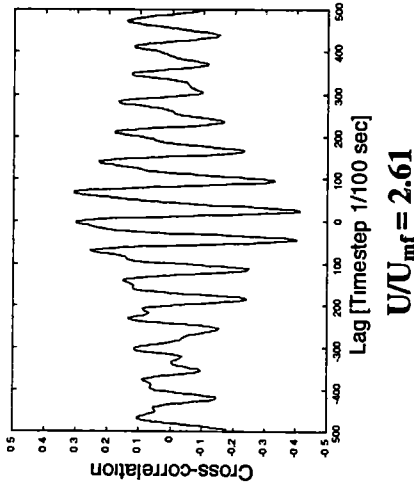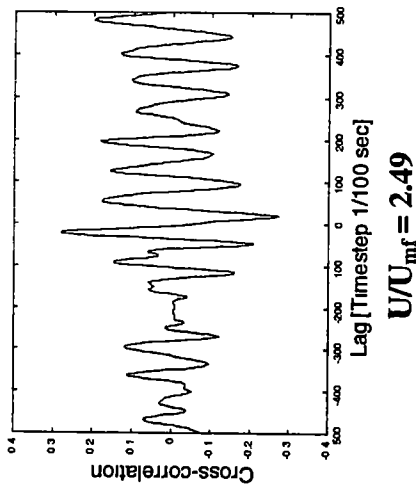
Figure B28. Cross-correlation of acoustic and pressure signals for 18x50 mesh stainless steel over a velocity range of U/U_{mf} = 2.49 to 2.85.
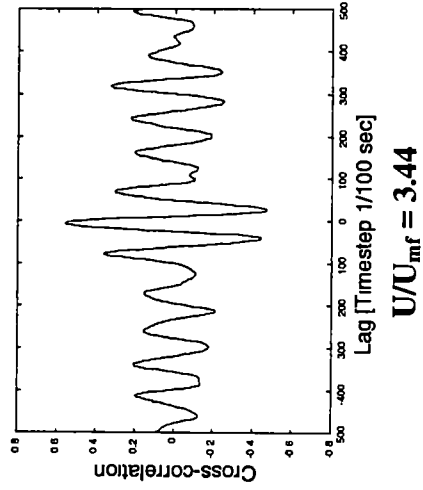
Figure B29. Cross-correlation of acoustic and pressure signals for 18x50 mesh stainless steel over a velocity range of $U/U_{mf} = 3.09$ to 3.44.

102

Figure B30. Cross-correlation of acoustic and pressure signals for 18x50 mesh stainless steel over a velocity range of U/U_{mf} = 3.56 and 4.40.

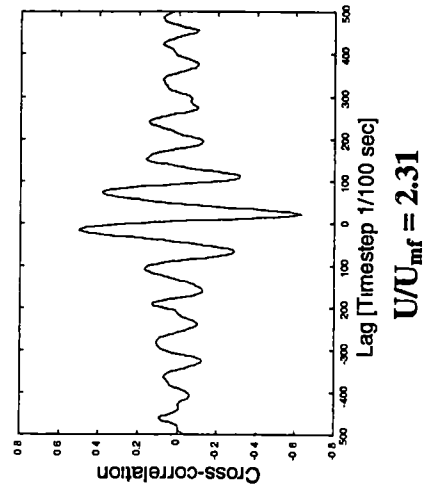**Figure B31.** Cross-correlation of acoustic and pressure signals for glass particles over a velocity range of $U/U_{mf} = 1.01$ to 1.16.
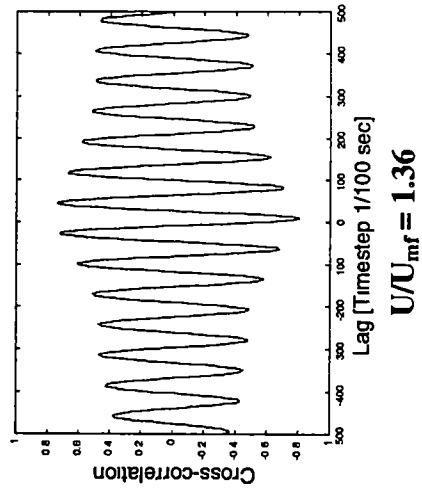
Figure B32. Cross-correlation of acoustic and pressure signals for glass particles over a velocity range of $U/U_{mf} = 1.21$ to 1.36.
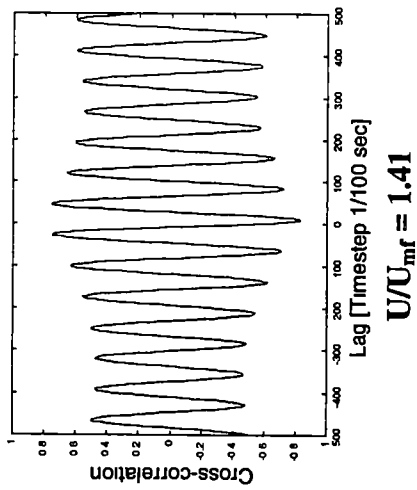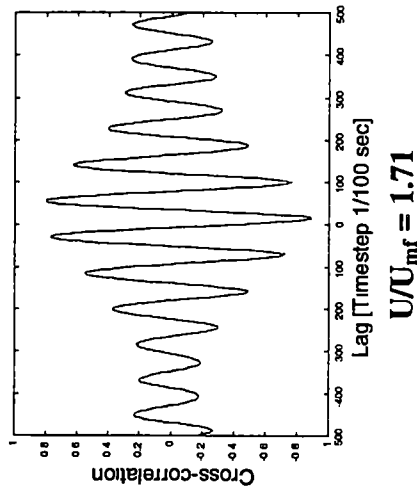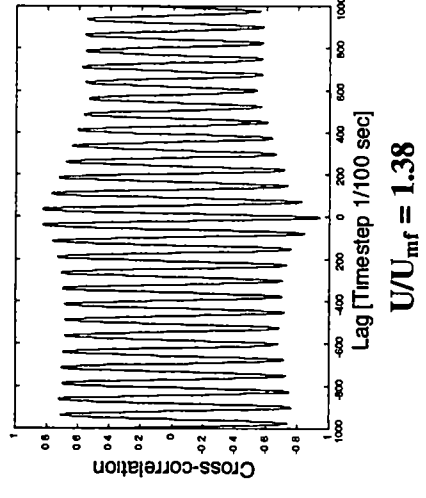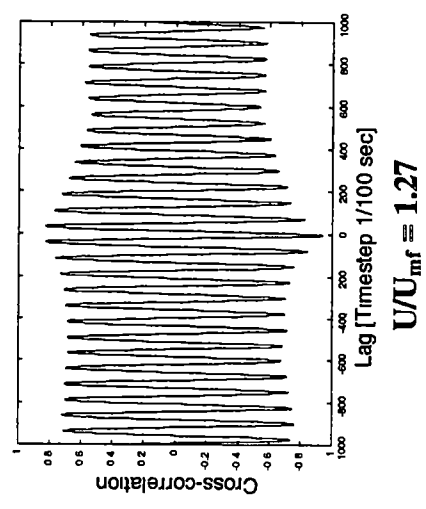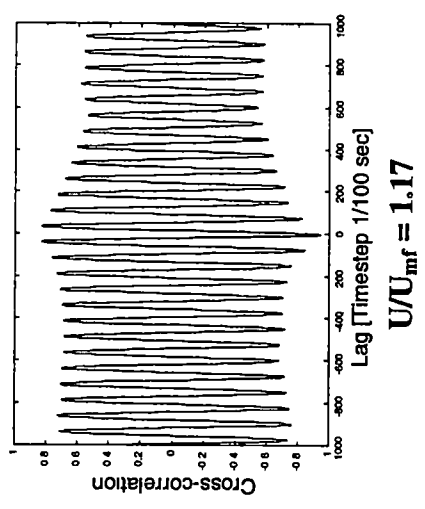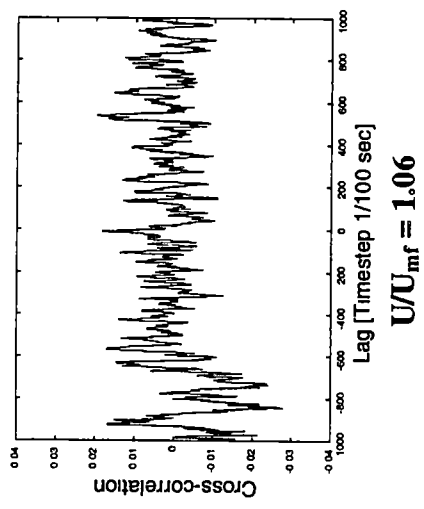
Figure B33. Cross-correlation of acoustic and pressure signals for glass particles over a velocity range of $U/U_{mf} = 1.41$ to 1.71.
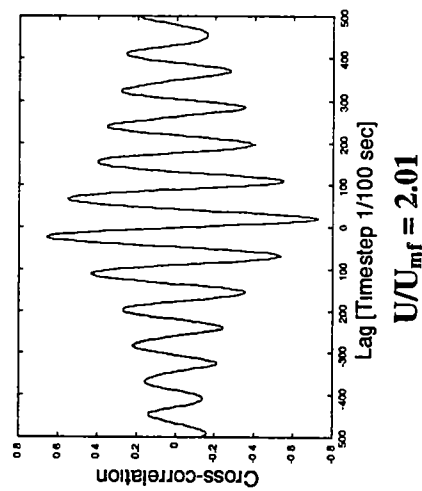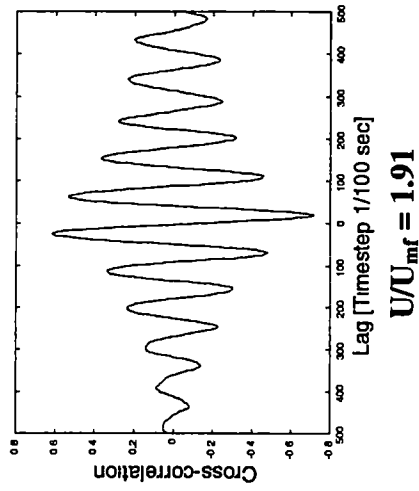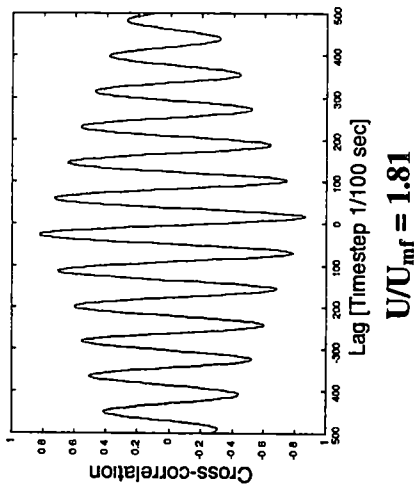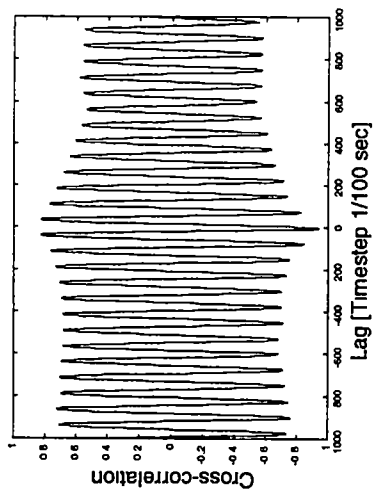
Figure B34. Cross-correlation of acoustic and pressure signals for glass particles over a velocity range of $U/U_{mf} = 1.81$ to 2.12.
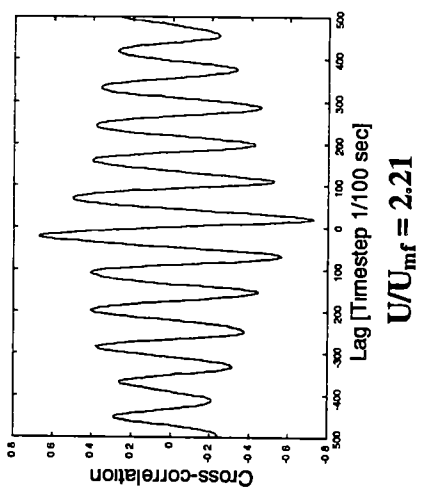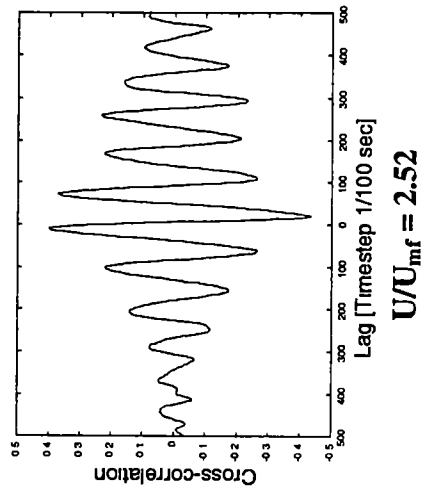
Figure B35. Cross-correlation of acoustic and pressure signals for glass particles over a velocity range of U/U$_{mf}$ = 2.21 to 2.52.
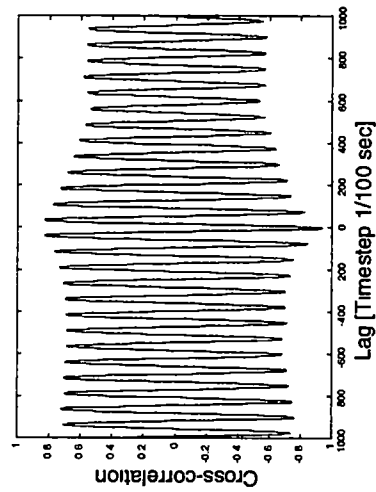
108
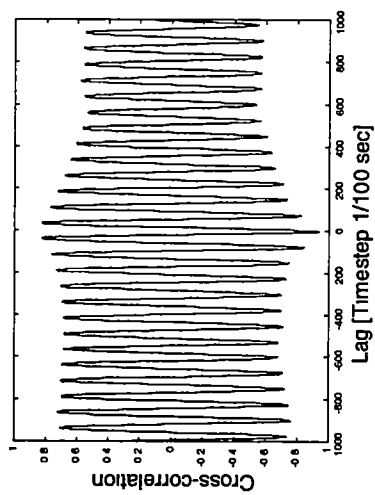
Figure B36. Cross-correlation of acoustic and pressure signals for BB particles over a velocity range of $U/U_{mf} = 1.06$ to 1.38.

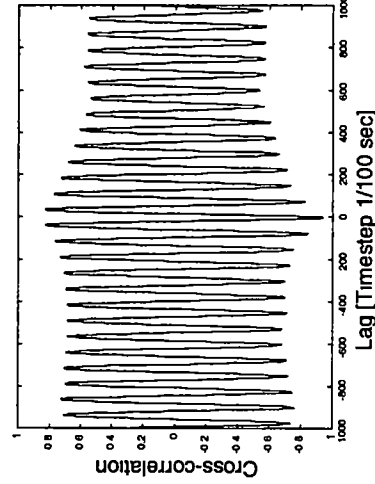**Figure B37.** Cross-correlation of acoustic and pressure signals for BB particles over a velocity range of U/U$_{mf}$ = 1.49 to 1.76.
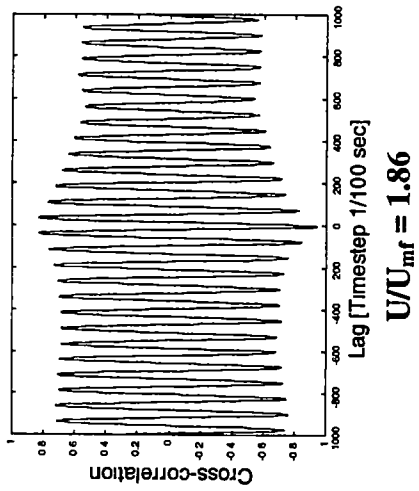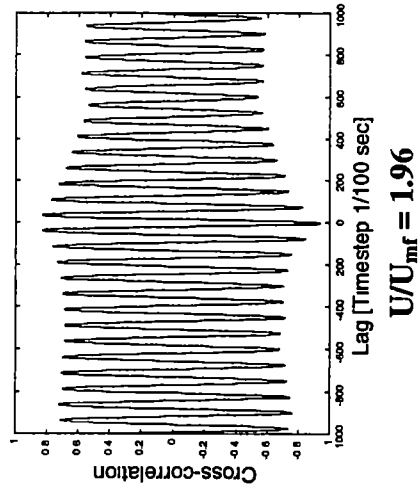
Figure B38. Cross-correlation of acoustic and pressure signals for BB particles over a velocity range of $U/U_{mf} = 1.86$ and 1.96.

VITA

Tiang-Yong Teh was born in Ipoh, Perak, Malaysia on June 30, 1976. He was a transferred student from Metropolitan College, Malaysia in August 1996 and graduated from University of Tennessee, Knoxville in August 1998 earning the degree of Bachelor of Science in Mechanical Engineering. He then began graduate study at the University of Tennessee, Knoxville where he received the degree of Master of Science in Mechanical Engineering in August 2000.